Journal of Energy Chemistry 61 (2021) 104–134

Contents lists available at ScienceDirect

Journal of Energy Chemistry

journal homepage: www.elsevier.com/locate/jechem

http://www.journals.elsevier.com/journal-of-energy-chemistry/

Review

Rechargeable metal (Li, Na, Mg, Al)-sulfur batteries: Materials and advances

Xue Liu [a], Yan Li [a], Xu Xu [a,*], Liang Zhou [a], Liqiang Mai [a,b,*]

[a] State Key Laboratory of Advanced Technology for Materials Synthesis and Processing, International School of Materials Science and Engineering, Wuhan University of Technology, Wuhan 430070, Hubei, China
[b] Foshan Xianhu Laboratory of the Advanced Energy Science and Technology Guangdong Laboratory, Xianhu Hydrogen Valley, Foshan 528200, Guangdong, China

ARTICLE INFO

Article history:
Received 29 January 2021
Revised 21 February 2021
Accepted 24 February 2021
Available online 11 March 2021

Keywords:
Lithium sulfur batteries
Sodium sulfur batteries
Magnesium sulfur batteries
Aluminum sulfur batteries
Energy materials

ABSTRACT

Energy and environmental issues are becoming more and more severe and renewable energy storage technologies are vital to solve the problem. Rechargeable metal (Li, Na, Mg, Al)-sulfur batteries with low-cost and earth-abundant elemental sulfur as the cathode are attracting more and more interest for electrical energy storage in recent years. Lithium-sulfur (Li-S), room-temperature sodium-sulfur (RT Na-S), magnesium-sulfur (Mg-S) and aluminum-sulfur (Al-S) batteries are the most prominent candidates among them. Many obvious obstacles are hampering the developments of metal-sulfur batteries. Li-S and Na-S batteries are encumbered mainly by anode dendrite issues, polysulfides shuttle and low conductivity of cathodes. Mg-S and Al-S batteries are short of suitable electrolytes. In this review, relationships between various employed nanostructured materials and electrochemical performances of metal-sulfur batteries have been demonstrated. Moreover, the selections of suitable electrolytes, anode protection, separator modifications and prototype innovations are all crucial to the developments of metal-sulfur batteries and are discussed at the same time. Herein, we give a review on the advances of Li-S, RT Na-S, Mg-S and Al-S batteries from the point of view of materials, and then focus on perspectives of their future developments.

Contents

1. Introduction . . . 105
2. Lithium-sulfur batteries . . . 106
 2.1. Mechanism . . . 107
 2.2. Carbon materials . . . 109
 2.3. Polymers . . . 110
 2.4. Metal oxides and sulfides . . . 111
 2.5. Emerging nanomaterials . . . 114
 2.6. Li metal anode protection . . . 117
 2.7. Electrolytes for Li-S batteries . . . 118
  2.7.1. Conventional electrolytes . . . 118
  2.7.2. Redox mediators . . . 118
  2.7.3. Solid state electrolytes . . . 118
  2.7.4. New liquid electrolytes . . . 119
 2.8. Practical applications of Li-S batteries . . . 119
3. Sodium-sulfur batteries . . . 119
 3.1. Mechanism . . . 120
 3.2. Cathode materials . . . 120
  3.2.1. Nonpolar carbon materials . . . 120

* Corresponding authors.
E-mail addresses: xuxu@whut.edu.cn (X. Xu), mlq518@whut.edu.cn (L. Mai).

https://doi.org/10.1016/j.jechem.2021.02.028

3.2.2. Polar host materials . . . 121
3.3. Electrolytes and Na metal anode protection . . . 121
4. Magnesium-sulfur batteries and aluminum-sulfur batteries . . . 122
4.1. Mg-S batteries . . . 122
4.1.1. Electrolytes for Mg-S batteries . . . 122
4.1.2. Cathodes for Mg-S batteries . . . 123
4.2. Al-S batteries . . . 125
4.2.1. Electrolytes for Al-S batteries . . . 125
4.2.2. Cathodes for Al-S batteries . . . 125
5. Separators for metal-sulfur batteries . . . 126
6. In situ/in operando characterization techniques for rechargeable metal-sulfur batteries . . . 127
7. Conclusions and outlook . . . 130
Declaration of Competing Interest . . . 131
Acknowledgments . . . 131
References . . . 131

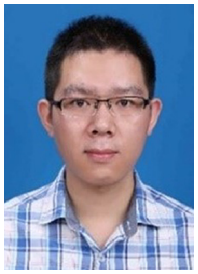

Xue Liu obtained his Bachelor's degree in 2014 from School of Materials Science and Engineering, Wuhan University of Technology. And he is now a Ph.D. candidate with Prof. Liqiang Mai at Wuhan University of Technology. He carried out research as a visiting student in Prof. Liangbing Hu's group at the University of Maryland in 2017–2019. His research interests focus on nanostructured energy storage materials.

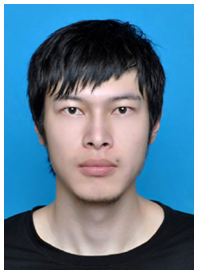

Yan Li received his M.S. degree in Department of Materials Science and Engineering from Wuhan University of Technology in 2019. He is currently working toward the Ph.D. degree. His current research involves the energy storage/conversion materials, nanoscale devices and DFT calculation.

Xu Xu received his Ph.D. degree in Materials Science from Wuhan University of Technology (WUT). He is currently working as an Associate Professor in the International School of Materials Science and Engineering, WUT. His research interests are mainly focused on energy storage materials and devices.

Liang Zhou received his B.S. (2006) and Ph.D. (2011) from Fudan University (with Prof. Dongyuan Zhao and Prof. Chengzhong Yu). He then carried out postdoctoral research in Prof. Xiong Wen (David) Lou's group at Nanyang Technological University and Prof. Chengzhong Yu's group at the University of Queensland. He is currently a Professor at Wuhan University of Technology. His research interests focus on functional nanomaterials for energy storage and conversion applications.

Liqiang Mai is a Chair Professor of Materials Science and Engineering at Wuhan University of Technology (WUT), Dean of School of Materials Science and Engineering at WUT, Fellow of the Royal Society of Chemistry. He received his Ph.D. from WUT in 2004 and carried out his postdoctoral research at Georgia Institute of Technology in 2006-2007. He worked as an advanced research scholar at Harvard University and University of California, Berkeley. His current research interests focus on new nanomaterials for electrochemical energy storage and micro/nano energy devices.

1. Introduction

In this new century, human beings are faced with unprecedented challenges related to energy and environmental issues, which are attributed to the increasing growth of global population and the increasing demand for energy [1–3]. As we know, non-renewable fossil fuels will be depleted one day. However, they are still the main source of the energy that human beings rely on to live a life with high standards. More seriously, the burning of these carbon-containing energy resources in a large scale will contribute to the emission of greenhouse gas-carbon dioxide, which will exacerbate the progressive adverse effect of global warming. This environmental phenomenon can cause serious climate changes, such as precipitation changes and acidation, temperature rise of oceans, and sea-level rise, which will threaten the sustainable developments of human beings. Through sustainable and clean energy technologies [4–10], such as photovoltaics, artificial photosynthesis, fuel cells, batteries and supercapacitors, new energy generation and higher storage capacity can be achieved to accelerate the adoption of the renewable energy. What's more, it will solve energy and environmental issues simultaneously. During this evolution, materials are both central and critical and will play

an important role in enabling these technologies for sustainable developments of our society [2]. For example, when it comes to terms with energy storage, there is a long history to look back. Wood was the oldest energy carrier in antiquity, after industrial evolution, fossil fuels became ubiquitous energy carriers. In recent decades, electrochemical energy storage devices enabled mainly by nanomaterials emerged as new energy carriers. During this evolution, materials have always been playing a key role everywhere [3].

In recent years, there is a growing demand for high-energy batteries with a long cycle life at a low cost [11,12]. As a typical prototype of electrochemical energy storage, lithium-ion batteries (LIBs) have been a mature technology for energy storage after tremendous developments for decades. However, as the needs for energy storage are diversifying from small, medium to large systems in recent years, the high cost of lithium and the limited energy density of LIBs are far from satisfying. Nonetheless, it is demanding for LIBs to meet these growing standards even though tremendous developments have been achieved in the last decades [13–16]. Elemental sulfur, with its earth-abundant advantage, is considered to be a rising cathode material for secondary batteries [17–20]. Low-cost elemental sulfur is produced as a side product of oil refining nowadays and the world production of it has been increasing. Elemental sulfur usually exists in its best-known allotrope octasulfur (S_8), which is a bright-yellow and soft solid. It has a melting point of 112.8 °C and a lowest viscosity in the temperature range of 130–160 °C [21]. When coupled with monovalent metals (Li, Na) or multivalent metals (Mg, Al), sulfur can be employed to make batteries with interesting specific properties.

As shown in Fig. 1, typical materials such as nanocarbon materials, polymers and inorganics used in composites for cathodes, different kinds of electrolytes such as organic solvents, ionic liquids and solid-state electrolytes used in different battery systems, and different metals (Li, Na, Mg, Al) as anodes, are illustrated together. The applications of these batteries are from electric vehicles (EV), grid energy storage, unmanned vehicles to consumer electronics. Fig. 2 depicts the typical prototypes of four different metal-sulfur batteries. Main electrolytes used in these four systems are described in the area of electrolytes. Fig. 3(a–d) describes the typical charge/discharge processes of Li-S, RT Na-S, Mg-S and Al-S batteries. Lithium-sulfur (Li-S) batteries, proposed since 1960s, are now regarded as one of gifted candidates for energy storage beyond lithium-ion batteries [19,22,23]. Sodium-sulfur (Na-S) batteries, known for high-temperature molten cells [24–26], are now gaining attention again for its room-temperature Na-S (RT Na-S) prototype [26–28]. Magnesium-sulfur (Mg-S) batteries, are characterized by magnesium's high theoretical volumetric capacity (near twice as much as that of lithium) and relatively low reduction potential (only 0.6 V higher than Li) [17]. Aluminum-sulfur (Al-S) batteries, with features that aluminum has the third highest earth-abundance and ultrahigh volumetric specific capacity (8040 mAh cm^{-3}), are under deep concern at present [20]. Table 1 lists some theoretical parameters of these four metals. Fig. 3(e) illustrates these specific parameters. Table 2 gives a list of some key parameters of these four kinds of metal-sulfur batteries and an illustration of them is shown in Fig. 3(f). Much effort has been put into the research on Li-S batteries and we have a clearer understanding of it in both academia and industry. RT Na-S batteries, as a low-cost choice for large-scale electrical energy storage, are gaining much attention. Mg-S batteries and Al-S batteries, which are free of dendrites issues existing in Li-S or Na-S batteries, are hampered by the developments of electrolytes.

In this review, considering the importance of ubiquitous materials existing in rechargeable metal-sulfur batteries, we will first concentrate mainly on recent advances in cathode materials for Li-S and Na-S batteries, and subordinately on mechanisms, anode protection and electrolytes. Then, based on the inspiring developments of Li-S and Na-S batteries, we will provide a summary of advances mainly on electrolyte materials in both Mg-S and Al-S batteries. A timeline of important developments of metal-sulfur batteries is shown in Scheme 1. At last, prospects of monovalent metal (Li, Na) and multivalent metal (Mg, Al) sulfur batteries will be given.

2. Lithium-sulfur batteries

Li-S batteries, which have a theoretical specific gravimetric capacity of 1675 mAh g^{-1}, are regarded as one of most prominent competitors for renewable energy storage [19,22,29–35]. However, the development of the Li-S system is encumbered by several problems, which are distributed from cathodes, separators, electrolytes

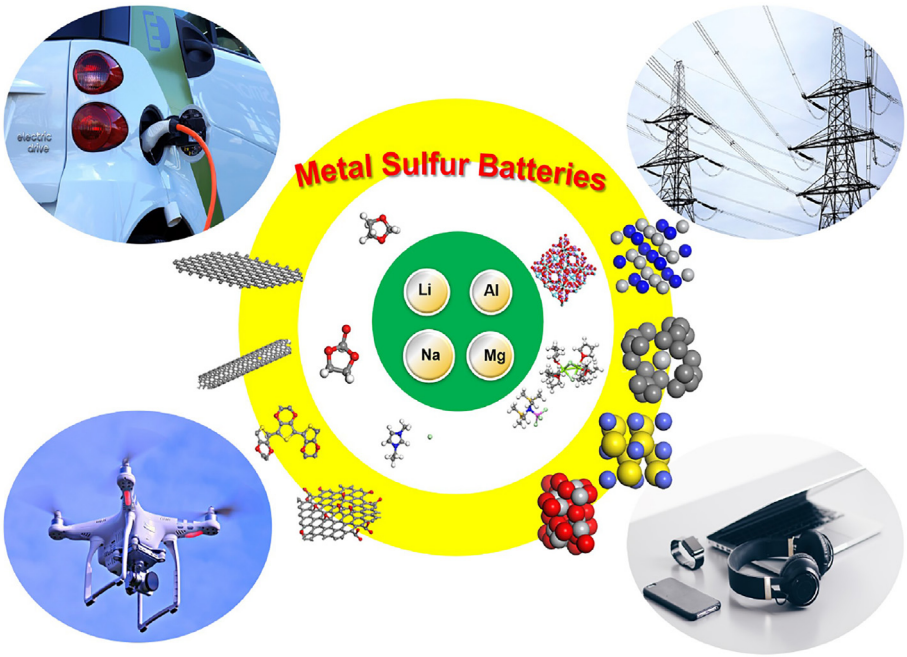

Fig 1. Metal-sulfur batteries and its applications from electric vehicles, grid energy storage, unmanned vehicles to consumer electronics, etc.

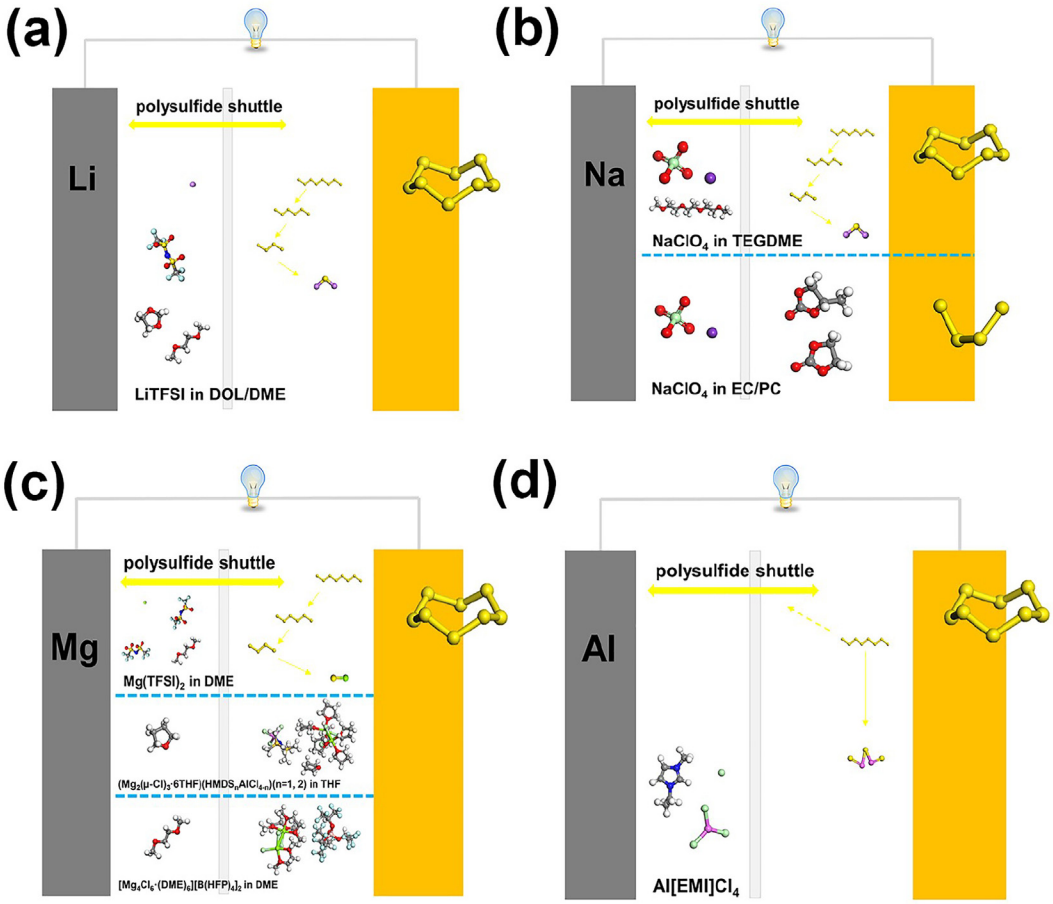

Fig 2. Different types of rechargeable metal-sulfur batteries, i.e. (a) Li-S batteries, (b) RT Na-S batteries, (c) Mg-S batteries and (d) Al-S batteries. All are composed of a metal anode, a sulfur cathode, an electrolyte and a separator. Li-S batteries use the electrolyte of LiTFSI in DOL/DME. Na-S batteries usually use the electrolyte of $NaClO_4$ in TEGDME. For small molecular sulfur cathodes, Na-S batteries use the electrolyte of $NaClO_4$ in EC/PC. The electrolyte for Mg-S batteries here is $Mg(TFSI)_2$ in DME, $Mg_2(\mu\text{-}Cl)_3\cdot 6THF)(HMDS_nAlCl_{4-n})$ (n = 1, 2) in THF and $[Mg_4Cl_6(DME)_6]$ $[B(HFP)_4]_2$ in DME. The electrolyte for Al-S batteries is the mixed $AlCl_3$ and 1-ethyl-3-methylimidazolium chloride (EMIC) ionic liquid solvent. DOL: dioxolane, DME: dimethoxyethane, TEGDME: tetraethylene glycol dimethyl ether, THF: Tetrahydrofuran, EMI: 1-ethyl-3-methylimidazolium.

to anodes. Carbonate electrolytes, which are widely used in lithium-ion batteries (LIBs), are not applicable to Li-S batteries [36,37]. Ether electrolytes have been extensively employed in Li-S systems [38–41]. Polysulfides shuttle (Fig. 2a) related to the intricate electrochemical reactions of sulfur cathode is the toughest problem, which has not been solved perfectly until now. The low conductivity of sulfur and its counterpart lithium sulfide can be made up for through the integration of diverse conductive nanostructured materials. The minor flaw, such as the structural variations of cathodes, compared with former issues, seems to have less influence on the performance and can be easily settled by creating voids in the cathode materials. The growth of lithium dendrites during cycling is a long-term problem impeding the utilization of lithium-metal-based batteries, including Li-S batteries. Herein, we focus mainly on important works and recent progress on composite cathode materials for Li-S batteries, before which the electrochemical reaction mechanism is introduced. Nanostructured carbon materials, polymers for Li-S batteries are summarized concisely while nanostructured metal oxides and sulfides and emerging nanomaterials which are widely researched for Li-S batteries are discussed in detail.

2.1. Mechanism

The intricate intermediate reactions of Li-S batteries have attracted many researchers' interest and various methods have been tried to investigate the essence of the mechanism of Li-S chemistries. Here we present a simplified reaction mechanism of Li-S batteries, as shown in Eqs. (1)–(7), which is accepted by most scientists [29–31,42–45].

Overall:

$$S_8 + 16Li^+ + 16e^- \rightarrow 8Li_2S \text{ (cathode)} \quad (1)$$

$$16Li \rightarrow 16Li^+ + 16e^- \text{(anode)} \quad (2)$$

Charge and Discharge reactions:

$$S_8 + 2e^- + 2Li^+ \rightleftarrows Li_2S_8 \quad (3)$$

$$3Li_2S_8 + 2e^- + 2Li^+ \rightleftarrows 4Li_2S_6 \quad (4)$$

$$2Li_2S_6 + 2e^- + 2Li^+ \rightleftarrows 3Li_2S_4 \quad (5)$$

$$Li_2S_4 + 2e^- + 2Li^+ \rightleftarrows 2Li_2S_2 \quad (6)$$

$$Li_2S_2 + 2e^- + 2Li^+ \rightleftarrows 2Li_2S \quad (7)$$

Generally, as shown in Fig. 3(a), there exist two discharge plateaus at 2.3 and 2.1 V in glyme-based electrolytes. The first plateau is the solid–liquid two-phase reduction of sulfur to Li_2S_8, which can be described by Eq. (3). The second plateau is the liquid–solid two-phase reduction of low-order polysulfides to solid Li_2S_2 and Li_2S. There is usually one dip before the second plateau, which is caused

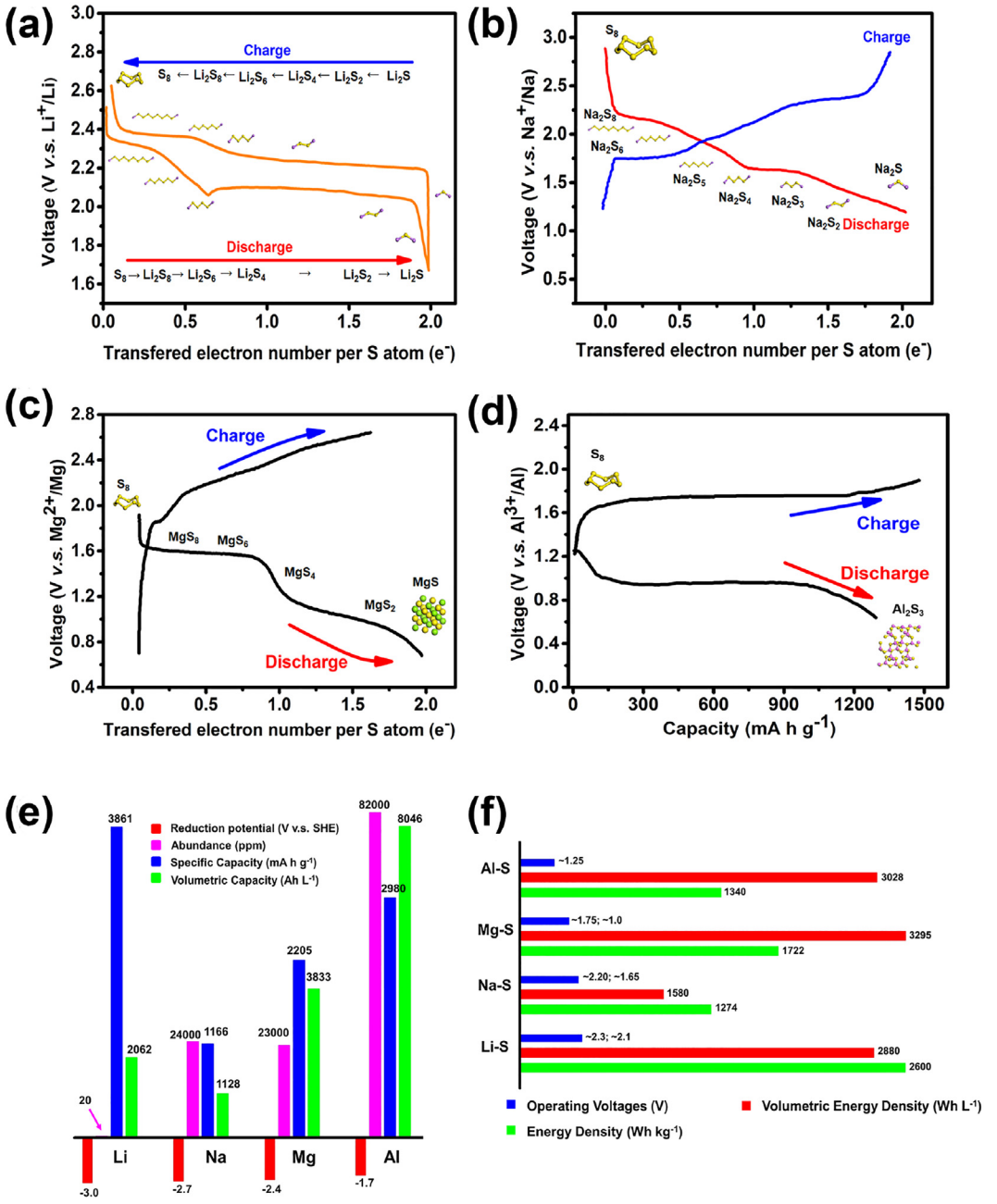

Fig 3. Typical discharge–charge voltage-capacity curves and reaction orders of (a) a Li-S battery (yellow ball: sulfur, purple ball: lithium). Reproduced with permission [30]. Copyright 2017, Royal Society of Chemistry. (b) A RT Na-S battery (yellow ball: sulfur, purple ball: sodium). Reproduced with permission [27]. Copyright 2015, Wiley-VCH. (c) A Mg-S battery (yellow ball: sulfur, green ball: magnesium). Reproduced with permission [188]. Copyright 2015, Wiley-VCH. (d) An Al-S battery (yellow ball: sulfur, purple ball: aluminum). Reproduced with permission [220]. Copyright 2017, Wiley-VCH. (e) Theoretical parameters of Li, Na, Mg and Al based on Table 1. (f) Some key parameters of metal (Li, Na, Mg, Al)-sulfur batteries based on Table 2.

Table 1
Key theoretical parameters of metal anodes for metal-sulfur batteries from literature.

Metals	Theoretical capacity [17]		Reduction potential [17] (V vs. SHE)	Abundance [267] (ppm)
	Specific capacity (mAh g^{-1})	Volumetric capacity (Ah L^{-1})		
Li	3861	2062	−3.0	20
Na	1166	1128	−2.7	24,000
Mg	2205	3833	−2.4	23,000
Al	2980	8046	−1.7	82,000

Table 2
Key theoretical parameters of metal-sulfur batteries from literature.

Batteries	Overall reactions	Energy density		Operating voltage (V)
		Wh kg^{-1}	Wh L^{-1}	
Li-S [23,29]	$2Li + S = Li_2S$	2600	2880[a]	~2.30; ~2.10
Na-S [171]	$2Na + S = Na_2S$	1274	1580[a]	~2.20; ~1.65
Mg-S [189]	$Mg + S = MgS$	1722	3295[a]	~1.75; ~1.0
Al-S [199]	$2Al + 3S = Al_2S_3$	1340	3028[a]	~1.25

a. This value is calculated based on the value of the energy density. The calculation is based on the equation below, in which Li (or Na, Mg, Al) is the anode and S is the cathode. $E_v = E_w \times \frac{\rho_c V_c + \rho_a V_a}{V_c + V_a}$ (E_v, volumetric energy density; E_w, specific energy density; ρ_c, density of cathode; ρ_a, density of anode; V_c, volume of cathode; V_a, volume of anode)

by the highest viscosity of the electrolyte as the polysulfides dissolve. During discharge, disproportionation and association reactions would happen and S_3^-, S_3^{2-}, S_5^{2-}, S_7^{2-} species could exist in the cell. However, upon charge process, the two plateaus during discharge are often overlapped, which should be ascribed to the sluggish conversion of solid Li_2S to soluble lithium polysulfides.

2.2. Carbon materials

Much effort has been paid in the research on nanostructured carbon–sulfur composite cathode materials because carbon materials possess high conductivity, robust stability and a large abundance. Carbon materials play the role of conductive frameworks for the reduction of sulfur and oxidation of lithium sulfide. The success of the pioneering combination of mesoporous carbon (CMK-3) and sulfur [22] in Li-S batteries should be ascribed to the physical confinement of lithium polysulfides and uniform distribution of sulfur in mesopores. After that, we have seen numerous works aiming at the construction of conductive nanocarbon frameworks as sulfur host materials. For different purposes, bimodal porous carbon [46], hollow carbon spheres [47], graphene [48,49], and carbon nanotubes [50–56] boomed in the research on sulfur composite cathodes for Li-S batteries. Distinctively, bimodal porous carbon developed by Nazar et al. [46] had two kinds of mesopores. 2 nm mesopores existed around 5.6 nm interconnected cylindrical mesopores, the former contained most sulfur while the latter provide free space for lithium ion transport and sulfur volume change. In order to improve the rate performance of Li-S batteries, Zhao et al. [48] introduced an unstacked graphene-sulfur composite as an ultrahigh-rate cathode for Li-S batteries (Fig. 4a). The high electrical conductive graphene enabled the sulfur cathode to deliver ~380 mAh g^{-1} at 10 C even after 1000 cycles.

Although nonpolar carbon materials above provided good electronic platform and ionic transport highways for sulfur cathodes, the interaction between carbon and sulfur species was very weak, which was proven experimentally and theoretically, and it would bring down the cycling performance because of the failure in trapping soluble lithium polysulfides. Doping can bring polar sites to the pristine graphene nanosheets. Along this thought, heteroatom doped nanostructured carbon materials, for instance, graphene oxide [57–62], were proposed to act as a polar sulfur host. Zhou et al. [60] reported a fibrous graphene-sulfur hybrid as the composite cathode material for Li-S batteries. With a sulfur loading of 63 wt%, at 0.3 A g^{-1}, it delivered an initial specific capacity of 1160 mAh g^{-1}. After the rate capability test, the capacity maintained 541 mAh g^{-1} for over 100 cycles at 0.75 A g^{-1}. The exciting result relied on the oxygen-containing functional groups on the graphene surface, which could increase the binding energy and induce larger charge transfer compared with pure graphene. Zhang and co-authors [63] reported another work on the influence of nitrogen doping. N-doped graphene was synthesized through a thermal nitridation process in the atmosphere of NH_3. With a sixty-percentage sulfur content, at 2 C, S@NG composite cathode showed its highest discharge capacity of 789 mAh g^{-1} and a capacity degradation rate as low as 0.038% per cycle across the 1000 cycles. DFT calculations [64] showed that both pyrrole-like and pyridine-like graphene had higher binding energy with Li, Li_2S, Li_2S_4, Li_2S_6, and Li_2S_8. Making full use of doping method and the advantages of nanocarbon frameworks, Tang et al. [65] compared the difference between N-doped aligned carbon nanotubes/-graphene sandwiches (N-ACNT/G) and aligned carbon nanotubes (ACNT) when employed in sulfur composite cathodes. Sulfur was infiltrated into N-ACNT/G and ACNT through the melt-diffusion method and the respective composite was named N-ACNT/G@S and ACNT@S. Fig. 4(b) depicts the illustration of the N-ACNT/G@S composite. With an around fifty-percentage sulfur loading, at 1 C, N-ACNT/G@S delivered an initial specific capacity of 1152 mAh g^{-1}, while that of ACNT@S was 865 mAh g^{-1} (25% lower). Even though N-ACNT/G held a lower specific surface area of 217 m^2 g^{-1} than that of ACNT of 259 m^2 g^{-1}, N-ACNT/G@S composite cathode still performed a specific capacity of around 880 mAh g^{-1} after 80 cycles at 1.0 C, 65% higher than ACNT@S. As to the effect of different elements on the doping of carbon, a systematic theoretical study on the interactions between doped carbon hosts and polysulfide guests was conducted by Hou and co-authors [66]. The result showed that N or O dopant significantly enhanced the interactions while B, F, S, P, Cl monodopants not. And they obtained an implicit volcano plot (similar to the volcano plot in electrocatalysis), which

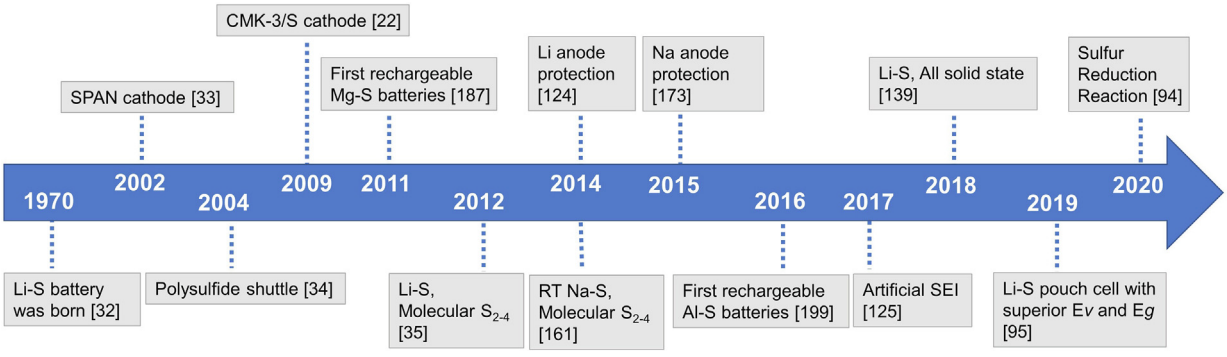

Scheme 1. A timeline of important developments of metal-sulfur batteries.

described the dependence of binding energies on electronegativity of dopants (Fig. 4c).

There is a large variety of nanostructured carbon materials including graphene, carbon nanotube and porous carbon materials and so on. The precise control of different properties of these carbon materials makes it easier to solve specific problems in Li-S batteries. Great effort has been achieved in carbon–sulfur composites and the science behind them has also been elucidated in a good way. However, the disadvantages of nanostructured carbon materials are obvious that they possess low density and it will lower the volumetric energy density, which is still an obstacle to be tackled in the future.

2.3. Polymers

Polymers cover a large variety of materials made up of macromolecules. Polymers for Li-S batteries were mainly used as sulfur hosts and binders. As sulfur hosts, conductive polymers play the role of conducting pathways and the structural change buffer. As binders, polymers increase the cohesion of active materials in sulfur cathodes, improve the adhesion to current collectors and buffer the volume changes. Here, we will discuss this part based on conductive polymers for sulfur hosts and polymers as binders in Li-S batteries.

Conductive polymers were considered to serve as an effective sulfur host in composite cathodes for Li-S batteries because of its flexibility and high conductivity. Li et al. [67] studied the effect of three typical conductive polymers in combination with sulfur on the electrochemical performance of Li-S batteries, which are poly(3,4-ethylenedioxythiophene) (PEDOT), polypyrrole (PPY) and polyaniline (PANI), respectively. Ab initio simulations showed that PEDOT had the strongest binding energy with Li_2S (1.08 eV) and Li-S· species (1.22 eV) (through O and S atoms) over PPY and PANI (through N atoms), which was corroborated by the proceeded experiment. Thermogravimetric analysis showed that elemental sulfur accounted for ~78 wt%, 74 wt% and 77 wt% in PEDOT-, PANI- and PPY- coated sulfur composites, respectively. At C/2 rate, with conductive polymer coatings of ~20 nm, PEDOT-S, PANI-S, PPY-S composite cathodes delivered the first discharge capacities of 1165, 1140, and 1201 mAh g^{-1}, respectively. As shown in Fig. 4(d), after 100 cycles, capacity retentions of 86%, 65% and 74% were obtained for PEDOT-S, PANI-S, and PPY-S, respectively. Electrochemical impedance spectroscopy (EIS) results showed that PEDOT-S had the smallest charge-transfer resistance. The strong interactions between PEDOT and sulfur species, the high conductivity of PEDOT and the perfect construction of the PEDOT-S composite at the nanoscale were three key factors to the excellent electrochemical performance of the PEDOT-S composite cathode.

Besides serving as effective coating layers in composite cathode materials, polymers also act as an important role in binders for Li-S batteries [68,69]. The most common binders used in Li-S batteries are fluoropolymers, such as poly(vinylidene fluoride) (PVDF), which has strong adhesive strength and high thermal stability and so on. However, with the utilization of PVDF, organic solvent (N-Methyl-2-pyrrolidone, NMP) is unavoidable, which is toxic and flammable. With different purposes, various alternative binders have been developed for Li-S batteries. For eco-friendliness and resource renewability, water-soluble biopolymer-based binders have found its place in improving electrochemical performances of Li-S batteries. Zhang et al. [70] reported a robust biopolymer network binder, which enabled high-areal specific capacities of Li-S batteries. It was constructed by guar gum (GG) and xanthan gum (XG). The copolymer interactions between GG and XG formed a mechanically robust network, which could support a high sulfur loading. The Li-S cell exhibited a very high areal capacity of 26.4 mAh cm^{-2} at a high sulfur loading of 19.8 mg cm^{-2}. It may inspire us to exploit the potential applications of biopolymers for binders of practical Li-S batteries. Moreover, polar polymers were found to be effective in alleviating polysulfides shuttle. Cui et al. [71] reported that poly(vinylpyrrolidone) (PVP)

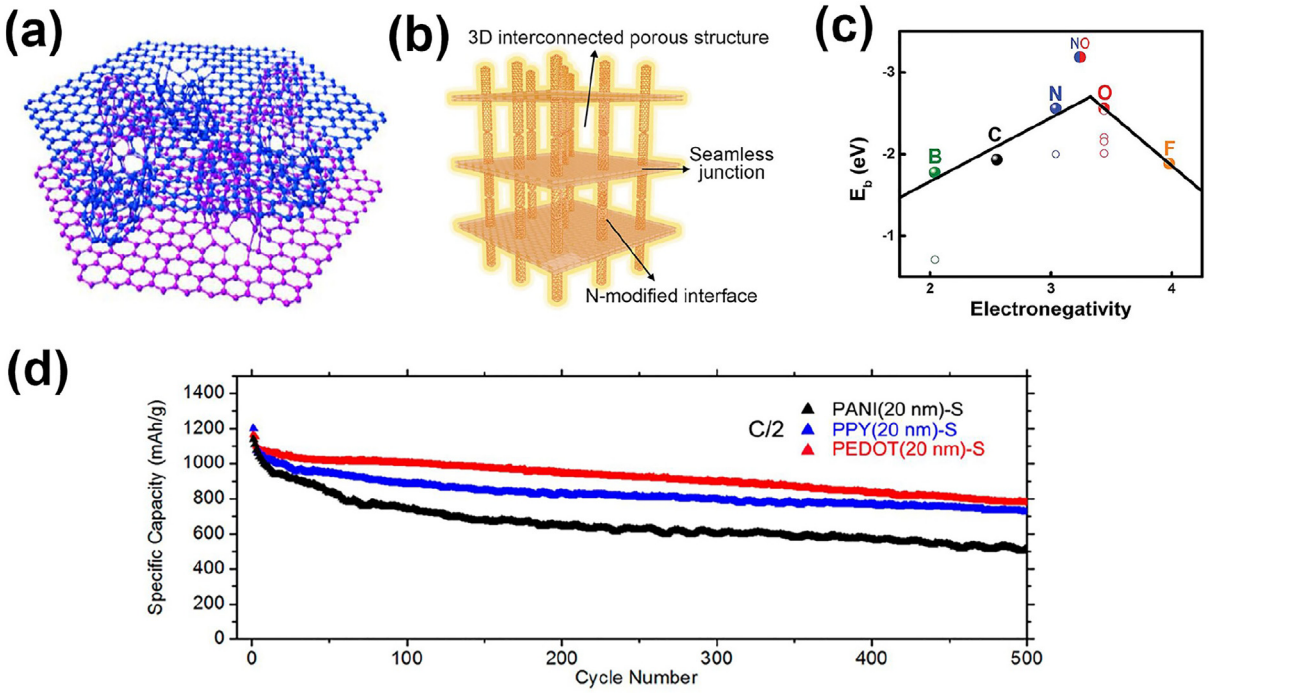

Fig 4. Carbon and polymers for Li-S batteries. (a) An illustration of the unstacked graphene for S cathodes. Reproduced with permission [48]. Copyright 2014, Springer Nature. (b) An illustration of the N-ACNT/G@S composite. Reproduced with permission [65]. Copyright 2014, Wiley-VCH. (c) A volcano plot illustrating the interaction between doped-carbon and Li_2S_4. X axis represents binding energy (E_b), y axis represents electronegativity of dopant element. Reproduced with permission [66]. Copyright 2016, Wiley-VCH. (d) Long-term discharge capacities of the PEDOT-S, PPY-S, and PANI-S cathodes. Reproduced with permission [67]. Copyright 2013, American Chemical Society.

could help stabilize Li_2S cathode through its oxygen-containing functional groups. DFT calculations showed that PVP had higher binding energy with Li_2S (1.14 eV) or Li-S· species (1.30 eV) than PVDF (0.64, 0.83 eV, respectively). PVP enabled Li_2S cathode delivered the first capacity of 760 mAh g^{-1} of Li_2S (1090 mAh g^{-1} of S) at 0.2 C and maintained 94% after 100 cycles.

In conclusion of this part, polymers have demonstrated their effectiveness in making better Li-S batteries from conductive polymers to biopolymers, cathode coating materials to innovative binders. It also exists in other parts of the batteries, such as polymer electrolytes, polymer separators and anode protective materials, which will not be discussed in detail. For future directions, taking advantage of the S-S bond in sulfur-rich polymers has been proven to be practical. It has much space to research on.

2.4. Metal oxides and sulfides

Because of the poor efficiency of carbon materials in anchoring polysulfides, much attention has been paid on nanostructured metal oxides and sulfides for Li-S batteries [72,73]. Metal oxides with specific catalytic functions such as MnO_2 can serve as efficient polysulfides oxidizers [64,74]. Usually, metal oxides exist in metal ions and O^{2-} ions with a specific crystal structure. Some oxides with oxygen vacancies such as Magnéli phase oxides have high conductivity [75]. Compared to metal oxides, sulfides have stronger sulfiphilic property to polysulfides and lower lithiation voltages vs. Li^+/Li. Metal sulfides mainly exist in metallic or half-metallic phases, which is the reason why they have high electronic conductivity. In this section, we will discuss the employment of metal oxides and sulfides in Li-S batteries.

First principle calculations predict that metal oxides and sulfides have a higher binding energy with polysulfides over graphene sheets, which confirms the effectiveness of them for Li-S batteries. Nazar research group has contributed much to this direction [31,39,74,76,77]. Pang et al. [77] harnessed conductive Magnéli phase oxide Ti_4O_7 (3.2 ± 0.1 S cm^{-1} at 298 K) with relatively high surface area (290 m^2 g^{-1}) to enhance the surface redox chemical reactions of polysulfides. A visualization experiment showed that Ti_4O_7 could more efficiently adsorb Li_2S_4 relative to graphite and VULCAN XC72 carbon. The interactions of terminal-sulfur and bridge-sulfur with Ti_4O_7 were confirmed by X-ray photon spectroscopy (XPS). With a sulfur loading of 60 wt%, at 2 C, Ti_4O_7/S composite cathode showed its first capacity of 850 mAh g^{-1} and only 0.06% per cycle decay rate over 500 cycles. Another work [75] on Ti_4O_7 for Li-S batteries gave a detailed crystal structure analysis of Ti_4O_7. It showed that Ti atoms with four and five coordination numbers accounted for 62.5% of titanium atoms of the Ti_4O_7 (1–20) surface, while 0% for the rutile TiO_2 (110) surface. A recent work reported by Wei et al. [78] on mesoporous Ti_4O_7 microspheres as sulfur composite cathode hosts corroborated the usefulness of Ti_4O_7 in improving the electrochemical performance of Li-S batteries.

As an efficient electrocatalyst, MnO_2 found its place in polysulfides mediator for Li-S batteries. Liang et al. [74] proposed that δ-MnO_2 could serve as a catalyst and oxidize polysulfides to form thiosulfate and it contributed to the conversion of long-chain polysulfides to short-chain polysulfides and lithium sulfide. A successional work [79] was on in situ formed core–shell hollow sulfur-MnO_2. It provided a scalable method to synthesize bifunctional (physical protection & chemical adsorption, catalysis) δ-MnO_2-sulfur composite. Along this thought, Lou and co-authors [80] constructed the sulfur infiltrated hollow carbon nanofiber with embedded δ-MnO_2 nanosheets composite. With a seventy-one-percentage sulfur loading and areal sulfur content of 3.5 mg cm^{-2}, at 0.5 C, it could still deliver an initial specific capacity of over 900 mAh g^{-1} and maintain 662 mAh g^{-1} after 300 cycles. By using MnO_2 nanowires as the template and oxidization initiator, the coaxial PPy-MnO_2 nanotubes were designed for sulfur composite cathodes. Hou and co-workers recently reported carbon nanoboxes filled with δ-MnO_2 to empower Li-S batteries [81]. Taking the (100) crystal surface δ-MnO_2 as anchoring support, DFT calculations [64] showed that MnO_2 could bind with S_8, Li_2S_8, Li_2S_6, and Li_2S_4 with energy of −1.60, −4.68, −3.86, and −5.15 eV, respectively (Fig. 5a). The interactions between MnO_2 and Li_2S were so strong (over −5.15 eV) that Li_2S may decompose into S = O and Li = O bonds. Besides used as composite cathode host materials, an ultrathin interlayer made up of MnO_2/graphene oxide/carbon nanotube was demonstrated to be efficient in polysulfides-trapping [82]. Moreover, recent works [81,83] showed that Mn_3O_4 was more stable than MnO_2 when employed in Li-S batteries. Depicted in Fig. 5(b), when interacting with polysulfides, in MnO_2, Mn^{4+} is reduced to Mn^{2+} and then dissolves into the electrolyte. While in Mn_3O_4, even though Mn^{4+} is reduced to Mn^{3+} and Mn^{2+} is reduced to Mn^{3+}, the structural balance attributed to the shrink of MnO_6 tetrahedra and the expansion of MnO_4 tetrahedra keeps the crystal structure of Mn_3O_4 stable. In all, the catalytic oxidation and proper binding of polysulfides by manganese oxides can indeed play an important role in achieving high-performance Li-S batteries.

Tao et al. [84] demonstrated a systematic research on nonconductive metal oxides for composite cathodes of Li-S batteries. Five kinds of nonconductive materials (MgO, Al_2O_3, CeO_2, La_2O_3 and CaO) were chosen to investigate the influence of adsorption and diffusion of lithium polysulfides on such non-conductive metal oxides. Li_2S_x adsorption capability and its diffusion properties in metal oxides were investigated and divided into three different situations (Fig. 5c). DFT calculations showed that the diffusion barriers of lithium ions on MgO (100), CeO_2 (111) and La_2O_3 (001) were smaller than on CaO (100) and Al_2O_3 (110) planes. Lithium diffusion coefficients derived from cyclic voltammetry indicated that lithium diffused fastest on La_2O_3 and MgO among all the five kinds of materials. Sulfur composite cathodes based on MgO, La_2O_3 and CeO_2 additives outperformed among all the materials. This paper highlighted the diffusion of polysulfides on the performance of Li-S batteries.

A "goldilocks" principle was proposed by Liang and co-authors [76]. They found that chemical reactivity of various metal oxides with lithium polysulfides could be plotted as function of redox potential vs. Li^+/Li (Fig. 5d). The higher the potential was, the stronger the oxidizability of metal oxides towards polysulfides. Only materials that oxidized polysulfides into thiosulfate rather than sulfate were suitable for hosts for Li-S batteries.

Compared to metal oxides, metal sulfides have sulfiphilic affinity towards polysulfides [21,85–89]. What's more, there are a large amount of metallic or half-metallic metal chalcogenides, existing in pyrite, spinel, and NiAs structures. Metallic pentlandite Co_9S_8 has a theoretical room-temperature conductivity of 290 S cm^{-1}. Pang et al. [39] reported a graphene-like Co_9S_8 cathode host for Li-S batteries, which had a surface area of 108 m^2 g^{-1} and a large pore volume of 1.07 cm^3 g^{-1}. As shown in Fig. 6(a), the (008) crystal surface of cubic Co_9S_8 is a purely Co-terminated plane. It can interact with polysulfides through $Sn^{2-} \rightarrow Co^{\delta+}$ and $Li^+ \rightarrow S^{\delta-}$ (in Co_9S_8) interactions with a binding energy of 6.93 eV with van der Waals force included. With a high sulfur loading of 4.5 mg cm^{-2}, at a rate of C/5, a reversible areal capacity of ~2.5 mAh cm^{-2} was achieved. Sulphifilic CoS_2 was incorporated into carbon–sulfur composite cathode by Yuan and co-authors [90]. They showed that CoS_2 could propel the polysulfides redox reaction. And it was confirmed by cyclic voltammetry test in a symmetrical Li_2S_6-Li_2S_6 cell, in which the electrode containing CoS_2 exhibited highest current density at an overpotential of 0.7 V. With a sulfur loading of 75 wt%, at 2 C, the sulfur electrode containing CoS_2 (15 wt%) deliv-

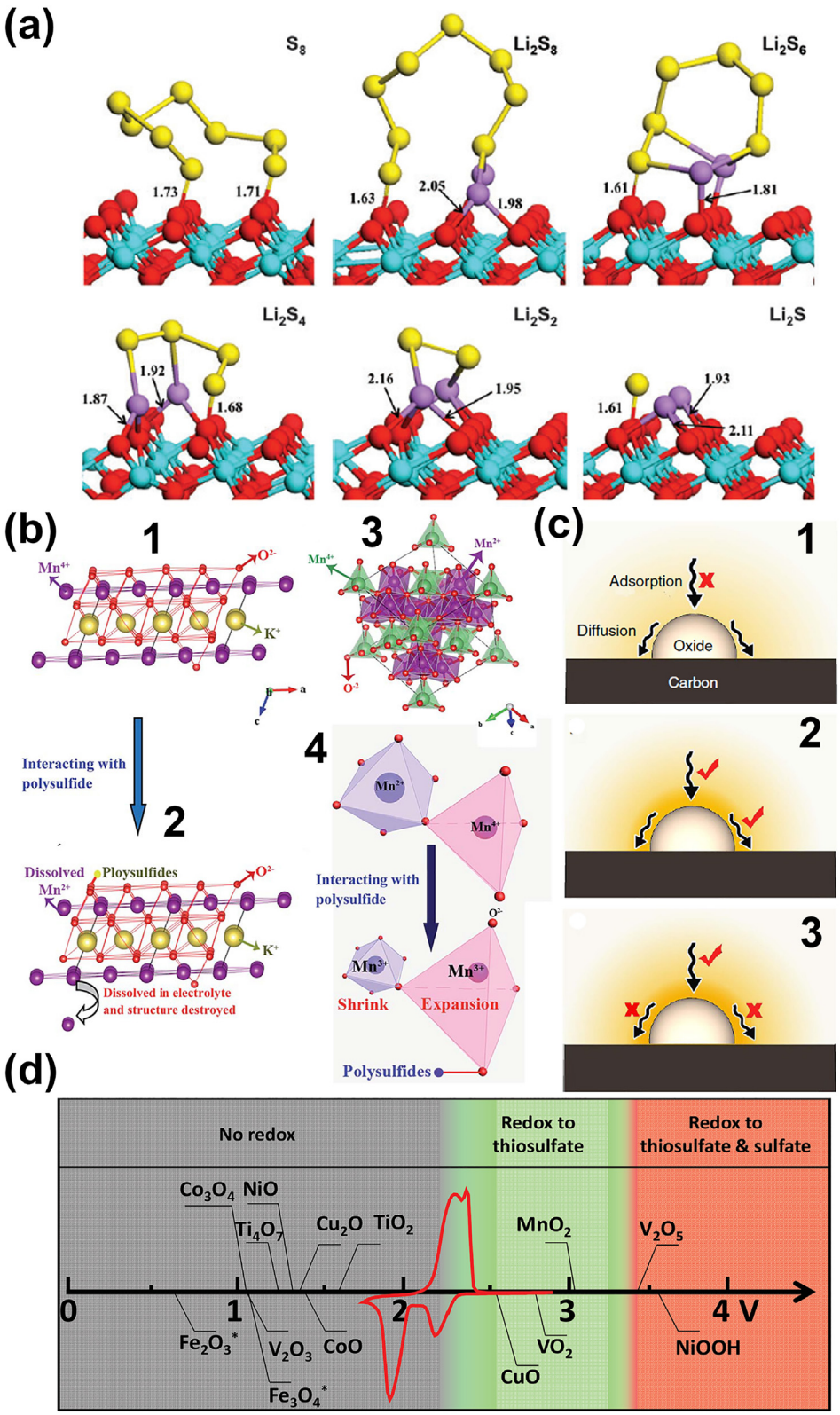

Fig 5. Metal oxides for Li-S batteries. (a) Optimized configurations of the binding between S_8, polysulfides, and Li_2S and the MnO_2. Reproduced with permission [64]. Copyright 2016, Royal Society of Chemistry. (b) An illustration describing the interactions between polysulfides and MnO_2 (1, 2), Mn_3O_4 (3, 4). Reproduced with permission [83]. Copyright 2017, Royal Society of Chemistry. (c) A schematic diagram of the Li_2S_x adsorption and diffusion on the surface of metal oxides with weak Li_2S_x adsorption capability (1), both strong Li_2S_x adsorption and good diffusion (2), strong binding but without good diffusion (3). Reproduced with permission [84]. Copyright 2016, Springer Nature. (d) Oxidability of different oxides towards lithium polysulfides as a function of redox potential versus Li^+/Li. Reproduced with permission [76]. Copyright 2016, Wiley-VCH.

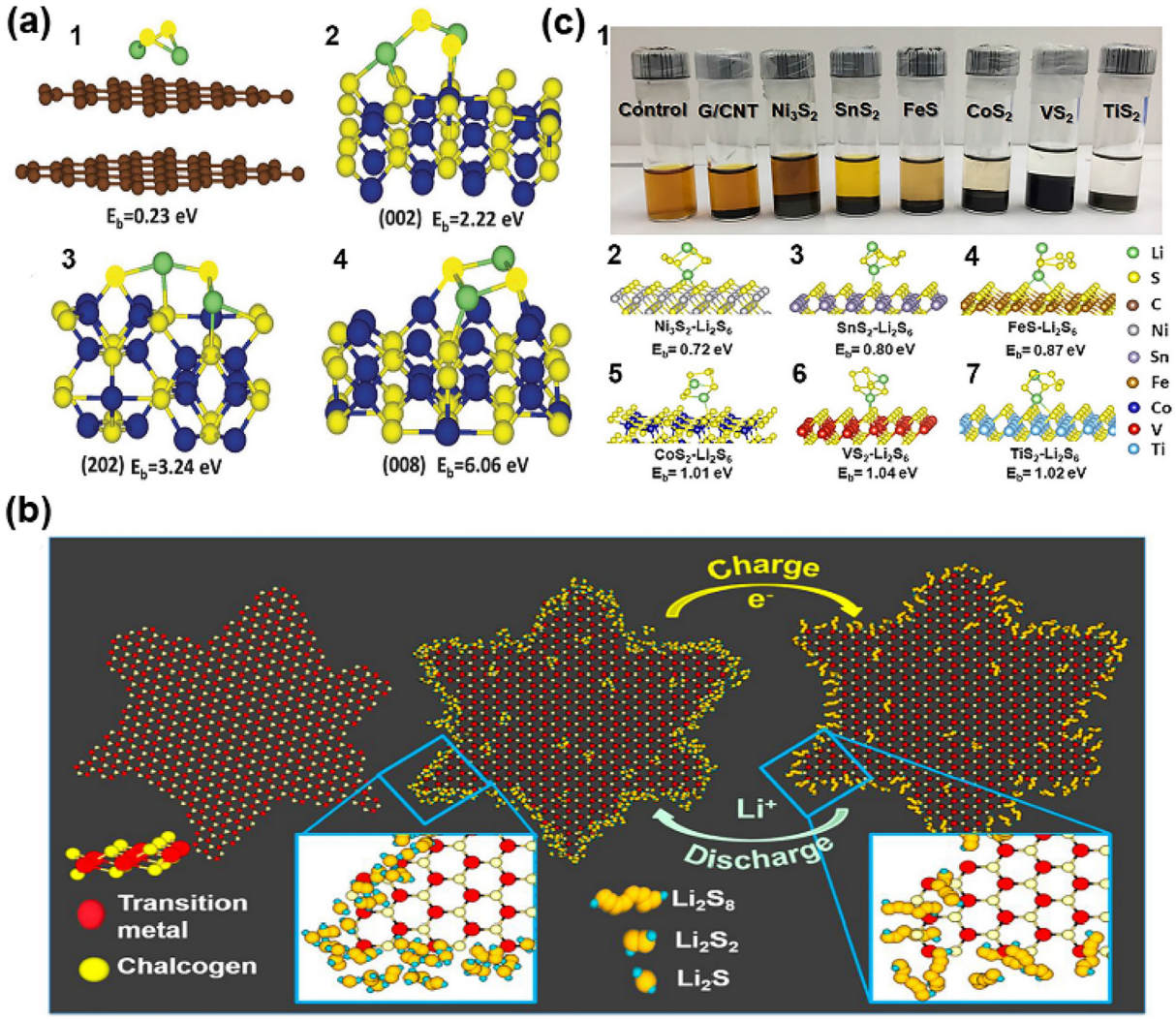

Fig 6. Metal sulfides for Li-S batteries. (a) Binding energies between Li_2S_2 and graphene (1), Co_9S_8 (2, 3, 4). Reproduced with permission [39]. Copyright 2016, Royal Society of Chemistry. (b) An illustration of preferential confined deposition of lithium polysulfides at catalytic sites of CVD-grown transition metal dichalcogenides during discharge–charge processes in a catholyte solution. Reproduced with permission [86]. Copyright 2016, American Chemical Society. (c) Adsorption experiments of Li_2S_6 with carbon and metal sulfides (1) and corresponding simulation of Li_2S_6 adsorbed on the surface of metal sulfides (2, 3, 4, 5, 6, 7). Reproduced with permission [85]. Copyright 2016, National Academy of Sciences.

ered a decay rate of only 0.034% per cycle over 2000 cycles. Also, the first specific capacity of 1368 mAh g^{-1} at 0.5 C was achieved.

In order to understand lithium polysulfides catalysis, Babu et al. [86] took advantage of WS_2 flakes to investigate the potential of transition metal chalcogenides in the acceleration of polysulfides redox reaction. Fig. 6(b) illustrates the preferential catalytic deposition sites of lithium sulfides on CVD-deposited metal dichalcogenide nanosheets. With the purpose of exploring the catalytic active sites of WS_2, they constructed a three-electrode electrochemical cell, in which CVD-synthesized WS_2 flakes served as the working electrode and metallic lithium as the counter/reference electrode. After immersed in a lithium polysulfides catholyte, galvanostatic discharge process was conducted. The morphology characterization showed that polysulfides tended to nucleate at the edge sites of WS_2 flakes in a dendrite-like arrangement, which is in good agreement with reports on materials for hydrogen evolution reaction (HER) [91] and lithium sulfide (Li_2S) [92] electrodeposition. Bulk WS_2 nanosheets were synthesized by a shear exfoliation method. Through an electrochemical test, WS_2 exhibited a higher reduction onset potential of 2.24 V (high plateau) and 1.78 V (low plateau) and a higher exchange current density of 11.8 μA cm^{-2} compared to carbon. For long cycling test of Li-S batteries, the cathode was consisted of WS_2 flakes and catholyte with Li_2S_8 was dissolved in TEGDME. At 0.5 C rate, stable discharge capacity of 596 mAh g^{-1} was achieved for 360 cycles. When serving as bulk sulfur composite cathode host materials, coupled with carbon nanofibers, WS_2 exhibited strong capability of polysulfides adsorption, which was confirmed by a visualizing discharge experiment of Li-S batteries [93]. DFT calculations showed that the interactions between WS_2 and polysulfides were in the mediate range, for example, it was 1.45 eV in the case of Li_2S. Because of the merits, a long-lasting cycling at 2 C with a stable ~600 mAh g^{-1} over 1500 cycles was achieved.

Besides the catalytic effect towards the conversion of polysulfides to sulfides, metal sulfides were found to catalyze the oxidation of Li_2S in Li-S batteries [85]. Six kinds of metal sulfides were chosen, including metallic Ni_3S_2, FeS, CoS_2, semimetallic VS_2, TiS_2, and semiconductive SnS_2, which were based on their electronic band structures. The barrier for Li_2S decomposition on different sulfides or graphene was also evaluated through the climbing-image nudged elastic band (CI-NEB) method. The Li_2S decomposition barriers for VS_2, CoS_2, TiS_2, FeS, SnS_2, Ni_3S_2, and graphene were

0.31, 0.56, 0.30, 0.63, 0.32, 1.03 and 1.81 eV, respectively. And this was in accordance with the charging overpotential of Li_2S on different metal sulfides. VS_2, CoS_2, TiS_2, FeS, SnS_2, Ni_3S_2 based Li_2S composite cathodes showed charging potential barriers of 2.91, 3.01, 2.88, 3.25, 3.53, and 3.47 V, respectively. The energy barrier for Li_2S electrochemical oxidation was related to not only the conductivity of anchoring materials but also the theoretical decomposition barriers. VS_2, TiS_2 and CoS_2 displayed the lowest energy barriers. When mixed with Li_2S_6 solution, as shown in Fig. 6(c), TiS_2, VS_2, and CoS_2 show the strongest ability in the adsorption of polysulfides, which is in accordance with the theoretical binding energy between metal sulfides and Li_2S_6. In order to investigate the long-cycle electrochemical performance, sulfur composite cathodes mixed with graphene/CNT material based on different metal sulfides were fabricated. Composite cathodes with VS_2 anchoring material outperformed others, whose lithium ion diffusion coefficient was the highest too. It delivered the first discharge capacity of 830 mAh g^{-1} and retained 701 mAh g^{-1} after 300 cycles at 0.5 C. This work elucidated that several key factors should be taken into consideration, such as inherent conductivity, interactions with lithium polysulfides, lithium ion transport, controlling of Li_2S precipitation, catalytic capability and so on.

Nanostructured metal oxides and sulfides used in sulfur composite cathodes have been proven to serve as polar host materials in Li-S batteries. Coupled with versatile conductive and high-surface-area nanostructured carbon materials, property optimization of them and improved electrochemical performances of batteries have been achieved. They can not only adsorb polysulfides efficiently but also catalyze the mutual conversion between soluble polysulfides and solid sulfides. Moreover, some metal oxides with high lithium ion diffusion capability can also promote batteries' performances. For future developments, nanostructured metal oxides and sulfides should participate more in high-sulfur-loading composite cathodes based on present fascinating results.

Tremendous efforts have been put into the utilization of nanostructured metal oxides and sulfides as polysulfides mediators for Li-S batteries. The electronic conductivity of the mediator is a key factor. The binding energy between the mediator and lithium polysulfides should be suitable because too strong binding energy may oxidize polysulfides to inactive sulfate while too weak binding energy can't adsorb polysulfides. Even though the sulfur redox catalysis was put forward, more systematic researches on the electrocatalytic sulfur reduction reaction based on metal oxides and sulfides like on doped carbon [94] are anticipated. Since metal oxides/sulfides-sulfur composites have a high tap density (usually >1 g cm^{-3}), Li-S batteries enabled by them will have higher volumetric energy density. From this perspective, the practical use of metal oxides and sulfides in Li-S batteries is promising. What's more, the nanostructured sulfides such as Mo_6S_8 [95] can improve the rheological properties of the slurry, which is very important in the scale-up of cathode foils. The consistent performances of coin cells and pouch cells in two important research on ZnS-containing [96] and Mo_6S_8-containing [95] hosts can validate it. This advantage makes the practical use of nanostructured sulfides for Li-S batteries more promising.

2.5. Emerging nanomaterials

Advanced nanomaterials are of great significance because it can provide driving force for the conversion and storage of renewable energy [97–99]. Last decade has seen the role of nanomaterials in providing sizeable increments in electrochemical performances of LIBs. Compared to micro ones, they can offer additional lithium storage sites, shorter ion conduction pathways, and quicker electron conduction capability and so on. Beyond lithium ion batteries, emerging nanomaterials especially two-dimensional nanomaterials have also been demonstrated to play a crucial role in Li-S batteries. Metal carbides, nitrides and phosphides are characterized by their intrinsic high conductivity. Metal organic frameworks are characterized by their proper Lewis interactions with polysulfides. In this section, we will mainly discuss their applications in Li-S batteries.

Gogotsi and co-workers pioneered the synthesis of two-dimensional metal carbides and named them MXenes [100]. Liang

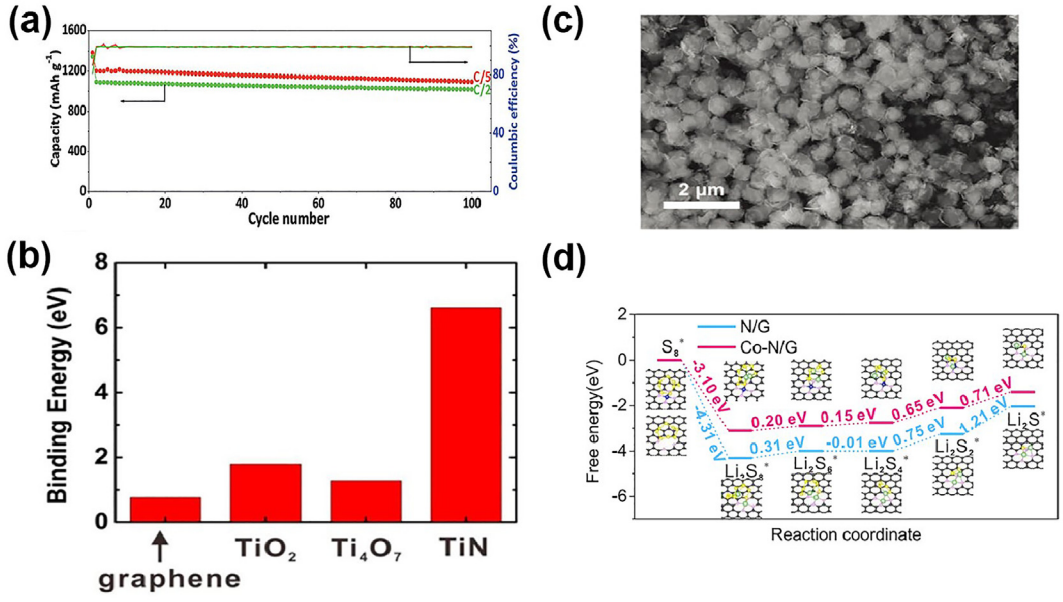

Fig 7. Emerging nanomaterials for Li-S batteries. (a) Cycling performance of 70S/d-Ti_2C tested at C/5 and C/2. Reproduced with permission [101]. Copyright 2015, Wiley-VCH. (b) Binding energies of graphene, TiO_2, Ti_4O_7 and TiN with polysulfides. Reproduced with permission [104]. Copyright 2016, Wiley-VCH. (c) SEM image of the single atom Zn-Mxene-sulfur spheres composite. Reproduced with permission [119]. Copyright 2020, Wiley-VCH. (d) Gibbs free energy diagram of different reaction coordinates. Reproduced with permission [120]. Copyright 2019, American Chemical Society.

et al. [101] first reported the use of conductive MXene nanosheets as the sulfur host material for the composite cathode of Li-S batteries. After melt with sulfur, d-Ti_2C had a different surface environment where hydroxyl groups were replaced by sulfur/sulfide species. With a sulfur loading of 70 wt%, at C/2, the S/d-Ti_2C composite cathode delivered an initial capacity of 1090 mAh g^{-1} and still maintained 723 mAh g^{-1} after 650 cycles (Fig. 7a). The stable electrochemical performance was attributed to two main factors. The first was the high conductivity of MXene phase, pure or with hydroxyl functionalization. The second was Lewis acid-base interaction between surface Ti atoms with unoccupied orbitals and sulfur species. The function of TiC in enhancing electrochemical kinetics of Li-S batteries was proven by Peng and co-authors [102]. This polar conductor had several advantages: (1) Strong binding with polysulfides; (2) more nucleation sites; (3) fast surface reaction. TiC was combined with mesoporous graphene (named TiC@G) when employed. Nucleation experiments showed that TiC@G delivered the highest capacity of 195 mAh g^{-1} in the process of Li_2S nucleation compared with TiO_2 on the carbon paper.

On the road to looking for polar conductive materials, mesoporous TiN was reported by Goodenough and co-workers [103]. It had a conductivity even higher than titanium metal and carbon while holding an excellent chemical stability because of a protective oxidation layer on the surface. Mesoporous TiN was made through a solid–solid phase separation method. With a sulfur loading of 58.8 wt%, at 0.5 C, TiN-S composite delivered a first discharge capacity of 988 mAh g^{-1} and obtained a 65.2% capacity retention after 500 cycles, which was superior to TiO_2-S and Vulcan carbon-S composites. N-S surface bonding played a vital role in the polysulfides reserving. DFT calculations [104] showed that the binding energy between TiN and S_8 was 6.6 eV, greater than Ti_4O_7 (Fig. 7b). And subsequent experiments (especially XPS) confirmed that sulfur could form a passivation layer on the surface of TiN, resulting in S-TiN. Theoretical calculations showed that this kind of material was similar to TiS_2 when interacting with sulfur species. As an analogue to TiN, composited with graphene, vanadium nitride (VN) [105] was reported recently to serve as a conductive composite cathode host with strong capability in polysulfides anchoring for lithium polysulfides batteries. Our group recently reported TiN nanowires grown in 3D N-doped graphene as the composite cathode for high-loading Li-S batteries [106]. The unique combination of three-dimensional N-graphene and polar TiN nanowires was of significance to its excellent performance in Li-S batteries with 9.6 mg cm^{-2} sulfur loading. This is a promising way to explore polar conductive materials for Li-S batteries with high sulfur loading. Moreover, heterostructures [107,108] based on metal nitrides are also attracting more and more attention. Yu research group [108] reported the dual-functional TiN-VN heterostructure as hosts for both sulfur cathode and lithium anode. TiN-VN heterostructured nanocrytsals were embedded in free-standing flexible carbon nanofibers. When employed in the full Li-S battery, even with a sulfur loading of 5.6 mg cm^{-2}, it showed over 4.5 mAh cm^{-2} at 0.1 C for more than 100 cycles. The synergy of the high adsorption ability toward lithium polysulfides of VN and low energy barrier of lithium diffusion in TiN endowed the TiN-VN heterostructure with the benefit in boosting the electrochemical performance in Li-S batteries.

Metal organic frameworks (MOFs) are composed of a metal ion or ion cluster and an organic linker. They are characterized by high surface area and tunable porosity. Due to its advantageous properties, it acted as versatile roles such as the cathode host materials [109,110], separator coatings [111] in Li-S batteries. Making use of the Lewis acid-base interactions, Xiao and co-workers [112] demonstrated a Ni-MOF based sulfur composite cathode for Li-S batteries. Compared with Co-MOF, Ni-MOF possessed a lower conductivity while higher binding energy with polysulfides. With a sulfur loading of no more than 60 wt%, Ni-MOF delivered less than 700 mAh g^{-1} during all the cycle. But this case was still better than Co-MOF. It was attributed to the low conductivity of MOF. In another work [113], three distinct MOFs, MIL-53 (Al), NH_2-MIL-53 (Al) and HKUST-1 were tried in sulfur composite cathodes. However, the sulfur loading (30 wt%) was too low to be compared with other works. Recently, Deng et al. reported a systematic work [110] on MOFs with ultrahigh electronic conductivity for Li-S batteries. They investigated three significant factors such as conductivity, porosity and polarity of cathode materials in affecting Li-S batteries' cycling performances. The sulfur composite cathode material comprising PCN-224's cross-linked pore and tunnels and ppy's coating outperformed other composites such as sulfur-carbon, sulfur-ppy, and sulfur-MOFs. Even at the rate of 5 C after 400 cycles, the ppy-S-PCN-224 composite showed a discharge capacity of 780 mAh g^{-1}, which was a 74% retention compared to the initial specific capacity. Besides, they found the pore geometries were also very powerful in ion diffusion, which influenced the rate capability of Li-S batteries.

As the compound of phosphorus, metal phosphides, which are characterized by metallic conductivity even superconductivity, are investigated much as electrocatalysts for oxygen reduction reactions. Because its beneficial properties in contributing to electrochemical reactions in Li-S batteries, metal phosphides showed much promise in Li-S batteries [114–118]. Wang et al. [115] found the surface oxidation layer of CoP played a crucial role in regulating its interaction with lithium polysulfides through Co-S and Li-O-P bindings. Zhu et al. [117] engineered CoP nanoparticles anchored in MOF-derived nitrogen-doped carbon arrays as a sulfur cathode host. The pouch cell enabled by it showed an initial capacity of 1100 mAh g^{-1} and decreased to 800 mAh g^{-1} after 50 cycles at 0.1 C.

Recently, single atom catalyst based composite materials were developed as host materials for Li-S batteries. For example, single atom Zn-MXene (SA-Zn-MXene) layers were synthesized by etching Al in molten $ZnCl_2$ [119]. The sulfur composite was fabricated by mixing SA-Zn-Mxene and sulfur in aqueous solution to form S@SA-Zn-MXene spheres (Fig. 7c). In order to optimize the sulfur cathode, 1,3-diisopropenylbenzene (DIB) treatment was used to improve the integrity. At a sulfur loading of 5.3 mg cm^{-2}, the cell delivered a high areal capacity of 5.3 mAh cm^{-2}. Single atom Co-N-graphene (Co-N/G) was synthesized successfully by Du et al. [120] to serve as a sulfur host material with a mass ratio of 90 wt% sulfur in Li-S batteries. The cell showed 1210 mAh g^{-1} at the first cycle and a decay rate of 0.029% per cycle over 100 cycles. Fig. 7(d) displays the optimized structures of the reaction intermediates and the corresponding Gibbs free energy profiles. Specifically, Co-N/G was effective in reducing the Gibbs free energy of the rate-limiting step (Li_2S_2 to Li_2S) in the discharge process compared to N/G, which meant the reduction of sulfur was more favorable on Co-N/G.

From nonpolar nanostructured carbon materials to emerging polar nanomaterials, a lot of materials have been applied into Li-S batteries. Table 3 summarizes the specific electrochemical performance of important researches mainly on host materials for sulfur composite cathodes of Li-S batteries. A detailed summary on metal oxides and sulfides for Li-S batteries was conducted in a former review [72], which is not listed again herein. There are several key parameters influencing the electrochemical performance of them. The ability to adsorbing polysulfides of host materials gradually becomes the most significant factor in determining the cycling performance of Li-S batteries. As electrode materials for batteries, higher conductivity is always welcome. Catalytic capability in contributing to the reciprocal conversion between soluble polysulfides and solid sulfides is attracting more and more attention because of its high theoretical specific capacity (more than

Table 3
Typical progress in host materials for sulfur cathodes of lithium-sulfur (Li-S) batteries.

Host materials	Some properties (Morphology; surface area with unit, $m^2 g^{-1}$; pore volume with unit, $cm^3 g^{-1}$; conductivity with unit, S cm^{-1} [some appear only when applicable])	Sulfur loading (mg cm^{-2}) & (sulfur content in cathode)	E/S ratio (μL mg^{-1})	Voltage window (V vs. Li^+/Li)	Electrochemical performance (initial capacity (mAh g^{-1}) and cycles) & decay rate claimed (per cycle)	Ref. & year
Nanostructured carbon materials						
CMK-3	Mesoporous structure; 0.2 S cm^{-1}	N/A & (59 wt%)	N/A	1.5–3.0	~1000 (80% after 20 cycles) at 0.1 C & N/A	[22] 2009
Bimodal porous carbon	Microporous and mesoporous carbon; 2300 $m^2 g^{-1}$	0.3–0.4 & (49 wt%)	N/A	1.5–3.0	718 (63% after 100 cycles) at 1 C & N/A	[46] 2011
Hollow carbon spheres	SnO_2 hard-templated synthesized double-shelled carbon; 748 $m^2 g^{-1}$; 1.685 $cm^3 g^{-1}$	N/A & (49 wt%)	N/A	1.5–3.0	1020 (68% after 100 cycles) at 0.1 C & N/A	[47] 2012
Unstacked graphene	MgAl LDH hard-templated synthesized unstacked graphene nanosheets; 438 S cm^{-1}; 1628 $m^2 g^{-1}$; 2 $cm^3 g^{-1}$	0.46–0.63 & (58 wt%)	N/A	1.7–2.8	1034 (80.5% after 200 cycles) at 5 C & N/A	[48] 2014
Carbon Nanotubes	Hierarchical Vine-Tree-Like Carbon Nanotube Architectures; 649 $m^2 g^{-1}$; 1.55 $cm^3 g^{-1}$	0.54–0.81 & (54 wt%)	12–18	1.7–2.8	844 (80.5% after 100 cycles) at 1 C & 0.08%	[50] 2014
Doped carbon materials						
Graphene oxide	Carbon nanosheets with several graphene layers	N/A & (46 wt%)	N/A	1.0–3.0	1000 (95.4% after 50 cycles) at 0.1 C & N/A	[57] 2011
N-doped graphene	Highly N-doped carbon (N: 20.5%); 606 $m^2 g^{-1}$; 0.53 $cm^3 g^{-1}$	N/A & (56 wt%)	N/A	1.6–2.8	1035 (43% after 500 cycles) at 0.5 C & 0.1%	[63] 2015
N-doped	CNT/graphene	N-doped aligned carbon nanotubes/graphene sandwiches; 217 $m^2 g^{-1}$; 0.77 $cm^3 g^{-1}$	1.0 & (52.6 wt%)	N/A	1.6–3.0	1152 (76% after 80
cycles) at 1 C & N/A	[65] 2014					
Polymers						
PEDOT	20 nm PEDOT (poly[3,4–ethylenedioxythiophene]) shell	~1.5 & (~78 wt%)	N/A	1.5–3.0	1165 (86% after 100 cycles) at 0.5 C & 0.066%	[67] 2013
PPY	20 nm PPY (polypyrrole) shell	~1.5 & (74 wt%)	N/A	1.5–3.0	1140 (74% after 100 cycles) at 0.5 C & 0.08%	[67] 2013
PANI	20 nm PANI (polyaniline) shell	~1.5 & (77 wt%)	N/A	1.5–3.0	1201 (65% after 100 cycles) at 0.5 C & 0.11%	[67] 2013
Metal oxides and sulfides						
MgO	Nanoparticles anchored on porous carbon nanoflakes	0.7–1.2 & (63 wt%–70 wt %)	N/A	1.8–2.6	~1110 (~83% after 300 cycles) at 0.5 C & 0.034%	[84] 2016
Al_2O_3	Nanoparticles anchored on porous carbon nanoflakes	0.7–1.2 & (63 wt%–70 wt %)	N/A	1.8–2.6	~1120 (~45% after 300 cycles) at 0.5 C & 0.171%	[84] 2016
CeO_2	Nanoparticles anchored on porous carbon nanoflakes	0.7–1.2 & (63 wt%–70 wt %)	N/A	1.8–2.6	~1190 (~73% after 300 cycles) at 0.5 C & 0.066%	[84] 2016
La_2O_3	Nanoparticles anchored on porous carbon nanoflakes	0.7–1.2 & (63 wt%–70 wt %)	N/A	1.8–2.6	~1170 (~76% after 300 cycles) at 0.5 C & 0.047%	[84] 2016
CaO	Nanoparticles anchored on porous carbon nanoflakes	0.7–1.2 & (63 wt%–70 wt %)	N/A	1.8–2.6	~1180 (~49% after 300 cycles) at 0.5 C & 0.136%	[84] 2016
γ-MnO_2	Core-shell structure (MnO_2-sulfur composites)	2 & (42.7 wt%)	N/A	1.7–2.8	936 (~86% after 300 cycles) at 0.5 C & 0.047%	[79] 2017
δ-MnO_2	Nanoboxes on the carbon matrix; 257 $m^2 g^{-1}$	0.7–1 & (~51 wt%)	N/A	1.7–2.8	1042 (~43% after 60 cycles) at 1 A g^{-1} & N/A	[81] 2017
VS_2	Commercial particles mixed with graphene/carbon nanotube hybrid	0.9–1.3 & (56 wt%)	N/A	1.5–2.8	830 (84.5% after 300 cycles) at 0.5 C & 0.052%	[85] 2017
CoS_2	Commercial particles mixed with graphene/carbon nanotube hybrid	0.9–1.3 & (56 wt%)	N/A	1.5–2.8	~690 (85.3% after 300 cycles) at 0.5 C & 0.049%	[85] 2017
TiS_2	Commercial particles mixed with graphene/carbon nanotube hybrid	0.9–1.3 & (56 wt%)	N/A	1.5–2.8	~710 (78.2% after 300 cycles) at 0.5 C & 0.073%	[85] 017
FeS	Commercial particles mixed with graphene/carbon nanotube hybrid	0.9–1.3 & (56 wt%)	N/A	1.5–2.8	~720 (~66% after 300 cycles) at 0.5 C & 0.175%	[85] 2017
SnS_2	Commercial particles mixed with graphene/carbon nanotube hybrid	0.9–1.3 & (56 wt%)	N/A	1.5–2.8	~610 (~59% after 300 cycles) at 0.5 C & 0.229%	[85] 2017
Ni_3S_2	Commercial particles mixed with graphene/carbon nanotube hybrid	0.9–1.3 & (56 wt%)	N/A	1.5–2.8	~540 (~59% after 300 cycles) at 0.5 C & 0.236%	[85] 2017
WS_2	Nanosheets grown on Carbon nanofiber	1.0–1.2 & (11 wt%)	N/A	1.7–2.7	954 (~47% after 500 cycles) at 1.0 C & N/A	[93] 2017
Co_9S_8	Nanocrystals inlaid hollow carbon nanopolyhedra	1.5–3.0 & (62 wt%)	5–10	1.7–2.8	950 (~59% after 1000 cycles) at 2.0 C & 0.041%	[87] 2017
	Honeycomb-like spherical tubules	N/A & (53 wt%)	N/A	1.7–2.8	893 (~85% after 600 cycles) at 1.0 C & 0.026%	[89] 2018
Emerging nanomaterials						

Table 3 (*continued*)

Host materials	Some properties (Morphology; surface area with unit, $m^2 g^{-1}$; pore volume with unit, $cm^3 g^{-1}$; conductivity with unit, S cm^{-1} [some appear only when applicable])	Sulfur loading (mg cm^{-2}) & (sulfur content in cathode)	E/S ratio (μL mg^{-1})	Voltage window (V vs. Li^+/Li)	Electrochemical performance (initial capacity (mAh g^{-1}) and cycles) & decay rate claimed (per cycle)	Ref. & year
d-Ti_2C	Two-dimensional nanosheets; 67.9 $m^2 g^{-1}$; 1.07 $cm^3 g^{-1}$	~1 & (56 wt%)	50	1.8–3.0	~958 (~75% after 650 cycles) at 0.5 C & 0.05%	[101] 2015
TiC	Nanoparticles on graphene; 1611 $m^2 g^{-1}$; above 2 $cm^3 g^{-1}$	3.5 & (55 wt%)	N/A	1.7–2.8	1032 (~65% after 100 cycles) at 0.2 C & N/A	[102] 2016
TiN	Mesoporous particles; 46 S cm^{-1}; ~70 $m^2 g^{-1}$; 0.32 $cm^3 g^{-1}$	~0.5 & (50 wt%)	N/A	1.6–2.8	988 (65.2% after 500 cycles) at 0.5 C & N/A	[103] 2016
TiN	Nanowires composited with 3D nitrogen-doped graphene	4.8 mg cm^{-2}; Li_2S_6 catholyte with 10 μL mg^{-1} sulfur	10	1.6–2.8	1510 (~84% after 100 cycles) at 0.5 C& N/A	[106] 2018
VN	Nanoribbon in the graphene matrix	3 mg cm^{-2}; 1/3 M Li_2S_6 catholyte	31	1.7–2.8	1131 (81% after 200 cycles) at 1.0 C & N/A	[105] 2017
Ni-MOF	Framework nanostructure; 5243 $m^2 g^{-1}$; 2.15 $m^2 g^{-1}$;	N/A & (48 wt%)	N/A	1.5–3.0	617 (~78% after 200 cycles) at 0.2 C & N/A	[112] 2014
Ppy-MOF	Conductive framework nanostructure	0.8–1.4 & (38 wt%)	40–71	1.8–2.7	1054 (74% after 400 cycles) at 5.0 C & 0.03%	[110] 2018
Phosphorene	Few-layer nanosheets; ~450 S cm^{-1}; ~70 $m^2 g^{-1}$; 0.32 $cm^3 g^{-1}$	5 mg cm^{-2}; 1M Li_2S_6 catholyte	3	1.5–3.0	~985 (67% after 500 cycles) at 1.0 C & 0.053%	[218] 2017
CoP	Nanoparticles grown on carbon nanotubes	7 & (N/A)	30	1.5–3.0	~866 (after 200 cycles) at 2.0 C & ~0.018%	[115] 2018
	Nanocrystals embedded in carbon cloth	1.81 & (60.74 wt%)	30	1.7–2.8	923 (~90% after 600 cycles) at 2.0 C & 0.016%	[117] 2019
FeP	Uniform nanotubes arrays deposited on carbon cloth	2.5 & (N/A)	50	1.7–2.8	1600 (~69% after 50 cycles) at 0.1 C & N/A	[116] 2019
MoN-VN	Two dimensional heterostructures	3.0 (58.5 wt%)	15	1.7–2.8	766 (72 wt% after 500 cycles) at 1.0 C & 0.068% at 2.0 C	[107] 2018
TiN-VN	Hetreostructured nanocrystals embedded in flexible carbon nanofibers	1.7 & 68 wt%	15	1.7–2.8	1388 (~80% after 100 cycles) at 0.2 C & 0.051% at 2.0 C	[108] 2019

half of the overall). It is worth noting that the real catalytic phase of host materials needs to be distinguished [115,121,122]. For example, when Ni_3FeN nanoparticles were employed in Li-S batteries, partial Fe was etched by polysulfides and $Ni_3Fe_{1-\delta}N$ was formed [121]. It was $Ni_3Fe_{1-\delta}N$ which had a higher catalytic performance. Similarly, Co_4N could be converted to CoS_x during cycling and the real catalytic phase was the mixture of pristine and new formed CoS_x [122]. Innovative works need to be done if we want to get more insights into this direction.

2.6. Li metal anode protection

Although successful endeavors have been made in host materials for sulfur composite cathodes, the counterpart, lithium anode, still lacks a systematic research on dendrites issues. Recent years have seen a revival in the area of lithium anode protection for Li metal based batteries, such as Li-S batteries and Li-O_2 batteries [123,124]. From the perspective of materials, we will mainly discuss about the artificial SEI and advanced nanostructured lithium metal anode designs for Li metal based batteries.

A good artificial SEI mainly has following advantages: Superior mechanical property (high shear modulus) to depress the growth of lithium dendrites; good lithium ion conductivity and electronic insulator; good chemical stability with lithium metal and electrolytes. By creating a Cu_3N + SBR artificial SEI layer which would react with lithium to form a Li_3N protection layer, Cui et al. [125] took advantage of its high Li ion conductivity, good flexibility and high mechanical strength to inhibit lithium dendrites successfully. An in situ generated Li_3PO_4 SEI layer [126] was proven to restrain the break and restoration of SEI layer. What's more, its high Young's modulus of ~10–11 GPa could effectively inhibit the growth of lithium dendrites. For the design of nanostructured lithium anode, advanced carbon host materials and inorganic matrix are mostly used. Cui et al. [127] reported a freestanding lithium alloy/graphene anode for Li metal batteries. However, lithiophilic sites should be introduced to the carbon matrix to enhance the affinity towards lithium. Lithiophilic N-doped graphene matrix was reported by Zhang research group [128] to guide the uniform nucleation lithium. Moreover, the high surface area of the 3D graphene could lower the local current density. The cycling electrochemical performance of the cells with N-doped graphene and Cu respectively as the counter electrode (the other is lithium) is shown in Fig. 9(a). N-doped graphene exhibits a more stable cycling performance than Cu foil electrode. A work by Hu research group [129] reported that silver nanoparticles decorated carbon nanofibers were taken advantage of to serve as a long-life lithium metal anode. In recent years, atomic layer deposition (ALD) has been emerging as an effective method to deposit conformal and ultrathin metal oxides or sulfides layers on the lithium metal anode [130,131]. Before used in lithium metal protection, atomic layer deposited Al_2O_3 thin layer was widely used in lithium ion batteries in the previous research [132,133]. Kozen et al. [130] reported an ALD Al_2O_3 layer (14 nm thick) protected lithium metal anode with stability towards moisture in the air for rechargeable Li-S batteries. In order to confirm the chemical stability of ALD Al_2O_3 protected lithium, they exposed lithium with (and without) Al_2O_3 protective layer to organic solvent, the thicker the Al_2O_3 layer was, the longer the onset time of H_2 evolution was. And the hydrogen pressure in the headspace of lithium with an Al_2O_3 protective layer was one order of magnitude lower than that of lithium without protection. With the purpose of exploring its potential use in Li-S batteries, they first compared the stability of lithium with (and without) ALD Al_2O_3 protection in the elemental sulfur (1 M)-containing DME solvent for 7 days. As shown in Fig. 9

(b), SEM images show that the surface of the ALD Al_2O_3 (14 nm thick)-protected lithium is nearly the same as the original lithium. Coupled with a sulfur-activated carbon cloth (ACC) composite as the sulfur composite cathode, ALD layer protected lithium anode performed better than the unprotected lithium in Li-S batteries. In the case of the former, the Coulombic efficiency (CE) of the first two cycles was higher than 95% while the latter was only 70% and 88%. A specific capacity of over 1000 mAh g^{-1} was attained in the ALD Al_2O_3 (14 nm thick) Li-S cells for more than 100 cycles. But the cell capacity decayed from ~1200 to ~800 mAh g^{-1} after 10 cycles in unprotected Li-S batteries. Lithium anode research is attracting more and more attention. Suppression of lithium dendrite growth and improvement of Columbic efficiency are two most key factors that need be kept in mind when designing new lithium anode structures and artificial SEI layers.

2.7. Electrolytes for Li-S batteries

The same to lithium ion batteries, electrolytes in Li-S batteries serve as the role of separating the anode and cathode while conducting ions. Differently, the reaction mechanisms in Li-S are highly associated with electrolytes. In this section, we will discuss the developments of electrolytes for Li-S batteries from conventional electrolytes, redox mediators in electrolytes, solid state electrolytes to new liquid electrolytes.

2.7.1. Conventional electrolytes

Dimethyl ether (DME) and dioxolane (DOL) are the most used electrolytes because widely used carbonate electrolyte can react with lithium polysulfides. $Li[CF_3SO_2)_2N]$ (LiTFSI) serves as the lithium salt and $LiNO_3$ acts as an additive to retard shuttle effect. DME has a low viscosity and solvates polysulfides well, while DOL is a co-solvent and has a low viscosity. DOL can break up its cyclic structure and form a protective layer on lithium anode during cycling. However, polysulfides shuttle exists in electrolytes based on DME and DOL. Besides, with a purpose of practical use, this electrolyte can't meet some high standards such as cost, safety and so on. Therefore, it is necessary to develop novel electrolytes.

2.7.2. Redox mediators

Different from insoluble host materials, soluble redox mediators exist in electrolytes and have also been proven to improve the performances of sulfur cathodes. The research on soluble redox mediators (RMs) are mainly on two points, the first is to improve the oxidation of Li_2S to polysulfides [134,135], the second is to control the growth of polysulfides to Li_2S [136,137]. On the first point, Aurbach et al. [134] reported that redox mediators such as decamethylferrocene, LiI and ferrocene could chemically oxidize Li_2S and therefore apparently lower its charge overpotential. They proved the result through comparing the intensities of XRD peaks of galvanostatically charged Li_2S cathodes using different electrolytes (i.e., with different RMs). With the same purpose, Cui research group [135] designed a quinone redox mediator named 1,5-bis(2-(2-(2-methoxyethoxy)ethoxy)ethoxy) anthra-9,10-quinone (AQT) for Li-S batteries. With AQT in the electrolyte, the original morphology of Li_2S didn't change even after 250 cycles. Thick Li_2S electrode test with AQT showed the cell delivered 606 mAh g^{-1} after 100 cycles at 0.1 C. On the second point, Helms, Chaing and co-authors [136] took advantage of Electrolyte Genome to screen suitable polycyclic aromatic hydrocarbons (PAHs) as RMs for Li-S batteries by considering electron affinities (E_{ea}) and ionization potentials (E_i). N-aryl-substituted benzo[ghi]peryleneimide (BPI) was discovered to have a calculated reduction potential at 1.99 V vs. Li/Li^+. Through ex situ analysis of Li-S cells at different states of charge, they found that BPI redox mediator promoted 3D growth of Li_2S and contributed its production to 6-fold. Inspired by them, Zhang et al. [137] introduced cobaltocene ($CoCp_2$) redox mediators into Li-S batteries under lean-electrolyte conditions. With ~26 mV smaller reduction potential than the formation potential of Li_2S, $CoCp_2$ redox mediators could also regulate the growth of Li_2S from 2D to 3D and the discharge capacities was enhanced to 8 times. Even with an electrolyte/sulfur (E/S) ratio of 4.7 μL mg_S^{-1}, at 0.05 C, Li-S cell with $CoCp_2$ RMs could deliver capacities over 800 mAh g^{-1} for 20 cycles while the cell without cobaltocene couldn't. Overall, the development of soluble redox mediators paved a new way to make Li-S batteries into practical use. Precise screen of redox mediators by theoretical calculation can accelerate this process.

2.7.3. Solid state electrolytes

Progress of research on all solid-state-electrolyte based lithium ion batteries inspires us to find its potential in Li-S batteries [138,139]. When used in a Li-S cell, the solid-state-electrolyte can not only prevent the shuttle of polysulfides but also block dendrites growth at the lithium anode. Hu and co-workers [140] introduced a 3D garnet-type nanofiber networks composed of $Li_{6.4}La_3Zr_2Al_{0.2}O_{12}$ (LLZO) embedded in PEO-LiTFSI matrix as a flexible solid-state electrolyte for rechargeable Li metal batteries. It exhibited a room-temperature ion conductivity of 2.5×10^{-4} S cm^{-1} and a stable voltage window up to 6 V versus Li^+/Li. Manthiram and co-workers [141] reported a NASICON-type lithium ion conductive solid-state electrolyte with a formula of $Li_{1+x}Y_xZr_{2-x}(PO_4)_3$ (LYZP) (x = 0–0.15) used in the hybrid Li||LYZP||Li_2S_6 cells (Fig. 8). This hybrid Li-S system consisted of solid-state electrolyte and liquid organic electrolyte, in which Li_2S_6 was dissolved. The indispensability of liquid electrolyte was attributed to the sluggish electrochemical reaction of all-solid-state Li-S batteries. Compared to commonly used NASICON-type $Li_{1+x}Al_xTi_{2-x}(PO_4)_3$ (LATP) solid electrolyte, LYZP was more stable in the media of polysulfides solution. Electrochemical characterization of this shuttle-free Li-S batteries showed that they could deliver the first specific capacity of 950 mAh g^{-1} and capacity retention of 89.5% after 150 cycles. However, the batteries using the Celgard membrane as separators decayed very rapidly with a capacity retention of only 20.0% after 150 cycles. Besides oxides, sulfides based solid state electrolytes usually possessed higher lithium ion conductivity and sulfiphilicity [138,142,143]. For example, superionic conductor $Li_{10}GeP_2S_{12}$ was reported to have a lithium ion conductivity of 12 mS cm^{-1} at RT [144]. Inspired by this, Fan et al. [145] synthesized $Li_{10}SnP_2S_{12}$ solid state electrolyte (3.2 mS cm^{-1} at RT) by high-energy ball-milling mixture of Li_2S, P_2S_5 and SnS_2. The solid-state Li-S batteries enabled by $Li_{10}SnP_2S_{12}$ delivered over 1200 mAh g^{-1} for 50 cycles. The research on solid-state electrolyte based lithium metal sulfur

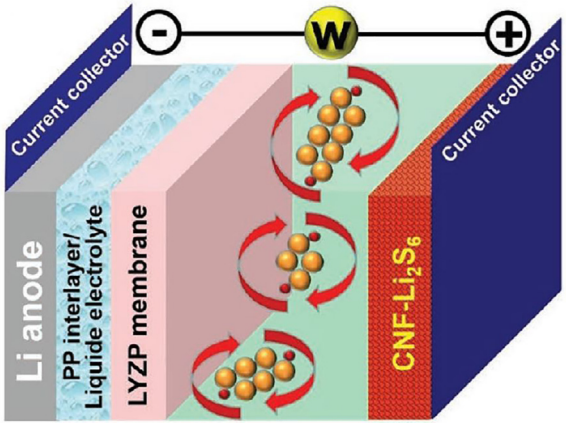

Fig 8. A prototype of a solid-state electrolyte based hybrid Li-S cell. Reproduced with permission [141]. Copyright 2016, Wiley-VCH.

batteries is still in its infancy and we believe much progress will be made in the future, not only in prototypes but also in boosting electrochemical performances.

2.7.4. New liquid electrolytes

Although ether-based electrolytes were widely used in Li-S batteries, the developments of other new liquid electrolytes for Li-S batteries didn't cease. Fluorinated ethers, ionic liquids and solvent-in-salt electrolyte were mostly concerned among them.

Because F-containing functional groups in solvents have a strong electron-withdrawing effect, fluorinated ethers have many advantages such as low viscosities and low flammability compared to conventional ethers. It was employed in adjusting electrolytes as an effective strategy to improve the stability of Li metal anodes. Shin et al. [146] reported a fluorinated solvent named 1,1,2,2-tetrafluoroethyl 2,2,3,3-tetrafluoropropyl ether (TFTFE) as a cosolvent in the electrolyte for Li-S batteries. Raman spectra analysis of chemical environment of electrolyte constituents showed that TFTFE didn't solvate ions in the electrolytes. For lean-electrolyte Li-S application, with an electrolyte/sulfur ratio of 2 μL mg^{-1} and a hybrid cathode made up of 45 wt% VS_2 mixed with ZnS-coated Li_2S@graphene (7.8 mg cm^{-2}), the Li-S cell demonstrated an energy density of 483 Wh kg^{-1}based on the mass of both electrodes and electrolytes. What's more, TFTFE enhanced battery's safety because of its high flash point, which was confirmed by flammability test.

Room temperature ionic liquid (RTIL) was applied in Li-S batteries because it was made up of entirely ions, which suppressed the dissolution of lithium polysulfides and many other attractive properties such as low volatility and low flammability. Previous research (mostly before 2015) mainly investigated the use of pyrrolidinium and imidazolium ionic liquids with $TFSI^-$ anions in Li-S batteries [37,147]. The solubility of lithium polysulfides in different ionic liquids was found to be related to the anionic parts. At the same time, solvate ionic liquids were developed as a new kind of ionic liquid to be applied in Li-S batteries. Watanabe and coworkers contributed much to this part [148–151]. Recently, Peng et al. [152] reported a zwitterionic ionic liquid, tris(dioxa-3,6-heptyl)aminesulfonate coupled with bis(trifluoromethane)sulfonimide lithium salt (named TLTFSI). It had an ionic conductivity of 3.2 mS cm^{-1} and a wide electrochemical window of 1.51–4.82 V. With TLTSI based electrolyte, Li-S batteries showed more than 400 mAh g^{-1} for 200 cycles at 0.5 C. In general, breakthroughs in this area like the use of CMK-3/S in cathode part still need to be anticipated in the future.

By increasing the concentration of lithium salt in electrolytes above 1 M, the dissolution of lithium polysulfides into the electrolytes would be prohibited, high-concentration electrolytes (i.e., solvent-in-salt electrolytes) attracted much interest in Li-S batteries. The breakthrough in this area was achieved by Suo and coworkers [153]. In the SIS#7 electrolyte (7 mol L^{-1} LiTFSI in DOL-DME electrolyte), lithium ion transfer number was up to 0.73, much higher than conventional electrolyte (0.2–0.4). What's more, this SIS#7 electrolyte reduced the corrosion and restrained the growth of lithium dendrites on lithium metal. Li-S batteries based on SIS#7 electrolyte delivered an initial specific capacity of 1041 mAh g^{-1} and maintained 74% after 100 cycles. In low-concentration electrolyte, lithium ions coordinated with oxygen in ethers and formed large solvation shell, which impeded the transport of solvated lithium cations. However, in solvent-in-salt electrolyte, solvated lithium cations decreased much, and the mobility of lithium ions improved. Although the viscosity of the electrolyte increased, it didn't make a big impact in the transport of lithium ions.

The exploration of new liquid electrolyte systems expanded the functionalities of Li-S batteries. The safety was greatly enhanced from mainly two points: (1) The suppression of the growth of lithium dendrites reduced short-circuits of cells; (2) the flame-retardant electrolytes avoided the explosion of cells. However, some issues such as higher cost of the solvent-in-salt electrolyte emerged if we considered the practical use of Li-S batteries. A compromise between cost and functionalities need to be reached.

2.8. Practical applications of Li-S batteries

The implementation of Li-S batteries from lab coin cell scale to practical applications remains challenging [154–156]. Pouch cells are the most useful prototype when it comes to practical use of Li-S batteries. Because there is a big gap between previous Li-S coin cells' research and demanding Li-S pouch cell products, new standards and key testing parameters need to be established by leaders in this area. For example, the ratio of electrolyte to sulfur (E/S ratio) determines the electrochemical performance of both Li-S coin cells and pouch cells. Most researchers recommend its value to be no more than 4 μL mg^{-1} and then the research based on it will be more meaningful. In order to achieve an energy density of 500 Wh kg^{-1}, high sulfur loading of >5 mg_S cm^{-2} and low E/S < 3. 0 μL mg_S^{-1} are necessary conditions. If the E/S ratio decreased, the viscosity of the electrolyte increased because of the polysulfides dissolution and the kinetics slowed down. At the same time, uneven reactions, severe shuttle happened, and unstable lithium anode formed. Besides, the ratio of negative to positive electrode in capacity (N/P) controls the actual energy density of Li-S pouch cells. A N/P value at no more than 2 will be of practical value. Besides, here emerge new significant parameters in Li-S pouch cells, such as the pressure control on cell stack, single- or double-sided coating and other engineering issues.

The cost of components of Li-S pouch cells determines the future of its practical applications. The cost of sulfur can be ignored compared to cathodes containing Co and Ni in Li-ion pouch cells. What's more, the cost of lithium foil anode in Li-S pouch cell is also lower than graphite in Li-ion pouch cells. However, the cost of electrolytes in Li-S pouch cells contributes more than 50%, while in Li-ion pouch cells it takes less than 5%. The large consumption of the solvents and expensive LiTFSI salt in Li-S pouch cells are two main reasons. It is apparent that decreasing the E/S ratio and developing cheap electrolytes for Li-S batteries are of great value.

In conclusion of the section of Li-S batteries, even though plentiful research work on Li-S batteries has been done to find its potential in high-energy storage devices, there are several points that are worth highly concerning. Increasing the areal sulfur content at low E/S while maintaining high performance of Li-S batteries at the same time is a challenging goal. The practical application of Li-S pouch cells enabled by different hosts and electrolytes with a target of 500 Wh kg^{-1} need more investigations. Besides, basic research is still of great value in solving these issues. All in all, Li-S batteries have been on the right track.

3. Sodium-sulfur batteries

Sodium-sulfur (Na-S) batteries are famous for the high-temperature Na-S (HT Na-S) batteries because of it being widely used in large-scale stationary energy systems [157]. HT Na-S batteries with its advantages manifested in the low cost of sodium and sulfur and the high theoretical specific energy of ~760 Wh kg^{-1}, are suitable for large-scale stationary energy storage. In the configuration, it is usually constructed in tubular designs, in which beta-alumina serves as the solid-state electrolyte and separator, molten sodium as the anode and molten sulfur as the cathode. The working temperature usually lies in the range of 300–350 °C and the working voltage window is in the range of 1.78–2.06 V. Nowadays,

for the sake of safety and cost, RT Na-S batteries have been emerging in recent years under the intriguing achievements of Li-S batteries. It has a higher theoretical specific density of 1274 Wh kg^{-1} compared to HT Na-S batteries.

3.1. Mechanism

Manthiram research group applied themselves to this field. Based on their plentiful research [158–160], they proposed a detailed reaction mechanism for RT Na-S batteries with glyme based electrolyte [27]. As shown in Fig. 3(b) and Eqs. (8)–(18), the discharge process is divided into four regions, where successive reactions take place.

Overall:

$$S_8 + 16Na^+ + 16e^- \rightarrow 8Na_2S \quad \text{(cathode)} \tag{8}$$

$$16Na \rightarrow 16Na^+ + 16e^- \quad \text{(anode)} \tag{9}$$

Charge and discharge reactions:

Process 1:

$$S_8 + 2e^- + 2Na^+ \rightleftarrows Na_2S_8 \tag{10}$$

Process 2:

Overall:

$$Na_2S_8 + 2e^- + 2Na^+ \rightleftarrows 2Na_2S_4 \tag{11}$$

Intermediate reactions:

$$3Na_2S_8 + 2e^- + 2Na^+ \rightleftarrows 4Na_2S_6 \tag{12}$$

$$5Na_2S_6 + 2e^- + 2Na^+ \rightleftarrows 6Na_2S_5 \tag{13}$$

$$4Na_2S_5 + 2e^- + 2Na^+ \rightleftarrows 5Na_2S_4 \tag{14}$$

Process 3:

$$3Na_2S_4 + 2e^- + 2Na^+ \rightleftarrows 4Na_2S_3 \tag{15}$$

$$Na_2S_4 + 2e^- + 2Na^+ \rightleftarrows 2Na_2S_2 \tag{16}$$

$$Na_2S_4 + 6e^- + 6Na^+ \rightleftarrows 4Na_2S \tag{17}$$

Process 4:

$$Na_2S_2 + 2e^- + 2Na^+ \rightleftarrows 2Na_2S \tag{18}$$

Similar to Li-S batteries, there exist two typical discharge plateaus at ~2.2 and ~1.6 V (Fig. 3b) in RT Na-S batteries. The high-voltage plateau corresponds to the sodiation of S_8 to Na_2S_8, which is a solid–liquid reaction. The lower-voltage plateau is the liquid–solid transition of Na_2S_4 to solid Na_2S_3, Na_2S_2 and Na_2S. The first descending region between the two plateaus in the voltage curve is related to the intermediate reactions from high-order Na_2S_8 to low-order soluble sodium polysulfides. The second descending region is the solid–solid process of Na_2S_2 to Na_2S. Upon charge, the processes are converse reactions of the discharge.

3.2. Cathode materials

The development of cathode materials for Na-S batteries is quite like that of Li-S batteries, namely, from nonpolar carbon materials to polar host materials. This part will be reviewed according to this order. Most cathode materials for Li-S batteries can be adopted in Na-S batteries. Differently, microporous carbon materials act as an interesting role in Na-S batteries.

3.2.1. Nonpolar carbon materials

Various nanostructured carbon material-sulfur composites have been investigated to serve as composite cathode materials for RT Na-S batteries with carbonate-based electrolytes. Xin et al. [161] reported a microporous carbon confined small sulfur molecule (S_{2-4}) composites as the cathode for RT Na-S batteries. Two stable reduction peaks at 1.55 and 1.1 V vs. Na^+/Na emerged after the second cycle. Upon oxidation, an obvious anodic peak at 1.75 V appeared. More than 200 cycles with a discharge capacity of over 500 mAh g^{-1} (750 Wh kg^{-1}) at 1 C and 2 C was achieved, which surpassed traditional HT Na-S batteries. And they thought there existed two reduction reactions: 2S + 2Na → Na_2S_2 (>1.4 V); Na_2S_2 + 2Na → $2Na_2S$ (<1.4 V). A sugar-derived microporous carbon was also applied in the RT Na-S batteries [162]. More than 300 mAh g^{-1} over 1500 cycles at 1 C rate was demonstrated. Wang et al. [163] proposed an interconnected mesoporous carbon hollow nanospheres as the conductive backbone for the electrochemical reactions of sulfur while providing active diffusion channels at the same time (Fig. 10a). Cycling results showed that the desodiation of Na_2S to Na_2S_4 was not reversible and the long-term cycling of RT Na-S batteries was highly dependent on the reversible reaction between long-chain Na_2S_x ($5 \leq x \leq 8$) and short-chain Na_2S_4.

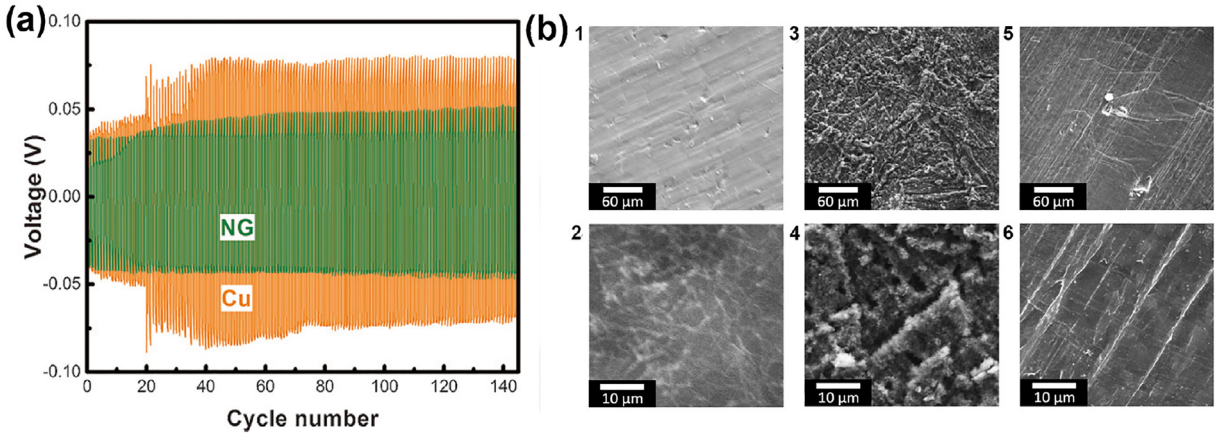

Fig 9. Lithium anode protection. (a) The cycling electrochemical performance of lithium metal cells with N-doped graphene and Cu as the counter electrode. Reproduced with permission [128]. Copyright 2016, Wiley-VCH. (b) The surface morphology of (1, 2) unprotected lithium before solvent exposure, (3, 4) unprotected lithium metal after seven days of exposure to DME/sulfur solution, and (5, 6) 14 nm ALD Al_2O_3-protected Li metal surface after 7 days of exposure to DME/sulfur solution. Reproduced with permission [130]. Copyright 2015, American Chemical Society.

3.2.2. Polar host materials

With the utilization of carbonate based electrolytes, Qiang et al. [164] reported a highly N, S-doped (~40 atom%) mesoporous carbon material as the sulfur host for RT Na-S batteries. Approximately a stable discharge specific capacity of 400 mAh g^{-1} over 350 cycles was obtained at 0.23 A g^{-1}. The successful prevention of reactions between polysulfides and carbonate electrolyte was attributed to the strong affinity of polysulfides to N atoms in the pores. Along the road to seeking for efficient polar host materials towards polysulfides, Zhu et al. [165] utilized ZIF-derived carbon as sulfur composite cathode materials for Na-S batteries. Inorganic compound-carbon hybrids as polar hosts were also investigated for Na-S batteries [166]. A recent paper [167] on atomic cobalt anchored on microporous hollow carbon (S@Co_n-HC) as the composite cathode material for high-performance Na-S batteries demonstrated an initial specific capacity of 1084 mAh g^{-1} and a reversible capacity of 508 mAh g^{-1} for 600 cycles at ~0.2 A g^{-1}. The catalytic function of atomic Co in contributing to the conversion of Na_2S_4 to Na_2S and lowering the dissolution of Na_2S_4 was the key factor to the excellent performance. What's more, the high binding energy between Na_2S_4 and Co_6 corroborated this host materials' high adsorption towards sodium polysulfides. The long cycling performance of Na-S batteries with S@Co_n-HC as the composite cathode is shown in Fig. 10(b). Proceeding this work, they reported transition Fe, Cu, and Ni nanoclusters based on hollow carbon spheres (HC) as sulfur cathode hosts to investigate different elements nanoclusters on the electrochemical performances of Na-S batteries [168]. MD simulation showed Na_2S_4 decomposed most quickly on the Fe nanocluster, which meant it had the most suitable reactivity for RT Na-S batteries. It could explain why Fe-HC delivered the highest specific capacity among the three materials.

In conclusion of this part, compared to nonpolar carbon materials, polar host materials can adsorb soluble sodium polysulfides and mediate the conversion of polysulfides, which will accelerate the kinetics and enhance the electrochemical performance of RT Na-S batteries. It is still worth noting to distinguish the true catalytic phase of polar host materials if the host reacted with soluble polysulfides during cycling.

3.3. Electrolytes and Na metal anode protection

Modifications to the electrolytes of RT Na-S batteries have also been tried in order to achieve stable RT Na-S batteries. The most used two kinds of electrolytes are carbonates and glymes. carbonate electrolytes are usually more stable and less volatile than glymes. When they are used as electrolytes for Na-S batteries, the situation becomes quite different from that in Li-S batteries.

Archer and co-workers [169] reported a liquid carbonate electrolyte (1 M $NaClO_4$ in the mixture of ethylene carbonate (EC) and propylene carbonate (PC)) with ionic liquid 1-methyl-3-propy limidazolium-chlorate tethered silica nanoparticle (SiO_2-IL-ClO_4) additives as a stabilizing agent for RT Na-S batteries. Fig. 10(c) illustrates the Na-S cell. It uses the reported electrolyte above and the SEM image on the left shows the surface of cycled sodium metal surface. Through the utilization of ZIF-8 derived microporous carbon polyhedron-sulfur composites as the composite cathode for RT Na-S batteries, they found that sulfur underwent a solid-state electrochemical reaction, for which this sort of featured carbonate-based electrolyte was compatible with the microporous carbon–sulfur composite cathode. Assembled batteries with this electrolyte (with 5 vol% SiO_2-IL-ClO_4) and the composite cathode showed a reversible capacity of more than 860 mAh g^{-1} for 50

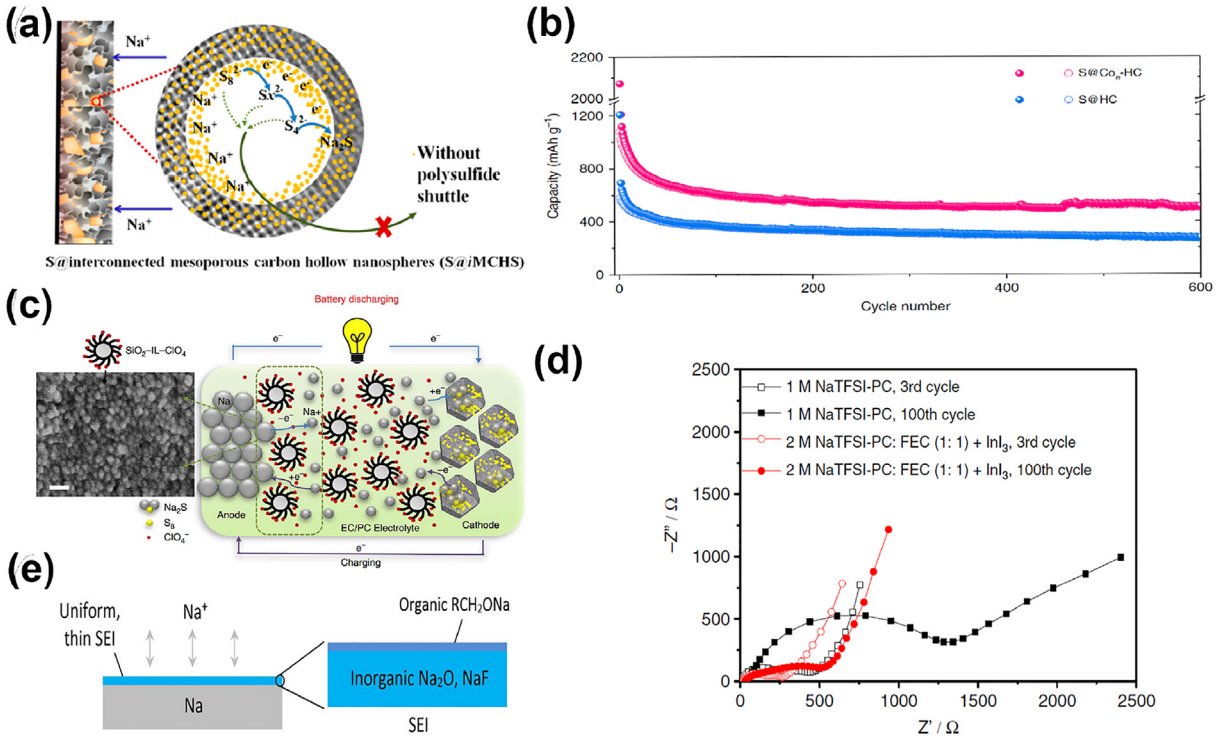

Fig 10. Advances in Na-S batteries. (a) Mesoporous carbon hollow nanospheres-sulfur composite materials. Reproduced with permission [163]. Copyright 2016, American Chemical Society. (b) The long-term cycling of S@Co_n-HC and S@HC cathode materials. Reproduced with permission [167]. Copyright 2018, Springer Nature. (c) A prototype of the SiO_2-IL-ClO_4 stabilized electrolyte-based Na-S cell (right) and the surface of cycled sodium metal anode (left). Reproduced with permission [169]. Copyright 2016, Springer Nature. (d) The Nyquist plots of Na-S cells using 1 M NaTFSI in PC and 2 M NaTFSI in PC/FEC with InI_3 as electrolytes. Reproduced with permission [170]. Copyright 2018, Springer Nature. (e) An illustration of the solid-electrolyte interface formed on the surface of Na metal when the electrolyte of $NaPF_6$ in glymes was used. Reproduced with permission [171]. Copyright 2016, American Chemical Society.

cycles at 0.1 C rate. At a higher rate, i.e. 0.5 C, in the potential range of 0.6–2.6 V vs. Na^+/Na, the discharge capacity of over 600 mAh g^{-1} for 100 cycles was obtained. The obvious difference in electrochemical reaction mechanisms of sulfur between microporous carbons and other carbons is of great significance for researchers to investigate afterwards if major improvement in this area is to be made. It should be noted that sulfur may exist in different allotropes (e.g. S_4, S_3, S_2) because of the differences of pore sizes of carbon materials. Therefore, the mechanisms will vary depending on the specific porous carbon–sulfur materials employed.

Carbonate electrolytes have been found to be reactive to polysulfides in Li-S batteries but it's feasible to use them in Na-S batteries because of the lower reactivity of Na^+-polysulfide$^-$ ion pairs. Wang research group [170] reported a new electrolyte made up of 2 M sodium trifluoromethanesulfonimide (NaTFSI) in polycarbonate (PC)/fluroethylene carbonate (FEC) (v:v = 1) with InI_3 as the additive for RT Na-S batteries. The higher concentration of the sodium salt suppressed the weak polysulfides shuttle, which degraded the cell. What's more, the In^{3+} could be reduced to indium metal on the Na metal anode, which inhibited the growth of sodium dendrites and contributed to the batteries' safety. The I_3^- catalyzed the conversion of solid Na_2S to sodium polysulfides and it increased the reversibility and specific capacity of the Na-S cells. Fig. 10(d) depicts the impedance analysis of Na-S cells using two kinds of electrolytes. The cell enabled by 2 M NaTFSI in PC/FEC with InI_3 showed lower charge transfer resistance and higher ionic conductivity.

It seems that carbonate electrolyte is well applicable to RT Na-S batteries based on the research above. However, a recent study on the effect of the electrolyte on the reversibility of sodium metal anode showed that electrolyte consisted of sodium hexafluorophosphate in glymes was more suitable for RT Na-S batteries. Seh et al. [171] found that there existed dendrite issues in sodium anode when $NaPF_6$-carbonate electrolyte system was employed. However, when $NaPF_6$-glyme system was used, an average Coulombic efficiency of 99.9% over 300 cycles in sodium plating-stripping was attained. It was attributed to the formation of uniform and compact inorganic SEI (Na_2O and NaF) which was impermeable to liquid electrolyte (Fig. 10e). What's more, the high shear moduli of Na_2O and NaF effectively suppressed the growth of sodium dendrites. The higher reduction potentials made carbonate electrolyte inferior to glymes, for the former was easier to decompose. In order to demonstrate its application in RT Na-S batteries, batteries made up of Na anode, $NaPF_6$ in tetraglyme and sulfur infiltrated carbon nanofibers composite cathode were tested at 0.1 C from 1.2 to 2.8 V versus Na^+/Na. It delivered a high specific capacity of 776 mAh g^{-1} and retained ~500 mAh g^{-1} after 20 cycles. This finding may provide inspiring ideas for research on high energy–density RT Na-S batteries and other sodium-based energy storage technologies. Even though in situ formed SEI was effective in depressing the growth of dendrites, its mechanical strength was not strong enough to bear the large volume change during sodium plating/stripping. With the same purpose employed in lithium metal anode protection, ALD was also used in depositing an Al_2O_3 thin film on Na metal anode. Hu and co-workers [172] reported that an artificial SEI was deposited on Na metal anode through a low-temperature plasma-enhanced ALD method. As expected, symmetric cells using the Al_2O_3 coated sodium metal could be cycled over 450 times stably while the bare one had a larger polarization all the time. The morphology characterization showed that symmetric cells using Al_2O_3 coated sodium metal exhibited a stable impedance while the impedance of bare ones increased with cycle times. This indicated that a stable artificial SEI was formed on Na metal anode. A similar but in-depth research by Sun and co-workers [173] found no voids in the Al_2O_3 layer through Rutherford backscattering spectrometry (RBS) measurements, which confirmed the uniform and fine growth of the Al_2O_3 layer.

We have summarized the recent advances in RT Na-S batteries, mainly on different electrolyte-based prototypes. Table 4 lists some important advances. Microporous carbon–sulfur composites have been demonstrated to act as promising cathodes of RT Na-S batteries towards low-cost large-scale stationary load-levelling energy-storage. Coupled with microporous carbon–sulfur composite cathodes, electrolyte based on carbonates is a good choice for RT Na-S batteries. On account of a definitely different application, RT Na-S batteries are not always an analogue to Li-S batteries. We can conclude that the reaction mechanisms of RT Na-S batteries still need further research in different systems (various electrolytes). Sulfur may undergo a solid-state reaction in the microporous carbon, which differs from that in other carbon hosts. It's too early to say which one is not suitable for RT Na-S batteries as to glymes and carbonates-based electrolytes.

For future developments of RT Na-S batteries, all solid-state sodium sulfur batteries are of great potential. It makes use of Na metal anodes, which is a holy grail for Na ion batteries. Progress on Na_3SbS_4 [174] and Na_3PS_4 [175] based all solid-state Na-S batteries paves a way for the development of solid-state Na-S batteries. The exploration of solid-state electrolytes for Na-S batteries still has a long way to go. Mimicking Li-S batteries, introducing Ge or Sn may be promising. Besides, whether to use ether electrolytes or carbonates electrolyte is still a topic of great value. It is anticipated to see further progress in this area both academically and industrially.

4. Magnesium-sulfur batteries and aluminum-sulfur batteries

Magnesium-sulfur (Mg-S) batteries are usually comprised of Mg metal anodes, Mg ion based electrolytes and sulfur cathodes. Similar to other metal-sulfur batteries, aluminum-sulfur (Al-S) batteries utilize Al metal anodes, Al ion based electrolytes and sulfur cathodes. As shown in Fig. 3(e) and Table 3, Mg-S batteries can provide a theoretical energy density of 1722 Wh kg^{-1} with an average operating voltage at ~1.7 V. Al-S batteries have a theoretical energy density of 1340 Wh kg^{-1} with an average voltage of ~1.25 V. The typical discharge–charge curves of Mg-S and Al-S batteries are shown in Fig. 3(c and d), respectively. Compared to Li-S batteries, Mg-S and Al-S batteries can provide the same energy at a lower cost. The minimum energy cost of Mg-S and Al-S batteries is 0.81 and 0.71 $ kW h^{-1}, respectively, whereas for Li-S batteries is up to 7.08 $ kW h^{-1}. The cost decreases nearly 90%, which is very fascinating and promising. In this section, we give a summary of the recent advances of Mg-S and Al-S batteries.

4.1. Mg-S batteries

4.1.1. Electrolytes for Mg-S batteries

As mentioned above, the developments of multivalent metal-sulfur batteries (Mg-S and Al-S batteries) are hampered by the lack of suitable electrolytes [17,176–181]. Up to now, electrolytes developed for Mg-S batteries can be classified into three main kinds, i.e. organic non-nucleophilic magnesium electrolyte, magnesium borate-based electrolyte, and $Mg(TFSI)_2$-$MgCl_2$ based ether electrolytes. Previous research shows that nucleophilic magnesium organohaloaluminate electrolyte reacted with electrophilic sulfur cathodes [180,182–186]. It is of great significance to develop a non-nucleophilic electrolyte for Mg-S batteries. Kim et al. [187] developed a $(Mg_2(\mu\text{-}Cl)_3\cdot 6THF)(HMDS_nAlCl_{4-n})$ (n = 1, 2) crystal (Fig. 11a) for the first rechargeable Mg-S batteries through the in situ reaction of Lewis acid $AlCl_3$ and hexamethyldisilazide magnesium chloride (HMDSMgCl) in THF (tetrahydrofuran). Through

Table 4
Progress in rechargeable room-temperature sodium-sulfur (RT Na-S) batteries.

Cathode materials	Morphology	Electrolyte	Sulfur loading (mg cm^{-2}) & (sulfur content in cathode)	Voltage window (V vs. Na^+/Na)	Energy density (Wh kg^{-1})	Electrochemical performance (initial capacity (mAh g^{-1}) and cycles) & decay rate (per cycle)	Ref. & year
Microporous Carbon	Coaxial cable-like structured microporous carbon;	Carbonate	0.4 & (40 wt%)	0.8–2.7	750 (based on sulfur)	1148 (~87% after 20 cycles) at 0.1 C & N/A	[161] 2014
ZIF-8 derived microporous carbon	Microporous carbon polyhedrons; 708 $m^2 g^{-1}$;	SiO_2-IL-ClO_4 stabled carbonate	1.8–2.5 & (37.6 wt%)	0.6–2.6	N/A	~900 (67% after 100 cycles) at 0.5 C	[169] 2016
Sugar-derived microporous carbon	Ordered microporous carbon spheres	TEGDME	N/A & (35 wt%)	0.8–2.6	180 (based on entire weight)	Nearly stable at 370 mAh g^{-1} after 1500 cycles at 1 C	[162] 2017
N, S-doped Mesoporous carbon	Highly doped (~40 atom%) mesoporous carbon	Carbonate	0.15–0.17 & (15.4 wt%)	0.8–2.7	150 (based on the total weight of cathode)	Stable at ~380 mAh g^{-1} for 350 cycles at 0.14 C	[164] 2017
Atomic Co-carbon	Atomic Co-anchored on hollow carbon nanospheres	Carbonate	N/A & (~33 wt%)	0.8–2.8	N/A	1084 (~47% for 600 cycles) at ~0.2 A g^{-1}	[167] 2018
Atomic Fe-carbon	Atomic Fe-nanoclusters anchored on hollow carbon spheres	Carbonate	0.9–1.1 (~28 wt%)	0.8–2.8	N/A	1023 (~39% after 1000 cycles) at 0.1 A g^{-1}	[168] 2019

the adoption of this electrolyte, much progress has been made in exploring the mechanism of Mg-S batteries. Zhao et al. [188] investigated the discharge mechanism of Mg-HMDS electrolytes based Mg-S batteries. The Mg-S cell reached its first upper flat voltage plateau at around 1.6 V. The reaction can be described as Eqs. (19) and (20) and an overall reaction Eq. (22). The second liquid–solid reaction was very sluggish compared to Li-S batteries, which can be described by Eqs. (23) and (24). Based on these results, Wang et al. [189] improved the reversibility of Mg-S batteries through the Li^+ mediation. They introduced LiTFSI into the non-nucleophilic $(HMDS)_2Mg$-based electrolytes. With Li ion in the electrolyte, the discharge capacity increased to ca. 1000 mAh g^{-1} compared to that of less than 200 mAh g^{-1} of the cells without Li ion mediation (Fig. 11b). They ascribed the phenomenon to these reasons: (1) The hard Lewis acid lithium ion enhanced the solubility of low order Mg polysulfides through coordinating the surface S^{2-} and their electrochemical activity was greatly improved; (2) lithium ions also participated in the reduction of sulfur and formed hybrid Mg/Li polysulfides during the process of discharge. This can provide a method to improving electrochemical performances of Mg-S or Al-S batteries in the future.

In order to achieve high-performance Mg-S batteries, Chen and co-workers [190] successfully developed a well-defined boron-centered anion-based magnesium electrolyte (BCM electrolyte) (Fig. 11c) and deployed it into Mg-S batteries. Through the use of this BCM electrolyte, coupled with a sulfur/carbon composite cathode, at 0.05 A g^{-1}, the cell showed the first discharge capacity of 1081 mAh g^{-1} and a retention of 86.4% after 30 cycles. The flat voltage plateau was at ~1.1 V vs. Mg^{2+}/Mg. Recently, Du et al. [191] reported an effective organic magnesium borate-based electrolyte whose effective cation was tetrakis(hexafluoroisopropyl)borate anions $[B(HFP)_4]^-$ and solvated cation was $[Mg_4Cl_6(DME)_6]^{2+}$. It showed some promising properties, such as high oxidation stability up to 3.0 V (vs. Mg^{2+}/Mg), high ionic conductivity of 5.58 mS cm^{-1}. When it was used in a Mg-S battery, coupled with an 80 wt% sulfur-carbon nanotubes (S-CNT) composite cathode, the battery showed a high specific capacity up to 1200 mAh g^{-1} and obtained specific capacity of over 1000 mAh g^{-1} for more than 100 cycles at 0.16 A g^{-1}. What's more, the overpotential could be as low as 0.3 V. This is a great improvement in electrolyte research compared to previous HMDS-based and monocarborane-based Mg electrolytes.

Charge and discharge reactions:

$$S_8 + 2e^- + Mg^{2+} \rightleftarrows MgS_8 \quad (19)$$

$$3MgS_8 + 2e^- + Mg^{2+} \rightleftarrows 4MgS_6 \quad (20)$$

$$2MgS_6 + 2e^- + 2Mg^{2+} \rightleftarrows 3MgS_4 \quad (21)$$

Overall:

$$S_8 + 4e^- + 2Mg^{2+} \rightleftarrows 2MgS_4 \quad (22)$$

$$MgS_4 + 2e^- + Mg^{2+} \rightleftarrows 2MgS_2 \quad (23)$$

$$MgS_2 + 2e^- + Mg^{2+} \rightleftarrows 2MgS \quad (24)$$

The aforementioned electrolytes are so complex that researchers begin to use widely used bis(trifluoromethane)sulfonimide(TFSI)-glyme electrolyte in Li-S batteries to find its potential in Mg-S batteries. Interestingly, Wang research group [192] reported that a new TFSI-glyme electrolyte could be implemented in Mg-S batteries. Through the use of 0.5 M $Mg(TFSI)_2$–1,2-dimethoxyethane(DME) as the electrolyte, they investigated the thermodynamics and kinetics of Mg-S batteries. And they also found two parallel but interacting magnesition pathways: (1) Dissolved polysulfides reacted with Mg^{2+} from the electrolyte; (2) bulk magnesition through the solid state transport of Mg^{2+}. The reaction mechanism was similar to the cells with Mg-HMDS electrolytes. It can also be described briefly by Eqs. (22)–(24). A consecutive work [193] on the $Mg(TFSI)_2$-$MgCl_2$-DME electrolyte for Mg-S batteries reported that a 69% capacity retention after 110 cycles was achieved at 0.1 A g^{-1}. The initial specific capacity was around 800 mAh g^{-1}. The sulfur composite cathode delivered better kinetics than intercalation- or conversion-type Mg batteries and showed a moderate voltage hysteresis of 0.25 V. However, the Mg anode showed a voltage hysteresis of 0.45 V, which need to be improved by using a better electrolyte. Both two works utilized the XPS to monitor the evolution of the Mg-S species, which is shown in Fig. 11(d).

4.1.2. Cathodes for Mg-S batteries

Besides the search of electrolytes for Mg-S batteries, new sulfur composite cathode materials for Mg-S batteries are also under investigation. Li et al. [194] introduced a hierarchical N- and Co-

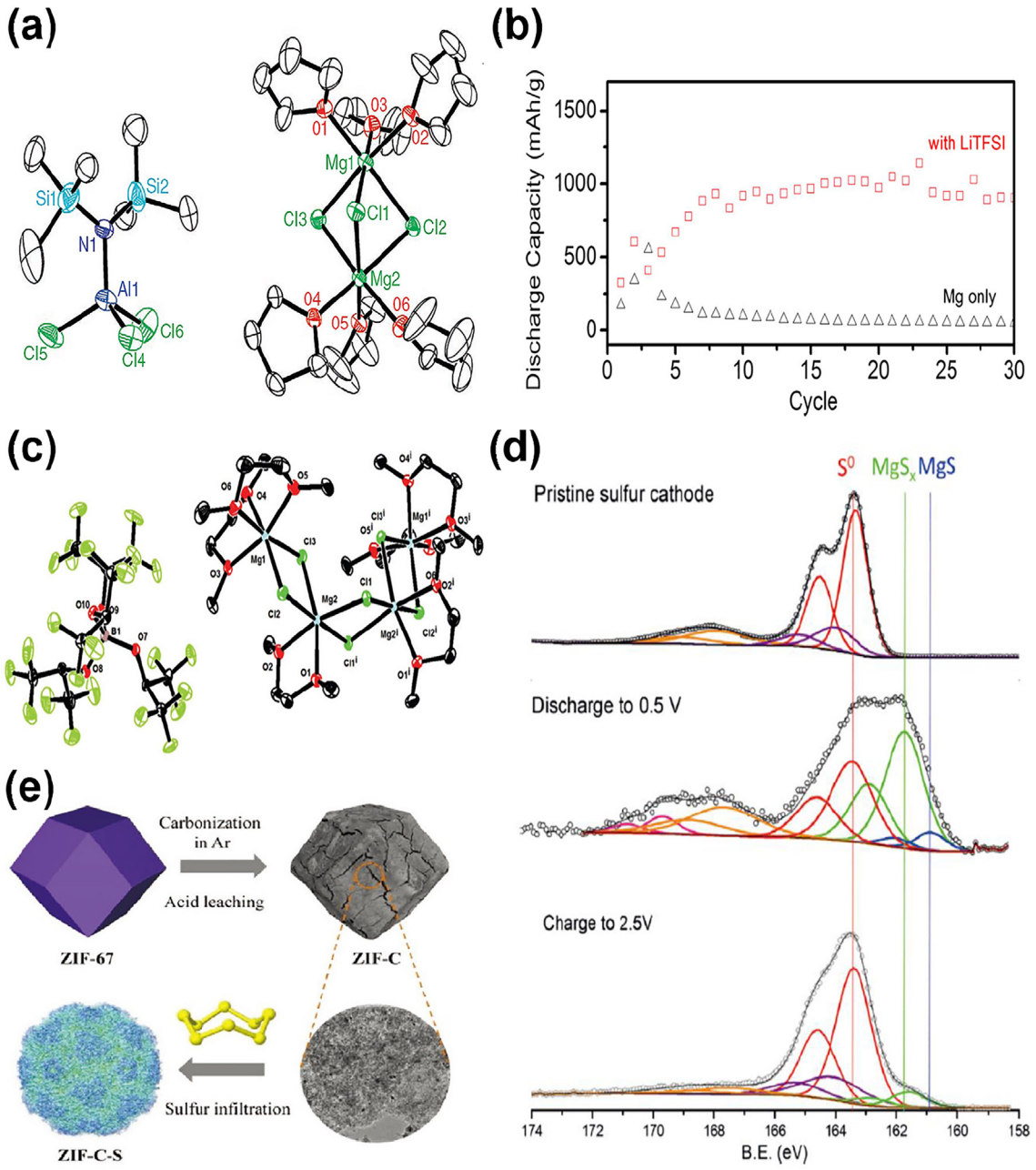

Fig 11. Advances in Mg-S batteries. (a) The structure of the crystallized product ($Mg_2(\mu\text{-}Cl)_3{\cdot}6THF)(HMDS_nAlCl_{4-n})$ (n = 1, 2) of the electrolyte used in the Mg-S battery. Reproduced with permission [187]. Copyright 2011, Springer Nature. (b) The cycling performance of the Mg-S battery with and without Li^+ mediation. Reproduced with permission [189]. Copyright 2015, American Chemical Society. (c) The structure of the crystalline $[Mg_4Cl_6(DME)_6][B(HFP)_4]_2$ used in the Mg-S battery. Reproduced with permission [190]. Copyright 2017, Wiley-VCH. (d) XPS curves of different states of the Mg-S battery. Reproduced with permission [193]. Copyright 2017, Wiley-VCH. (e) An illustration of the ZIF-S cathode. Reproduced with permission [194]. Copyright 2018, Wiley-VCH.

doped carbon derived from ZIF-67 as a sulfur host material (Fig. 11e). Through the use of a ternary electrolyte made up of $(HMDS)_2Mg$, $AlCl_3$, and LiTFSI in diglyme, at 1 C rate, an initial specific capacity of about 600 mAh g^{-1} and a preserved capacity of ~400 mAh g^{-1} were obtained for more than 200 cycles. What's more, even at higher rate of 5 C, the cells still delivered 300–400 mAh g^{-1}. Modifications to separators can also improve the electrochemical performances of Mg-S batteries. Yu and co-workers [195] modified the conventional separator (glassy fiber, GF) with a layer of activated carbon nanofibers. The cell's cycle stability was greatly enhanced compared to the ones without any modification. It showed an initial specific capacity of 1200 mAh g^{-1} and with a retention of more than 20 cycles at C/50. However, the cell with an unmodified separator showed a rapidly decayed capacity, i.e. no more than 400 mAh g^{-1} after 5 cycles. Similar to the case of the smaller sulfur molecule composite cathode used in Li-S and Na-S batteries, a sulfur cathode based on sulphide graphdiyne characterized with short sulfur energy-storing unites was coupled with a Grignard reagent-based electrolytes (a nucleophilic electrolyte) [196]. This may provide a new route to explore the potential use of Mg-S batteries.

Thanks to the much effort in previous research in Mg-S batteries, the reversibility and practical specific capacity of it have been greatly improved. The idea of the use of nonnucleophilic magnesium-based electrolytes has inspired researchers to develop different kinds of electrolytes for Mg-S batteries. Based on these

useful electrolytes, engineering of cathodes and separators becomes possible. In the future, modifications to the Mg anode are expected because large overpotential attributed to Mg anodes is very large [197]. Developing solid-state Mg-S batteries need to be paid attention since the development of magnesium solid ionic conductor such as $MgSc_2Se_4$ [198] is under way. Moreover, a big improvement in Mg-S batteries is highly expected based on the holistic design of all the components of it.

4.2. Al-S batteries

4.2.1. Electrolytes for Al-S batteries

Rechargeable aluminum-sulfur batteries have been little concerned until now. Room-temperature ionic liquid (RTIL) was widely used in nonaqueous Al-S batteries. Fig. 3(d) is a typical charge–discharge curve of the RT Al-S battery. Wang and co-workers [199] reported the first reversible Al-S battery with an ionic liquid electrolyte. The electrolyte was made through mixing $AlCl_3$ and 1-ethyl-3-methylimidazolium chloride (EMIC). The electrolyte's electrochemical stability was evaluated and shown in Fig. 12(a). A reaction mechanism in this system was proposed, as shown in Eqs. (25) and (26). The anion $Al_2Cl_7^-$ participated in the electrochemical reactions happening at both the anode and the cathode. The concentration of it had big influences on the overall

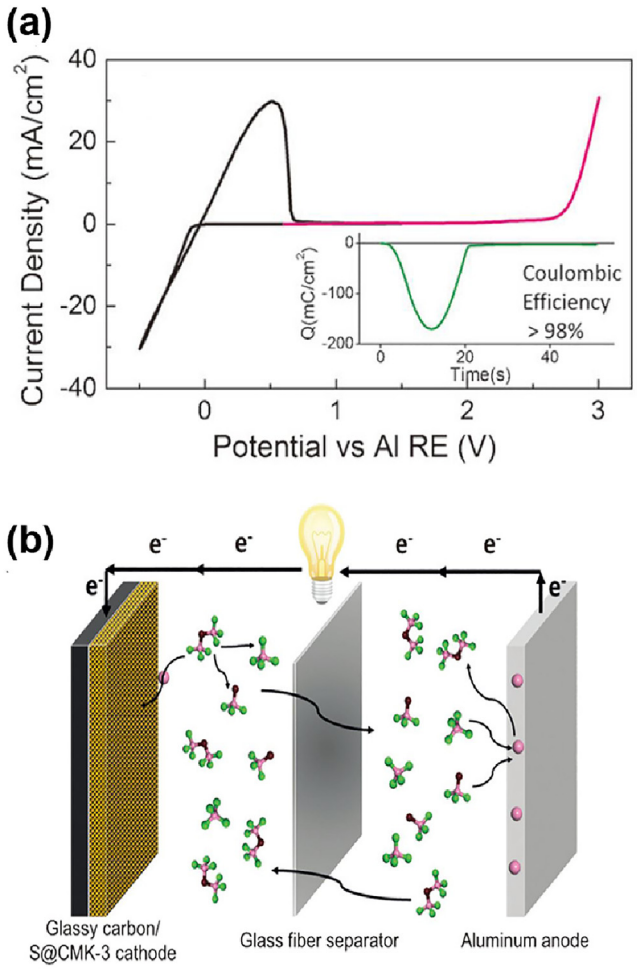

Fig 12. Advances in Al-S batteries. (a) Aluminum deposition/stripping in the EMIC: $AlCl_3$ (1:1.3) electrolyte (black) and the electrochemical stability of the electrolyte (pink), insert is the charge-time curve of aluminum deposition/stripping, glassy carbon was the working electrode, aluminum was both the counter and reference electrode. Reproduced with permission [199]. Copyright 2016, Wiley-VCH. (b) The discharge process of the Al-S battery with the NBMPBr/$AlCl_3$ electrolyte. Reproduced with permission [200]. Copyright 2018, Wiley-VCH.

electrochemical performance of Al-S batteries. With a sulfur/activated carbon cloth (ACC) composite cathode, the Al-S cell showed a discharge voltage plateau at ~0.65 V and charge voltage potential at 1.40 V at 0.05 A g^{-1}. A specific capacity of over 1000 mAh g^{-1} was achieved over 20 cycles.

$$2Al + 14AlCl^{4-} \rightleftarrows 8Al_2Cl_7^- + 6e^- \text{ (anode)} \quad (25)$$

$$Al_2Cl_7^- + 6e^- + 3S \rightleftarrows Al_2S_3 + 14AlCl^{4-} \text{ (cathode)} \quad (26)$$

Considering the present research, the rate-determining step of Al-S batteries should be determined by the electrolyte. Recently, Li and co-workers [200] utilized a kind of new ionic liquid composed of NBMPBr (N-Butyl-N-methylpiperidinium) and $AlCl_3$ as the electrolyte in Al-S batteries. At first, they took advantage of the EMIBr/$AlCl_3$ electrolyte, even though Al-S batteries using this electrolyte delivered high initial specific capacity, but it degraded rapidly because the electrophilic polysulfide intermediates reacted with the nucleophilic imidazole ring of EMI^+. So, they tried NBMPBr instead of EMIBr. Compared to the ionic liquid made up of EMIC and $AlCl_3$, the EMIBr/$AlCl_3$ electrolyte was easier to dissociate and had a higher reactivity towards sulfur cathodes. This was because Al_2Cl_6-Br^- had a higher formation energy and a smaller LUMO–HOMO gap than $Al_2Cl_6Cl^-$, which was confirmed by DFT calculations. In this point, the NBMPBr/$AlCl_3$ electrolyte shared some similarities with the EMIBr/$AlCl_3$ electrolyte. Fig. 12(b) is the discharge process of the Al-S battery enabled by the NBMPBr/$AlCl_3$ electrolyte. Al-S batteries utilizing this electrolyte and the CMK-3/S composite cathode showed an initial discharge capacity of 1390 mAh g^{-1} and retained more than 400 mAh g^{-1} after 20 cycles.

Similar to the mediation function of lithium ions in regulating the electrochemical performance of Mg-S batteries, Manthiram et al. [201] reported that the reversibility of Al-S batteries could be improved by Li^+ ion mediation. Conventional Al-S batteries using ionic liquids as the electrolyte undergo a solid-state electrochemical reaction, during which polysulfides shuttle disappears. However, after the addition of LiTFSI into the Al[EMI]Cl_4 electrolyte, the solubility of intermediate polysulfides in this ionic liquid was promoted and polysulfides shuttle came back. This was proven by the UV–visible absorption experiment, which showed that the solubility of S_4^{2-} species increased in the Li ion mediated electrolyte. It was the presence of Li ions that activated the short-chain Al polysulfides and the kinetic barrier in the reduction/oxidation of the discharged products was reduced. An initial specific capacity of more than 1000 mAh g^{-1} and a maintained capacity of up to 600 mAh g^{-1} was achieved in their Al-S batteries.

4.2.2. Cathodes for Al-S batteries

On the cathode part, Wan et al. [202] took advantage of carbonized HKUST-1 as the sulfur cathode host for Al-S batteries. The copper ions in carbonized HKUST-1 had a vital effect in regulating the interactions with lithium polysulfides through forming ionic clusters with polysulfides. The S@HKUST-1-C composite started to exhibit a reversible capacity of 600 mAh g^{-1} from the 75th cycle and maintained 460 mAh g^{-1} after 500 cycles.

Al-S batteries are still in its infancy and much research need to be conducted. There are still some uncertain things in the reaction mechanism of Al-S batteries using ionic liquid as the electrolyte. For example, many papers said the reduction of sulfur underwent a full solid-state reaction, but some observed the existence of soluble polysulfides. If there existed a large amount of polysulfides, it could diffuse to the anode side and cause shuttle effect like the phenomenon in Li-S batteries. Besides, as we can see, large voltage hysteresis and sluggish electrochemical rate still exist in present Al-S batteries, like the development of Mg-S batteries, there may

be a more suitable electrolyte for Al-S batteries. If a suitable electrolyte was developed, comprehensive design of Al-S batteries would be more practical.

In the conclusion of this part, because of the adaptability of sulfur composite cathodes, the improvements of Mg-S batteries and Al-S batteries are highly related to innovative designs of electrolytes. Table 5 gives a brief summary of important progress of both batteries. Reaction mechanisms are very different in prototypes with different electrolytes. If a robust system was established, much progress would be made.

5. Separators for metal-sulfur batteries

Separators in metal-sulfur batteries usually act as an electron-insulating and ion-conductive component to avoid the internal short-circuit of cells during cycling. Considering the polysulfides shuttle in metal-sulfur batteries, researchers redesigned the separator by coating active materials on the surface of conventional polypropylene (PP) or polyethylene (PE) membrane to alleviate polysulfides shuttle. The material development route for separators is quite similar to that of cathode host materials, from polymers, carbon materials, metal oxides and sulfides, to other polar emerging materials.

Zhang research group [203] reported a Nafion coated PP separator, which could regulate the ion transport between cathode and anode by selectively letting lithium ions go through while rejecting polysulfides. It should be ascribed to the existence of anionic SO_3^- on Nafion coated separator which could reject hopping of polysulfides because of the coulombic interactions. They optimized the amount of Nafion coated on the Celgard PP/PE/PP separator at 0.7 mg cm^{-2} because too less Nafion (0.15 mg cm^{-2}) couldn't spread the membrane while too much (3.5 mg cm^{-2}) could cause high polarization. Manthiram research group [204] investigated the use of sodiated Nafion membrane (Nafion 212) in RT Na-S batteries. It served as a sodium ion selective separator, which functioned similarly in Li-S batteries. Besides Nafion polymer coating, nanostructured carbon materials such as carbon nanotubes [205], graphene [59], graphene oxide [206] and activated carbon nanofibers [207] were widely used in modifying separators. For example, Zhang et al. [206] took advantage of GO-coated separator in Li-S batteries and improved the decay rate from 0.49% to 0.23% per cycle compared to the conventional separator.

Besides carbon materials, metal oxides, sulfides, nitrides and other metallic compounds showed promising performances in separator coating for Li-S batteries. Our group [208] engineered oxygen vacancies in TiO_2 (OVs-TiO_2) and made good use of it in Li-S batteries. The density of states of OVs-TiO_2 near Fermi energy level was quite different from original TiO_2. More polarized OVs-TiO_2 could adsorb more polysulfides. The cell enabled by OVs-TiO_2@PP separator showed 5.83 mAh cm^{-2} even at 7.1 g cm^{-2} sulfur loading after 100 cycles. Kim et al. [209] coated ferroelectric material $BaTiO_3$ particles on PE separator and found its distinctive mechanism in Li-S batteries. When an external electric field existed, permanent dipoles formed in $BaTiO_3$ particles and they didn't disappear even the field terminated. Poled $BaTiO_3$ rejected the transport of polysulfides and permitted the hooping of lithium ions because of electrostatic repulsion. With poled $BaTiO_3$ coated PE as the separator, the Li-S cell showed an initial capacity of 1122.1 mAh g^{-1} and retained 82.8% after 50 cycles. Tang et al. [210] reported the significant function of lithium conductive MoS_2/Celgard separator in Li-S batteries. Through comparing the electrochemical impedance spectra of three different Li-S cells enabled by conventional Celgard, GO/Celgard and MoS_2/Celgard separators, they found only one semicircle (R_{ct}, charge transfer) in the cell using the MoS_2/Celgard separator. Semicircles representing the insulating layer of Li_2S_2/Li_2S between cathode and separator or on the surface of lithium anode were disappeared. This result disclosed the effective function of MoS_2/Celgard separator in depressing polysulfides shuttle. Besides metal oxides and sulfides, antimony selenide with Se deficiencies (Sb_2Se_{3-x}) was composited with rGO to coat the separator in high-loading Li-S batteries [211]. It may intrigue more interest in metal chalcogenides for Li-S batteries. In order to maximize the advantages of different metal compounds, heterostructured materials were developed to bring

Table 5
Progress in rechargeable magnesium-sulfur (Mg-S) and aluminium-sulfur (Al-S) batteries.

Electrolyte	Cathode materials	Voltage window	Electrochemical performance (capacity unit, mAh g^{-1})	Ref. & year
Mg-S batteries				
Non-nucleophilic $(HMDS)_2Mg$ based glyme electrolytes	CMK-3-sulfur composite	0.5–2.1 (V vs. Mg^{2+}/Mg)	800 (initial) (second 350, stable at 260 for 20 cycles) at 0.02 A g^{-1}	[188] 2015
Mg-HMDS and LiTFSI	Activated carbon cloth-sulfur composite	0.5–3.0 (V vs. Mg^{2+}/Mg)	1000 (maximum) (stable for 30 cycles) at 0.071 A g^{-1}	[189] 2015
Boron-centered anion-based magnesium electrolyte	Disordered mesoporous carbon–sulfur composite	0.5–2.8 (V vs. Mg^{2+}/Mg)	1081 (initial) (86.4% after 30 cycles) at 0.05 A g^{-1}	[190] 2017
$[Mg_4Cl_6(DME)_6][B(HFP)_4]_2$ in DME	Carbon nanotubes-sulfur composite	0.4–2.0 (V vs. Mg^{2+}/Mg)	1247 (maximum) (80.4% after 100 cycles) at 0.16 A g^{-1}	[191] 2017
$(HMDS)_2Mg$ and LiTFSI in diglyme	ZIF-67 derived carbon–sulfur composite	0.3–3.0 (V vs. Mg^{2+}/Mg)	600 (stable above ~400 for 100 cycles) at 1 C rate	[194] 2018
$MgCl_2$ and YCl_3 (1:2) in $PYR_{14}TFSI$	MgS_8 catholyte, graphene-carbon nanotube matrix	0.3–2.4 (V vs. Mg^{2+}/Mg)	More than 1000 mAh g^{-1} for 50 cycles	[177] 2019
Al-S batteries				
Chloroaluminate room temperature ionic liquid electrolyte	Sulfur and Ketjen black carbon	0.5–1.9 (V vs. Al^{3+}/Al)	A sixth discharge capacity of 1400 mAh g^{-1} at 0.05 A g^{-1}	[263] 2015
$AlCl_3$ in 1-ethyl-3-methylimidazolium chloride	Activated carbon cloth-sulfur composite	0.2–1.6 (V vs. Al^{3+}/Al)	Over 1000 mAh g^{-1} for 20 cycles	[199] 2016
$AlCl_3$ in 1-ethyl-3-methylimidazolium chloride	S@HKUST-1-C	0.1–1.8 (V vs. Al^{3+}/Al)	1200 mAh g^{-1} (initial) and 500 mAh g^{-1} after 500 cycles	[202] 2019
$AlCl_3$/acetamide	S@CMK-3	0.2–1.6 (V vs. Al^{3+}/Al)	1500 mAh g^{-1} (initial) (stable at 500 mAh g^{-1} for 60 cycles)	[178] 2019

its functional interfaces into play in Li-S batteries. Zhao et al. [212] reported CoO decorated Co_9S_8 heterostructures through one-pot carbothermal reduction. The synergistic adsorption-electrocatalysis mechanism made Co_9S_8/CoO-G coated separator very effective in Li-S batteries. It showed the best 925 mAh g^{-1} and a decay rate of 0.049% per cycle in 1000 cycles. Yang et al. [213] reported the synthesis of heterostructured twinborn TiO_2-TiN particles, which were mixed with graphene as a separator coating layer in Li-S batteries. The synergy of TiO_2 and TiN enabled the heterostructure to provide both high adsorption of polysulfides and fast electron transfer.

Phosphorene was found to be a potential polysulfide immobilizer and catalyst for Li-S batteries [214]. The intriguing characteristic of few layer phosphorene (FLP) was that it had a very high electrical conductivity of ~450 S cm^{-1}, higher than other reported oxides and carbon nitride. What's more, the low synthesis price of FLP was also very fascinating. Black phosphorus was reported by Sun et al. [215] to act as separator modification layer materials. In situ Raman tests corroborated the effective trapping of polysulfides of black phosphorus. And ex situ XPS confirmed the interaction between black phosphorus and polysulfides through both a P-S and P-Li bonds. Zhou et al. [216] reported the MOF@GO coated separator used in Li-S batteries. Crystalline MOF nanoparticles and GO layers were formed adjacently. The polysulfide permeation test showed that the MOF@GO coated separator could effectively block polysulfides over time while GO coated separator couldn't. Coupled with CMK-3/sulfur cathode, the cell showed the first capacity of 1126 mAh g^{-1} and retained 799 mAh g^{-1} at the 500th cycle. Recently, Yang et al. [217] synthesized in-situ crafted well-distributed TiO_2 nanoparticles on MXene sheets and the surface fluorine is removed largely. Mxenes were characterized by its 2D high electronic conductive structures. $Ti_3C_2T_x$ after 4 h hydrothermal reaction had the highest conductivity of 1490 S cm^{-1}. $Ti_3C_2T_x$ was composited with graphene nanosheets to coat the separator. At an ultrahigh sulfur loading of 7.3 mg cm^{-2}, the cell retained 57.7% at 0.2 C after 200 cycles.

Compared to the boom of separators in Li-S and Na-S batteries, the developments of separators in Mg-S and Al-S are slow [218,219]. Fortunately, the functions of separators in metal-sulfur batteries are similar in suppressing polysulfides shuttle. Progress in any kind of metal-sulfur batteries can inspire the others. Zhou et al. [218] designed a sandwiched multifunctional separator for Mg-S and Li-S batteries. It was composed of a copper nanowire-graphene nanosheet (CuNWs-GN) film, electrospinning polyimide (PI) nonwovens and a rigid lithium lanthanum zirconium oxide-polyethylene oxide (LLZO-PEO) film. The PI nonwovens provided a stable support and were flame-retardant. The rigid LLZO-PEO film could suppress the growth of lithium dendrites. The CuNWs-GN film was powerful in blocking polysulfides. With this separator, Mg-S batteries that operated at 50 °C showed a stable specific capacity of 915.3 mAh g^{-1} at 0.1 A g^{-1} after 25 cycles. Li-S batteries with this separator at 80 °C showed an initial specific capacity of 1402.1 mAh g^{-1} at 0.1 A g^{-1} and a decay rate of 0.24% in 300 cycles at 0.5 A g^{-1}. It's obvious that the reaction kinetics of Mg-S batteries were slow compared to Li-S batteries. For Al-S batteries, Yu et al. modified the glassy fiber (GF) separator with a thin layer of single walled carbon nanotubes (SWCNT) [220]. The function of the SWCNT thin layer here was to help alleviate high-order polysulfides (S_6^{2-}) and reduce the polarizations of Al-S batteries. The illustration of the mechanism of it is shown in Fig. 13(d). With this layer, the Al-S batteries delivered more than 600 mAh g^{-1} while the batteries with pure GF delivered less than 300 mAh g^{-1} in the 8 cycles.

In conclusion of this part, it's very clear that materials for sulfur cathode host materials are also widely used in separator coating. Different ion sieves capable of repelling polysulfides and permitting lithium ions have been constructed on separators, such as Nafion coating, metal oxides, sulfides and their heterostructures coating, emerging nanomaterials coating such as MOFs, Mxenes and so on. It's noteworthy that present research is mainly on separator coating for Li-S and Na-S batteries, novel separators for Mg-S and Al-S batteries need to be developed in the future.

6. In situ/in operando characterization techniques for rechargeable metal-sulfur batteries

Batteries are a very sophisticated system, where cathodes, electrolytes, anodes and other components change instantly and continuously during the electrochemical process. The mechanism of the emerging high-energy batteries such as metal-sulfur batteries is often unclear. Only when the mechanism is elucidated clearly can we improve the overall electrochemical performance in a right and efficient way. While it's hard for traditional characterization techniques (ex situ characterization techniques) to qualify for capturing the intermediate states of the components of batteries and the clear processes during charging/discharging. Fortunately, in situ/in operando characterization tools [221–227] (such as in situ XRD [228–231], in situ TEM [97,224,232–238], in situ AFM [239–242]) provide a real-time monitoring method to observe the electrochemical process of energy storage devices, such as nanowires powered devices [222] and rechargeable metal-sulfur batteries [221]. The term "in situ" means "on site", it means that data is collected at the site of the experiment. The term "in operando" means "in operation", i.e. the experiment is conducted at conditions similar to the real-life operating condition [1,243]. For example, if we carried out an XRD experiment while a specimen was being heated, the experiment was carried out "in situ". If the heating conditions were the same as the operating conditions of the material, it was also "in operando". The electrochemical reduction and oxidation of sulfur are complex during which many polysulfides molecules are generated and sometimes the intermediates disappear rapidly. It's very hard for ex situ characterization methods to capture the signals of these polysulfides intermediates. However, in situ techniques such as in situ X-ray absorption near-edge structure (XANES) [244–246] test can be equal to this both qualitatively and quantificationally. In this part, we will review on the effective in situ/in operando characterization techniques used in metal-sulfur batteries, especially in Li-S batteries.

In order to record the phase changes of the cathode/anode crystal materials during lithium insertion/deinsertion real-timely, in situ/in operando XRD characterization methods have been widely used in the area of lithium ion batteries. In metal-sulfur batteries, only sulfur and lithium sulfide are crystalized, it's very hard to use in situ XRD to characterize the intermediate electrochemical process of sulfur reduction/oxidation. Cui et al. [230] pioneered the use of in operando XRD in Li-S batteries. Recently, Villevieille et al. [231] reported that they observed the existence of lithium polysulfides by in operando XRD test through the strong interactions between long-chain polysulfides and SiO_2. As shown in Fig. 14(a), two broad peaks at 25.56° and 28.32° appeared during the electrochemical process of a Li-S cell containing fumed SiO_2 as the electrolyte additive. Inspired by this strong interaction, they achieved a high- performance Li-S cell with SiO_2 compared to the cell without SiO_2. In order to investigate the mechanism of Mg-S batteries, Dominko et al. [247] took advantage of some in operando characterizations such as in operando XRD, XANES and resonant inelastic X-ray scattering (RIXS). In operando XRD showed the disappearance of sulfur diffraction peaks and the emergence of diffraction peaks from MgS. The crys-

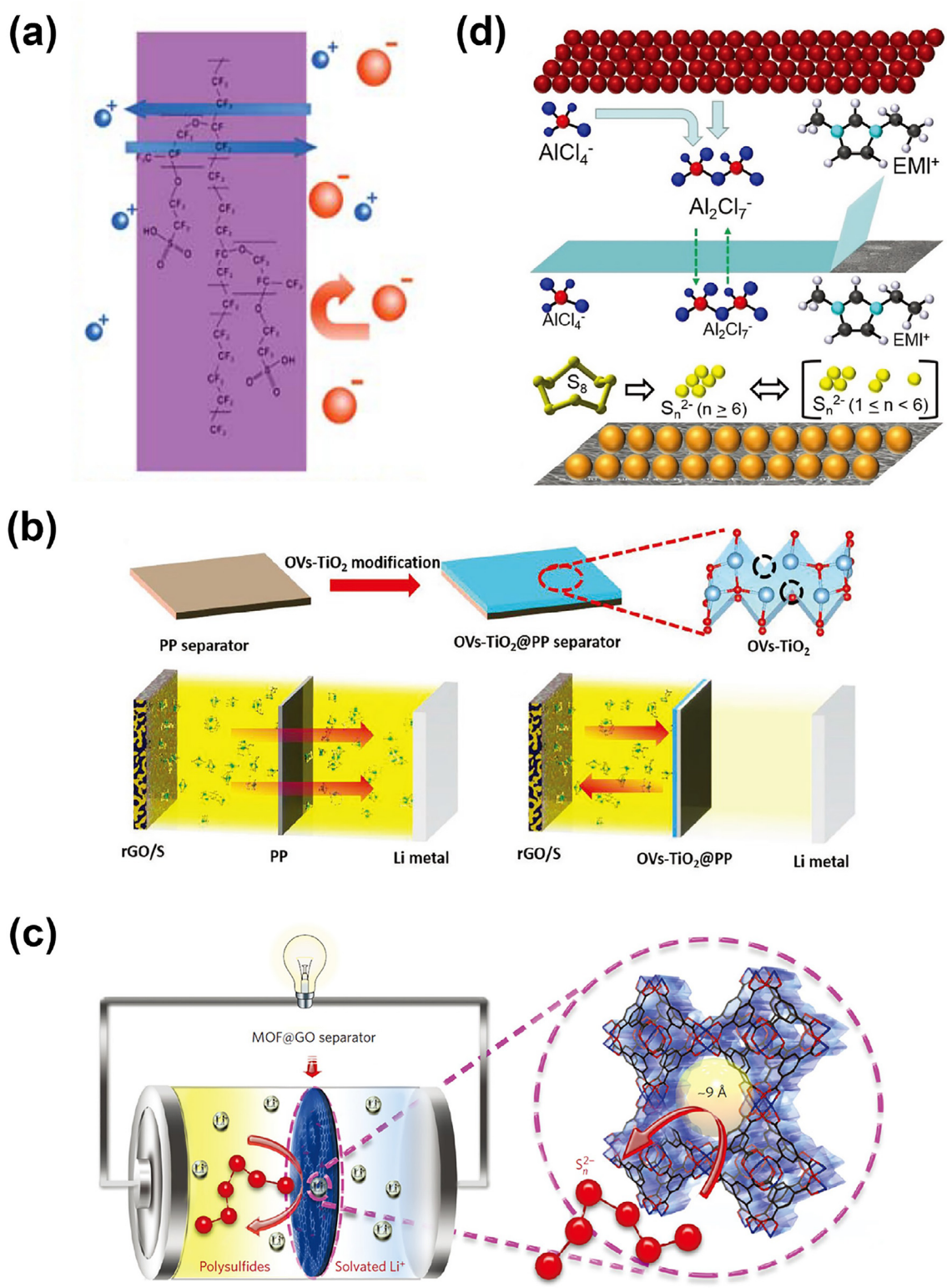

Fig 13. Separators used in metal-sulfur batteries. (a) The mechanism of Nafion in repelling polysulfides and permitting lithium ions. Reproduced with permission [203]. Copyright 2014, Royal Society of Chemistry. (b) The fabrication process and mechanism in inhibiting polysulfides of OVs-TiO_2@PP separator. Reproduced with permission [208]. Copyright 2020, Wiley-VCH. (c) Schematic MOF@GO separator in sieving soluble polysulfides. Reproduced with permission [216]. Copyright 2016, Springer Nature. (d) An illustration of the mechanism of the reported Al-S batteries. Reproduced with permission [220]. Copyright 2017, Wiley-VCH.

talline structure of MgS was similar to wurtzite, which also indicated large volume changes during electrochemical charge/discharge in Mg-S batteries.

In situ TEM provides a powerful tool to monitor the structural evolution of electrode materials during an electrochemical process (lithium or sodium insertion/deinsertion), especially in SnO_2 [234], Sn [235], Si [236] and P [237] anodes. The volume changes of sulfur cathodes (up to after lithiation) are strong enough to destroy the electrode structure which will deteriorate the performance of the electrodes. It is of great importance to visualize the morphological

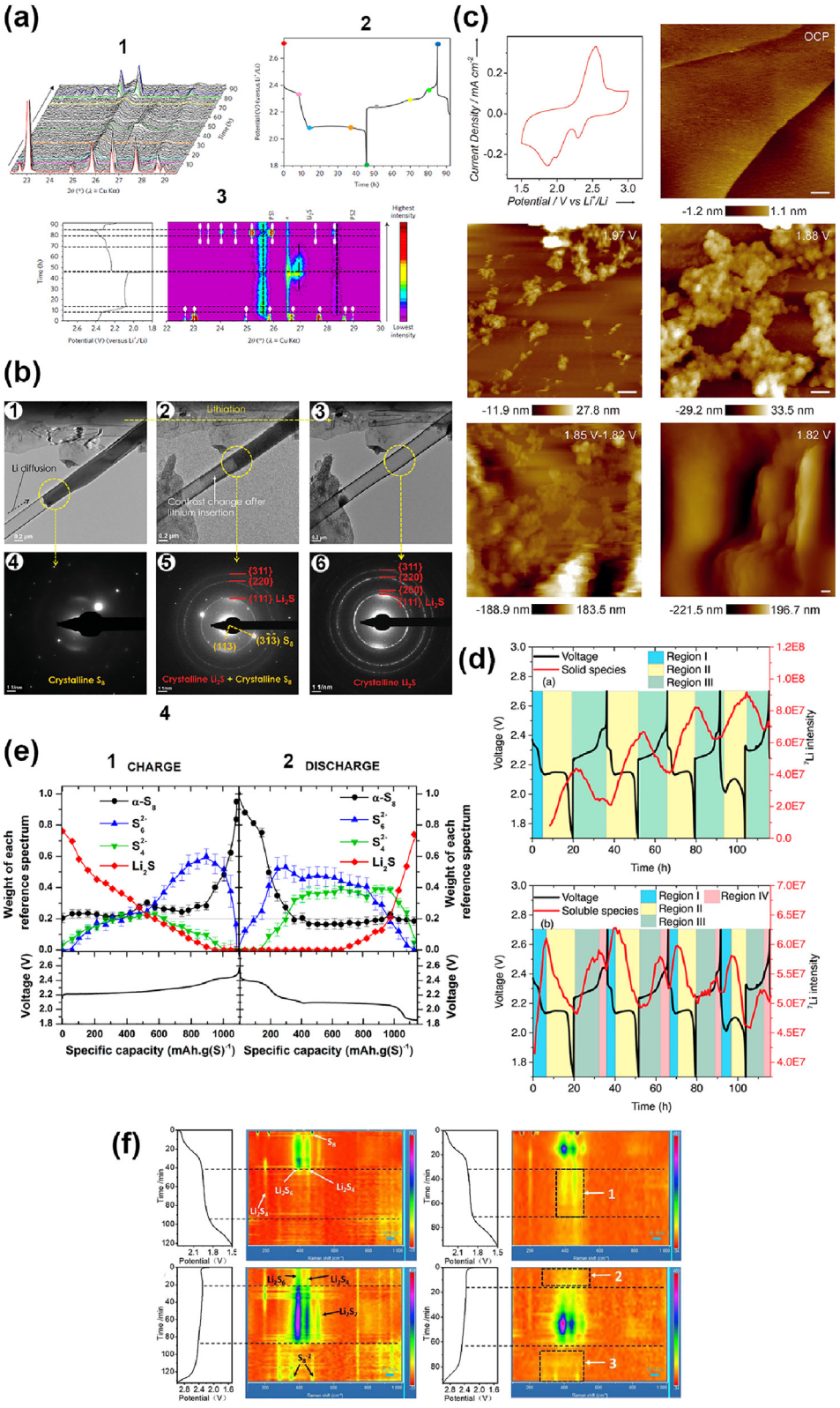

Fig 14. In situ characterization techniques for metal-sulfur batteries. In situ XRD: (a) The waterfall curve of XRD patterns (1), the corresponding galvanostatic curve (2), and the intensity chart is given at the right of XRD contour part (3). Reproduced with permission [231]. Copyright 2017, Springer Nature. In situ TEM: (b) TEM images taken during lithiation of sulfur nanoconfined in a CNT reaction vessel (1–3), and their corresponding EDP patterns (4–6). Reproduced with permission [248]. Copyright 2015, Wiley-VCH. In situ AFM: (c) The representative cyclic voltammetry curve of the first cycling in a lithium polysulfides (Li/PS) cell (1), and (2–6) AFM topography images of highly oriented pyrolytic graphite (HOPG) in an in situ Li/PS cell at various potentials. Reproduced with permission [242]. Copyright 2016, Wiley-VCH. In situ NMR: (d) Formation of solid species in Li-S batteries upon cycling. Reproduced with permission [251]. Copyright 2017, American Chemical Society. In situ XANES: (e) Evolution of sulfur K-edge XANES upon the electrochemical cycle based on linear combination analysis shown upon (1) charge and (2) discharge at a 0.1 C rate. Reproduced with permission [244]. Copyright 2013, American Chemical Society. In situ Raman: (f) The discharge (upper left) and charge (bottom left) process of the S@Nafion@GDY electrode, the discharge (upper right) and charge (bottom right) process of the S@GDY@Nafion electrode. The selected rectangular areas 1, 2 and 3 are the significant variations in the Raman spectra. Reproduced with permission [253]. Copyright 2020, Elsevier.

evolution of sulfur cathodes and guide the innovative design of sulfur composite cathodes. Yushin et al. [248] monitored the direct lithiation of sulfur confined in a cylindrical carbon (carbon nanotubes, CNT) pore through in situ TEM for the first time. Fig. 14 (b) showed the sample evolution during the lithiation process. They found that lithiation front was flat and oriented perpendicular to the confined sulfur cylinder. The lithiation process propagated along the cylinder length. They proposed that lithium ions had three transport ways: (1) Through the bulk of CNT; (2) through the surface of CNT; (3) through the bulk of Li_2S. At the same time, electrons had two transport ways: (1) Through the bulk of CNT; (2) along the Li_2S/S interface. The latter way was reasonable because it was confirmed by DFT calculations, which showed that energy bandgap disappeared in the intermediate lithiation product Li_2S_8.

In situ AFM is widely used to probe the interface between electrolyte and electrode in lithium batteries. Wan et al. [241] reported a series of in situ AFM study on the interfacial process of Li-S batteries. They took advantage of electrochemical atomic force microscopy (EC-AFM) to characterize the interphase process and mechanism in Li-S batteries. They found that the morphologies of Li_2S_2 and Li_2S were different and they existed in nanoparticles and lamella sediments respectively (Fig. 14c). The electrochemical performance degradation was ascribed to the unreversed deposition of some Li_2S_2 nanoparticles. Recently, they reported a protective LiF interface film was formed at high-temperature (60 °C) Li-S batteries [240]. It could trap polysulfides and form an amorphous film, which provided effective protection of polysulfides intermediates and alleviated polysulfides shuttle. The results confirmed the potential application of lithium bis(fluorosulfonyl) imide (LiFSI) salt for Li-S system. These exciting results have proven the effective function of in situ AFM in detecting the interface morphology.

Taking advantage of the ^{7}Li signal (spin value is 3/2, 92.5% abundance), in situ NMR is well applied to monitor the evolution of lithium polysulfides (both soluble and insoluble) [249–252]. Nazar et al. [251] observed the temporal speciation of Li-S batteries through in situ NMR. There exist three Li environments in the spectrum, one is at around −0.06 ppm (signals of solid lithium-containing species), and the other two are at around 3.67 ppm and −0.16 ppm (signals of soluble lithium-containing species). As shown in Fig. 14(d), through the monitoring of soluble and solid species through in situ NMR, a four-step evolution during a complete charge/discharge cycle can be seen. First is the formation of soluble species because of the reaction between elemental sulfur and lithium; second is the consumption of soluble species due to solid species formation; third is the formation of soluble species through the decomposition of solid species; fourth is the consumption of soluble species due to the formation of elemental sulfur. Peaks at around 250 ppm are ascribed to Li metal. Interestingly, the differences between the chemical shifts of Li metal can distinguish dendritic/mossy (247 ppm) lithium from lithium metal (259 ppm).

Synchrotron X-ray absorption spectroscopy (XAS) can detect element-specific information no matter the material is crystalline or not. The spectrum of XAS is made up with the pre-edge, XANES and the extended X-ray absorption fine structure (EXAFS). Through detecting sulfur K-edge spectrum, different sulfur-containing species can be identified [244,245]. Nazar et al. [244] used in operando XANES technique to monitor sulfur or lithium polysulfides. It was worth mentioning that radical anion ($S_3^{\cdot -}$) was observed and characterized by a pre-peak at around 2468.5 eV. As shown in Fig. 14 (e), through making a linear combination analysis of S K-edge XANES during a charge/discharge cycle, changes of polysulfides intermediates are depicted.

Because in situ Raman spectroscopy [253–256] is sensitive to the signals of sulfur and lithium polysulfides, it was used to monitor the electrochemical reaction process of Li-S batteries. In order to distinguish the heterostructure of S@Nafion@GDY in regulating the polysulfides in Li-S batteries, Li et al. [253] took advantage of in situ Raman to track the changes of polysulfides during discharge and charge processes in S@Nafion@GDY- and S@GDY@Nafion-enabled Li-S batteries. During discharge, the reaction kinetics of Li_2S_6 and Li_2S_4 were slow in the S@GDY@Nafion electrode, which resulted in the phenomenon in rectangular area 1 (Fig. 14f). During charge, the retarded appearance of Li_2S_6 and Li_2S_4 in rectangular area 2 (Fig. 14f) and weak signals of Li_2S_8 in rectangular area 3 (Fig. 14f) confirmed the Nafion@GDY could accelerate the phase transformation. Moreover, in situ Raman can monitor the interactions between polysulfides and $VOPO_4$ host. Zhou et al. [255] found that the Raman peaks didn't increase after 75 min when $VOPO_4$ host aged in the Li_2S_6 solution. This should be ascribed to the saturation of the adsorption of polysulfides.

We have summarized many useful in situ techniques in this part for metal-sulfur batteries, including in situ XRD (phase transformation), in situ TEM (morphology evolution), in situ AFM (surface tomography), in situ NMR (soluble polysulfides), in operando XANES (soluble polysulfides) and in situ Raman (soluble polysulfides). There also exist many other useful in situ/in operando characterization techniques for metal-sulfur batteries, such as transmission X-ray microscopy (TXM) [257], X-ray fluorescence microscopy [258], ultraviolet visible (UV–vis) absorption spectroscopy [259–261], which will not be discussed in detail. In situ electrochemical method such as in situ EIS test of Li-S batteries during discharge and charge was achieved by a four-electrode Li/CP/CP/Li configuration. [262] In situ characterization techniques are still under rapid developments and we believe the progress in this area will have great advancements in exploring the underlying mechanisms and methods of performance optimizations of battery materials. For example, in situ characterization of strain during cycling of batteries is a very good direction. Much work has been done on Li-S batteries whereas minor was on RT Na-S, Mg-S and Al-S batteries. In the future, much attention should be paid to the latter and the mechanism behind them will be elucidated in a clearer way.

7. Conclusions and outlook

In conclusion, developments of high-energy rechargeable metal-sulfur batteries are of big significance to the storage of renewable energy. Various materials have been taken advantage of to realize high-performance Li-S batteries, including carbon materials, polymers, metal oxides and sulfides and other emerging nanomaterials. Li-S batteries are the most prominent candidate for high-energy storage amongst not only metal-sulfur batteries but also lithium batteries. Polar host materials have been sought after mainly on sulfur composite cathodes and separators of Li-S batteries. Appropriate ones bind polysulfides efficiently while not decomposing it. Anode protection is gaining more and more interest. Solid-state electrolyte may be a good solution to Li-S batteries, because it can solve the safety issues related to lithium anode and flammable organic electrolytes. RT Na-S batteries designed for low-cost large-scale electrical energy storage is worth anticipation. Prototypes based on microporous carbon–sulfur composite based composite cathodes coupled with carbonate electrolytes are attracting more and more attention. Developments of new electrolytes have been paid much attention to by many researchers. Research results on sodium metal anode aimed at realizing practical low-cost Na-S batteries are exciting at present. When it comes to terms with the volumetric energy density, magnesium or aluminum based batteries are very fascinating. Even though belonging to metal-sulfur batteries like Li-S and Na-S batteries, the reaction

mechanisms of Mg-S and Al-S batteries are quite different because of the different electrolyte used. Nucleophilic magnesium organohaloaluminate electrolyte has been developed to serve as electrolytes for rechargeable Mg-S batteries. In the same way, electrolytes based on an ordinary ionic liquid were developed for rechargeable Al-S batteries. In that case, polysulfides shuttle no longer exists. When coupled with sulfur counterpart, practical performances of Mg-S and Al-S batteries need to be under deep consideration. The electrolyte is still the stumbling block on the road to achieving high-performance Mg-S and Al-S batteries.

For the perspectives of future developments, Li-S batteries are promising in its industrialization before which several issues need to be solved. (i) Through composite cathodes engineering, sulfur loading of more than 15 mg cm^{-2} at low E/S ratio can be achieved. In the future, only when high-areal-loading sulfur was achieved would the application of Li-S batteries seem practical. New synthetic method may be an innovative way to give a solution [263,264]. (ii) Safety issues related to lithium anode should be given a good solution. Moreover, thermal management including experiments and simulations of Li-S batteries like Na-ion batteries [265] need to be investigated more. Nanostructured carbon materials including graphene have been demonstrated to play a crucial role in lithium anode protection. As a bright alternative way, solid-state electrolyte may be a holy grail for Li-S batteries. Solid-state electrolyte materials with lithium super ionic conductor (LISICON), sodium super ionic conductor (NASICON) or garnet structures are promising. Towards low-cost large-scale stationary energy storage, Na-S batteries are of great potential to come into play. Future directions for improvements are listed below. (i) Thermodynamics and kinetics of the reaction mechanisms of Na-S batteries are highly in demand. It will guide the developments of composite cathode materials for Na-S batteries. (ii) Low sulfur loading of microporous carbon–sulfur composites is a big hurdle. Innovative methods are needed. (iii) Similar to lithium metal protection, sodium metal anode protection is significant to the developments of Na-S batteries. As for rechargeable Mg-S and Al-S batteries, large amount of work needs to be conducted in the fundamental research especially in developing suitable electrolytes. Since Mg^{2+} and Al^{3+} ions possess higher charge density compared to Li^{+} and Na^{+} ions, it will make them difficult to participate in sulfur redox reactions. What's more, the strong solvation effect of Mg^{2+} and Al^{3+} ions will also impede the electrochemical reactions. Organic chemists can do much more than material scientists. Optimizing non-nucleophilic electrolytes is a right direction to proceed for Mg-S batteries. Commonly used glyme electrolytes are also a reasonable choice. Besides electrolytes, the electrochemical activity of Mg anodes has been found to be very low and should be improved if we wanted to achieve better battery performances. High-cost room temperature ionic liquids are widely used in non-aqueous aluminum-ion batteries and it applies to Al-S batteries. The slow reaction kinetics of present Al-S batteries should be considered more. These issues are all relied on the developments of suitable electrolytes (lower cost, lower dissociation barrier) for Al-S batteries. On new prototypes, flexible batteries are a very promising direction. On implementing emerging technologies, 3D printing [266] has been used to enable advanced battery manufacturing. We believe there is a bright future for the developments of rechargeable metal-sulfur batteries. What's more, it can give insights on sulfur redox chemistries and so on.

Declaration of Competing Interest

The authors declare that they have no known competing financial interests or personal relationships that could have appeared to influence the work reported in this paper.

Acknowledgments

This work was supported by the National Natural Science Foundation of China (51702247, 51832004, 51521001), the National Key Research and Development Program of China (2020YFA0715004, 2016YFA0202603), the Natural Science Foundation of Hubei Province (2019CFA001), the Foshan Xianhu Laboratory of the Advanced Energy Science and Technology Guangdong Laboratory (XHT2020-003).

References

[1] C.P. Grey, J.M. Tarascon, Nat. Mater. 16 (2017) 45–56.
[2] D.S. Ginley, D. Cahen, Fundamentals of Materials for Energy and Environmental Sustainability, Cambridge University Press, 2011.
[3] R.A. Huggins, Energy Storage, Springer, 2010.
[4] S. Chu, A. Majumdar, Nature 488 (2012) 294.
[5] S. Chu, Y. Cui, N. Liu, Nat. Mater. 16 (2017) 16–22.
[6] A. Polman, M. Knight, E.C. Garnett, B. Ehrler, W.C. Sinke, Science 352 (2016) aad4424.
[7] N.S. Lewis, Nat. Nanotechnol. 11 (2016) 1010.
[8] M.S. Faber, S. Jin, Energy Environ. Sci. 7 (2014) 3519–3542.
[9] L. Mai, X. Tian, X. Xu, L. Chang, L. Xu, Chem. Rev. 114 (2014) 11828–11862.
[10] L.-Q. Mai, F. Yang, Y.-L. Zhao, X. Xu, L. Xu, Y.-Z. Luo, Nat. Commun. 2 (2011) 381.
[11] J. Lu, Z. Chen, Z. Ma, F. Pan, L.A. Curtiss, K. Amine, Nat. Nanotechnol. 11 (2016) 1031.
[12] D. Larcher, J.-M. Tarascon, Nat. Chem. 7 (2015) 19.
[13] J.B. Goodenough, K.-S. Park, J. Am. Chem. Soc. 135 (2013) 1167–1176.
[14] J.B. Goodenough, Y. Kim, Chem. Mat. 22 (2009) 587–603.
[15] J.R. Croy, A. Abouimrane, Z. Zhang, MRS Bull. 39 (2014) 407–415.
[16] K. Amine, R. Kanno, Y. Tzeng, MRS Bull. 39 (2014) 395–401.
[17] J. Muldoon, C.B. Bucur, T. Gregory, Chem. Rev. 114 (2014) 11683–11720.
[18] D.A. Boyd, Angew. Chem. Int. Ed. 55 (2016) 15486–15502.
[19] A. Manthiram, Y. Fu, S.-H. Chung, C. Zu, Y.-S. Su, Chem. Rev. 114 (2014) 11751–11787.
[20] G.A. Elia, K. Marquardt, K. Hoeppner, S. Fantini, R. Lin, E. Knipping, W. Peters, J.-F. Drillet, S. Passerini, R. Hahn, Adv. Mater. 28 (2016) 7564–7579.
[21] N.N. Greenwood, A. Earnshaw, Chemistry of the Elements, Elsevier, 2012.
[22] X. Ji, K.T. Lee, L.F. Nazar, Nat. Mater. 8 (2009) 500.
[23] P.G. Bruce, S.A. Freunberger, L.J. Hardwick, J.-M. Tarascon, Nat. Mater. 11 (2012) 19.
[24] T. Oshima, M. Kajita, A. Okuno, Int. J. Appl. Ceram. Technol. 1 (2004) 269–276.
[25] Z. Wen, J. Cao, Z. Gu, X. Xu, F. Zhang, Z. Lin, Solid State Ion. 179 (2008) 1697–1701.
[26] D. Kumar, S.K. Rajouria, S.B. Kuhar, D.K. Kanchan, Solid State Ion. 312 (2017) 8–16.
[27] A. Manthiram, X. Yu, Small 11 (2015) 2108–2114.
[28] Y.-X. Wang, B. Zhang, W. Lai, Y. Xu, S.-L. Chou, H.-K. Liu, S.-X. Dou, Adv. Energy Mater. 7 (2017) 1602829.
[29] A. Manthiram, Y. Fu, Y.-S. Su, Acc. Chem. Res. 46 (2012) 1125–1134.
[30] Y. Yang, G. Zheng, Y. Cui, Chem. Soc. Rev. 42 (2013) 3018–3032.
[31] Q. Pang, X. Liang, C.Y. Kwok, L.F. Nazar, Nat. Energy 1 (2016) 16132.
[32] N.P. Yao, L.A. Heredy, R.C. Saunders, J. Electrochem. Soc. 117 (1970) C247.
[33] J. Wang, J. Yang, J. Xie, N. Xu, Adv. Mater. 14 (2002) 963–965.
[34] Y.V. Mikhaylik, J.R. Akridge, J. Electrochem. Soc. 151 (2004) A1969.
[35] S. Xin, L. Gu, N.-H. Zhao, Y.-X. Yin, L.-J. Zhou, Y.-G. Guo, L.-J. Wan, J. Am. Chem. Soc. 134 (2012) 18510–18513.
[36] Z. Li, L. Yuan, Z. Yi, Y. Sun, Y. Liu, Y. Jiang, Y. Shen, Y. Xin, Z. Zhang, Y. Huang, Adv. Energy Mater. 4 (2014) 1301473.
[37] S. Zhang, K. Ueno, K. Dokko, M. Watanabe, Adv. Energy Mater. 5 (2015) 1500117.
[38] G. Zhou, D.-W. Wang, F. Li, P.-X. Hou, L. Yin, C. Liu, G.Q.M. Lu, I.R. Gentle, H.-M. Cheng, Energy Environ. Sci. 5 (2012) 8901–8906.
[39] Q. Pang, D. Kundu, L.F. Nazar, Mater. Horizons 3 (2016) 130–136.
[40] H.-J. Peng, J.-Q. Huang, X.-Y. Liu, X.-B. Cheng, W.-T. Xu, C.-Z. Zhao, F. Wei, Q. Zhang, J. Am. Chem. Soc. 139 (2017) 8458–8466.
[41] L. Kong, X. Chen, B.-Q. Li, H.-J. Peng, J.-Q. Huang, J. Xie, Q. Zhang, Adv. Mater. 30 (2018) 1705219.
[42] S.S. Zhang, J. Power Sources 231 (2013) 153–162.
[43] M. Wild, L. O'neill, T. Zhang, R. Purkayastha, G. Minton, M. Marinescu, G.J. Offer, Energy Environ. Sci. 8 (2015) 3477–3494.
[44] Z.W. Seh, Y. Sun, Q. Zhang, Y. Cui, Chem. Soc. Rev. 45 (2016) 5605–5634.
[45] B. Yan, X. Li, Z. Bai, X. Song, D. Xiong, M. Zhao, D. Li, S. Lu, J. Power Sources 338 (2017) 34–48.
[46] G. He, X. Ji, L. Nazar, Energy Environ. Sci. 4 (2011) 2878–2883.
[47] C. Zhang, H.B. Wu, C. Yuan, Z. Guo, X.W.D. Lou, Angew. Chem. Int. Ed. 124 (2012) 9730–9733.
[48] M.-Q. Zhao, Q. Zhang, J.-Q. Huang, G.-L. Tian, J.-Q. Nie, H.-J. Peng, F. Wei, Nat. Commun. 5 (2014) 3410.
[49] T. Lin, Y. Tang, Y. Wang, H. Bi, Z. Liu, F. Huang, X. Xie, M. Jiang, Energy Environ. Sci. 6 (2013) 1283–1290.

[50] M.-Q. Zhao, H.-J. Peng, G.-L. Tian, Q. Zhang, J.-Q. Huang, X.-B. Cheng, C. Tang, F. Wei, Adv. Mater. 26 (2014) 7051–7058.
[51] Z. Yuan, H.-J. Peng, J.-Q. Huang, X.-Y. Liu, D.-W. Wang, X.-B. Cheng, Q. Zhang, Adv. Funct. Mater. 24 (2014) 6105–6112.
[52] X.-B. Cheng, J.-Q. Huang, Q. Zhang, H.-J. Peng, M.-Q. Zhao, F. Wei, Nano Energy 4 (2014) 65–72.
[53] H.-J. Peng, J.-Q. Huang, M.-Q. Zhao, Q. Zhang, X.-B. Cheng, X.-Y. Liu, W.-Z. Qian, F. Wei, Adv. Funct. Mater. 24 (2014) 2772–2781.
[54] L. Zhu, H.-J. Peng, J. Liang, J.-Q. Huang, C.-M. Chen, X. Guo, W. Zhu, P. Li, Q. Zhang, Nano Energy 11 (2015) 746–755.
[55] H.-J. Peng, T.-Z. Hou, Q. Zhang, J.-Q. Huang, X.-B. Cheng, M.-Q. Guo, Z. Yuan, L.-Y. He, F. Wei, Adv. Mater. Interfaces 1 (2014) 1400227.
[56] M.-Q. Zhao, X.-F. Liu, Q. Zhang, G.-L. Tian, J.-Q. Huang, W. Zhu, F. Wei, ACS Nano 6 (2012) 10759–10769.
[57] L. Ji, M. Rao, H. Zheng, L. Zhang, Y. Li, W. Duan, J. Guo, E.J. Cairns, Y. Zhang, J. Am. Chem. Soc. 133 (2011) 18522–18525.
[58] H. Wang, Y. Yang, Y. Liang, J.T. Robinson, Y. Li, A. Jackson, Y. Cui, H. Dai, Nano Lett. 11 (2011) 2644–2647.
[59] G. Zhou, S. Pei, L. Li, D.-W. Wang, S. Wang, K. Huang, L.-C. Yin, F. Li, H.-M. Cheng, Adv. Mater. 26 (2014) 625–631.
[60] G. Zhou, L.-C. Yin, D.-W. Wang, L. Li, S. Pei, I.R. Gentle, F. Li, H.-M. Cheng, ACS Nano 7 (2013) 5367–5375.
[61] Y. Qiu, W. Li, W. Zhao, G. Li, Y. Hou, M. Liu, L. Zhou, F. Ye, H. Li, Z. Wei, Nano Lett. 14 (2014) 4821–4827.
[62] C. Zu, A. Manthiram, Adv. Energy Mater. 3 (2013) 1008–1012.
[63] J. Liu, W. Li, L. Duan, X. Li, L. Ji, Z. Geng, K. Huang, L. Lu, L. Zhou, Z. Liu, Nano Lett. 15 (2015) 5137–5142.
[64] X. Wang, G. Li, J. Li, Y. Zhang, A. Wook, A. Yu, Z. Chen, Energy Environ. Sci. 9 (2016) 2533–2538.
[65] C. Tang, Q. Zhang, M.-Q. Zhao, J.-Q. Huang, X.-B. Cheng, G.-L. Tian, H.-J. Peng, F. Wei, Adv. Mater. 26 (2014) 6100–6105.
[66] T.-Z. Hou, X. Chen, H.-J. Peng, J.-Q. Huang, B.-Q. Li, Q. Zhang, B. Li, Small 12 (2016) 3283–3291.
[67] W. Li, Q. Zhang, G. Zheng, Z.W. Seh, H. Yao, Y. Cui, Nano Lett. 13 (2013) 5534–5540.
[68] H. Yuan, J.-Q. Huang, H.-J. Peng, M.-M. Titirici, R. Xiang, R. Chen, Q. Liu, Q. Zhang, Adv. Energy Mater. 8 (2018) 1802107.
[69] P.T. Dirlam, R.S. Glass, K. Char, J. Pyun, J. Polym. Sci. Pol. Chem. 55 (2017) 1635–1668.
[70] J. Liu, D.G. Galpaya, L. Yan, M. Sun, Z. Lin, C. Yan, C. Liang, S. Zhang, Energy Environ. Sci. 10 (2017) 750–755.
[71] Z.W. Seh, Q. Zhang, W. Li, G. Zheng, H. Yao, Y. Cui, Chem. Sci. 4 (2013) 3673–3677.
[72] X. Liu, J.-Q. Huang, Q. Zhang, L. Mai, Adv. Mater. 29 (2017) 1601759.
[73] Y. Song, W. Cai, L. Kong, J. Cai, Q. Zhang, J. Sun, Adv. Energy Mater. 10 (2020) 1901075.
[74] X. Liang, C. Hart, Q. Pang, A. Garsuch, T. Weiss, L.F. Nazar, Nat. Commun. 6 (2015) 5682.
[75] X. Tao, J. Wang, Z. Ying, Q. Cai, G. Zheng, Y. Gan, H. Huang, Y. Xia, C. Liang, W. Zhang, Nano Lett. 14 (2014) 5288–5294.
[76] X. Liang, C.Y. Kwok, F. Lodi-Marzano, Q. Pang, M. Cuisinier, H. Huang, C.J. Hart, D. Houtarde, K. Kaup, H. Sommer, Adv. Energy Mater. 6 (2016) 1501636.
[77] Q. Pang, D. Kundu, M. Cuisinier, L.F. Nazar, Nat. Commun. 5 (2014) 4759.
[78] H. Wei, E.F. Rodriguez, A.S. Best, A.F. Hollenkamp, D. Chen, R.A. Caruso, Adv. Energy Mater. 7 (2017) 1601616.
[79] X. Liang, L.F. Nazar, ACS Nano 10 (2016) 4192–4198.
[80] Z. Li, J. Zhang, X.W.D. Lou, Angew. Chem. Int. Ed. 54 (2015) 12886–12890.
[81] S. Rehman, T. Tang, Z. Ali, X. Huang, Y. Hou, Small 13 (2017) 1700087.
[82] W. Kong, L. Yan, Y. Luo, D. Wang, K. Jiang, Q. Li, S. Fan, J. Wang, Adv. Funct. Mater. 27 (2017) 1606663.
[83] J. Guo, X. Zhang, X. Du, F. Zhang, J. Mater. Chem. A 5 (2017) 6447–6454.
[84] X. Tao, J. Wang, C. Liu, H. Wang, H. Yao, G. Zheng, Z.W. Seh, Q. Cai, W. Li, G. Zhou, Nat. Commun. 7 (2016) 11203.
[85] G. Zhou, H. Tian, Y. Jin, X. Tao, B. Liu, R. Zhang, Z.W. Seh, D. Zhuo, Y. Liu, J. Sun, Proc. Natl. Acad. Sci. U. S. A. 114 (2017) 840–845.
[86] G. Babu, N. Masurkar, H. Al Salem, L.M.R. Arava, J. Am. Chem. Soc. 139 (2016) 171–178.
[87] T. Chen, L. Ma, B. Cheng, R. Chen, Y. Hu, G. Zhu, Y. Wang, J. Liang, Z. Tie, J. Liu, Nano Energy 38 (2017) 239–248.
[88] X. Liu, Q. He, H. Yuan, C. Yan, Y. Zhao, X. Xu, J.-Q. Huang, Y.-L. Chueh, Q. Zhang, L. Mai, J. Energy Chem. 48 (2020) 109–115.
[89] C. Dai, J.-M. Lim, M. Wang, L. Hu, Y. Chen, Z. Chen, H. Chen, S.-J. Bao, B. Shen, Y. Li, Adv. Funct. Mater. 28 (2018) 1704443.
[90] Z. Yuan, H.-J. Peng, T.-Z. Hou, J.-Q. Huang, C.-M. Chen, D.-W. Wang, X.-B. Cheng, F. Wei, Q. Zhang, Nano Lett. 16 (2016) 519–527.
[91] Z. Wu, B. Fang, Z. Wang, C. Wang, Z. Liu, F. Liu, W. Wang, A. Alfantazi, D. Wang, D.P. Wilkinson, ACS Catal. 3 (2013) 2101–2107.
[92] H. Wang, Q. Zhang, H. Yao, Z. Liang, H.-W. Lee, P.-C. Hsu, G. Zheng, Y. Cui, Nano Lett. 14 (2014) 7138–7144.
[93] T. Lei, W. Chen, J. Huang, C. Yan, H. Sun, C. Wang, W. Zhang, Y. Li, J. Xiong, Adv. Energy Mater. 7 (2017) 1601843.
[94] L. Peng, Z. Wei, C. Wan, J. Li, Z. Chen, D. Zhu, D. Baumann, H. Liu, C.S. Allen, X. Xu, A.I. Kirkland, I. Shakir, Z. Almutairi, S. Tolbert, B. Dunn, Y. Huang, P. Sautet, X. Duan, Nat. Catal. 3 (2020) 762–770.
[95] W. Xue, Z. Shi, L. Suo, C. Wang, Z. Wang, H. Wang, K.P. So, A. Maurano, D. Yu, Y. Chen, L. Qie, Z. Zhu, G. Xu, J. Kong, J. Li, Nat. Energy 4 (2019) 374–382.
[96] C. Zhao, G.-L. Xu, Z. Yu, L. Zhang, I. Hwang, Y.-X. Mo, Y. Ren, L. Cheng, C.-J. Sun, Y. Ren, X. Zuo, J.-T. Li, S.-G. Sun, K. Amine, T. Zhao, Nat. Nanotechnol. (2020) 1–8.
[97] Y. Zhao, J. Feng, X. Liu, F. Wang, L. Wang, C. Shi, L. Huang, X. Feng, X. Chen, L. Xu, Nat. Commun. 5 (2014) 4565.
[98] N. Liu, W. Li, M. Pasta, Y. Cui, Front. Phys. 9 (2014) 323–350.
[99] L. Ma, K.E. Hendrickson, S. Wei, L.A. Archer, Nano Today 10 (2015) 315–338.
[100] M. Naguib, M. Kurtoglu, V. Presser, J. Lu, J. Niu, M. Heon, L. Hultman, Y. Gogotsi, M.W. Barsoum, Adv. Mater. 23 (2011) 4248–4253.
[101] X. Liang, A. Garsuch, L.F. Nazar, Angew. Chem. Int. Ed. 54 (2015) 3907–3911.
[102] H.-J. Peng, G. Zhang, X. Chen, Z.-W. Zhang, W.-T. Xu, J.-Q. Huang, Q. Zhang, Angew. Chem. Int. Ed. 128 (2016) 13184–13189.
[103] Z. Cui, C. Zu, W. Zhou, A. Manthiram, J.B. Goodenough, Adv. Mater. 28 (2016) 6926–6931.
[104] T.-G. Jeong, D.S. Choi, H. Song, J. Choi, S.-A. Park, S.H. Oh, H. Kim, Y. Jung, Y.-T. Kim, ACS Energy Lett. 2 (2017) 327–333.
[105] Z. Sun, J. Zhang, L. Yin, G. Hu, R. Fang, H.-M. Cheng, F. Li, Nat. Commun. 8 (2017) 14627.
[106] Z. Li, Q. He, X. Xu, Y. Zhao, X. Liu, C. Zhou, D. Ai, L. Xia, L. Mai, Adv. Mater. 30 (2018) 1804089.
[107] C. Ye, Y. Jiao, H. Jin, A.D. Slattery, K. Davey, H. Wang, S.-Z. Qiao, Angew. Chem. Int. Ed. 57 (2018) 16703–16707.
[108] Y. Yao, H. Wang, H. Yang, S. Zeng, R. Xu, F. Liu, P. Shi, Y. Feng, K. Wang, W. Yang, Adv. Mater. (2019) 1905658.
[109] Y. Mao, G. Li, Y. Guo, Z. Li, C. Liang, X. Peng, Z. Lin, Nat. Commun. 8 (2017) 14628.
[110] H. Jiang, X.-C. Liu, Y. Wu, Y. Shu, X. Gong, F.-S. Ke, H. Deng, Angew. Chem. Int. Ed. 57 (2018) 3916–3921.
[111] S. Bai, X. Liu, K. Zhu, S. Wu, H. Zhou, Nat. Energy 1 (2016) 16094.
[112] J. Zheng, J. Tian, D. Wu, M. Gu, W. Xu, C. Wang, F. Gao, M.H. Engelhard, J.-G. Zhang, J. Liu, Nano Lett. 14 (2014) 2345–2352.
[113] J. Zhou, R. Li, X. Fan, Y. Chen, R. Han, W. Li, J. Zheng, B. Wang, X. Li, Energy Environ. Sci. 7 (2014) 2715–2724.
[114] H. Yuan, X. Chen, G. Zhou, W. Zhang, J. Luo, H. Huang, Y. Gan, C. Liang, Y. Xia, J. Zhang, ACS Energy Lett. 2 (2017) 1711–1719.
[115] Y. Zhong, L. Yin, P. He, W. Liu, Z. Wu, H. Wang, J. Am. Chem. Soc. 140 (2018) 1455–1459.
[116] J. Shen, X. Xu, J. Liu, Z. Liu, F. Li, R. Hu, J. Liu, X. Hou, Y. Feng, Y. Yu, ACS Nano 13 (2019) 8986–8996.
[117] Z. Wang, J. Shen, J. Liu, X. Xu, Z. Liu, R. Hu, L. Yang, Y. Feng, J. Liu, Z. Shi, Adv. Mater. (2019) 1902228.
[118] S. Yu, W. Cai, L. Chen, L. Song, Y. Song, J. Energy Chem. 55 (2021) 533–548.
[119] D. Zhang, S. Wang, R. Hu, J. Gu, Y. Cui, B. Li, W. Chen, C. Liu, J. Shang, S. Yang, Adv. Funct. Mater. (2020) 2002471.
[120] Z. Du, X. Chen, W. Hu, C. Chuang, S. Xie, A. Hu, W. Yan, X. Kong, X. Wu, H. Ji, L.-J. Wan, J. Am. Chem. Soc. 141 (2019) 3977–3985.
[121] M. Zhao, H.-J. Peng, Z.-W. Zhang, B.-Q. Li, X. Chen, J. Xie, X. Chen, J.-Y. Wei, Q. Zhang, J.-Q. Huang, Angew. Chem. Int. Ed. 58 (2019) 3779–3783.
[122] M. Zhao, H.-J. Peng, B.-Q. Li, X. Chen, J. Xie, X. Liu, Q. Zhang, J.-Q. Huang, Angew. Chem. Int. Ed. 59 (2020) 9011–9017.
[123] D. Lin, Y. Liu, Y. Cui, Nat. Nanotechnol. 12 (2017) 194.
[124] G. Zheng, S.W. Lee, Z. Liang, H.-W. Lee, K. Yan, H. Yao, H. Wang, W. Li, S. Chu, Y. Cui, Nat. Nanotechnol. 9 (2014) 618–623.
[125] Y. Liu, D. Lin, P.Y. Yuen, K. Liu, J. Xie, R.H. Dauskardt, Y. Cui, Adv. Mater. 29 (2017) 1605531.
[126] N.-W. Li, Y.-X. Yin, C.-P. Yang, Y.-G. Guo, Adv. Mater. 28 (2016) 1853–1858.
[127] J. Zhao, G. Zhou, K. Yan, J. Xie, Y. Li, L. Liao, Y. Jin, K. Liu, P.-C. Hsu, J. Wang, Nat. Nanotechnol. 12 (2017) 993.
[128] R. Zhang, X.-R. Chen, X. Chen, X.-B. Cheng, X.-Q. Zhang, C. Yan, Q. Zhang, Angew. Chem. Int. Ed. 56 (2017) 7764–7768.
[129] C. Yang, Y. Yao, S. He, H. Xie, E. Hitz, L. Hu, Adv. Mater. 29 (2017) 1702714.
[130] A.C. Kozen, C.-F. Lin, A.J. Pearse, M.A. Schroeder, X. Han, L. Hu, S.-B. Lee, G.W. Rubloff, M. Noked, ACS Nano 9 (2015) 5884–5892.
[131] E. Kazyak, K.N. Wood, N.P. Dasgupta, Chem. Mat. 27 (2015) 6457–6462.
[132] X. Meng, X.-Q. Yang, X. Sun, Adv. Mater. 24 (2012) 3589–3615.
[133] L. Wen, M. Zhou, C. Wang, Y. Mi, Y. Lei, Adv. Energy Mater. 6 (2016) 1600468.
[134] S. Meini, R. Elazari, A. Rosenman, A. Garsuch, D. Aurbach, J. Phys. Chem. Lett. 5 (2014) 915–918.
[135] Y. Tsao, M. Lee, E.C. Miller, G. Gao, J. Park, S. Chen, T. Katsumata, H. Tran, L.-W. Wang, M.F. Toney, Joule 3 (2019) 872–884.
[136] L.C. Gerber, P.D. Frischmann, F.Y. Fan, S.E. Doris, X. Qu, A.M. Scheuermann, K. Persson, Y.-M. Chiang, B.A. Helms, Nano Lett. 16 (2016) 549–554.
[137] M. Zhao, H.-J. Peng, J.-Y. Wei, J.-Q. Huang, B.-Q. Li, H. Yuan, Q. Zhang, Small Methods (2019) 1900344.
[138] Z. Zhang, Y. Shao, B. Lotsch, Y.-S. Hu, H. Li, J. Janek, L.F. Nazar, C.-W. Nan, J. Maier, M. Armand, L. Chen, Energy Environ. Sci. 11 (2018) 1945–1976.
[139] C. Dietrich, R. Koerver, M.W. Gaultois, G. Kieslich, G. Cibin, J. Janek, W.G. Zeier, Phys. Chem. Chem. Phys. 20 (2018) 20088–20095.
[140] K.K. Fu, Y. Gong, J. Dai, A. Gong, X. Han, Y. Yao, C. Wang, Y. Wang, Y. Chen, C. Yan, Proc. Natl. Acad. Sci. U. S. A. 113 (2016) 7094–7099.
[141] X. Yu, Z. Bi, F. Zhao, A. Manthiram, Adv. Energy Mater. 6 (2016) 1601392.
[142] Y.-Z. Sun, J.-Q. Huang, C.-Z. Zhao, Q. Zhang, Sci. China Chem. 60 (2017) 1508–1526.
[143] E. Umeshbabu, B. Zheng, Y. Yang, Electrochem. Energy Rev. (2019) 1–32.

[144] N. Kamaya, K. Homma, Y. Yamakawa, M. Hirayama, R. Kanno, M. Yonemura, T. Kamiyama, Y. Kato, S. Hama, K. Kawamoto, A. Mitsui, Nat. Mater. 10 (2011) 682–686.
[145] J. Yi, L. Chen, Y. Liu, H. Geng, L.-Z. Fan, ACS Appl Mater. Interfaces 11 (2019) 36774–36781.
[146] W. Shin, L. Zhu, H. Jiang, W.F. Stickle, C. Fang, C. Liu, J. Lu, X. Ji, Mater. Today 40 (2020) 63–71.
[147] L. Wang, Y. Ye, N. Chen, Y. Huang, L. Li, F. Wu, R. Chen, Adv. Funct. Mater. 28 (2018) 1800919.
[148] J.-W. Park, K. Ueno, N. Tachikawa, K. Dokko, M. Watanabe, J. Phys. Chem. C 117 (2013) 20531–20541.
[149] K. Ueno, J.-W. Park, A. Yamazaki, T. Mandai, N. Tachikawa, K. Dokko, M. Watanabe, J. Phys. Chem. C 117 (2013) 20509–20516.
[150] C. Zhang, K. Ueno, A. Yamazaki, K. Yoshida, H. Moon, T. Mandai, Y. Umebayashi, K. Dokko, M. Watanabe, J. Phys. Chem. B 118 (2014) 5144–5153.
[151] C. Zhang, A. Yamazaki, J. Murai, J.-W. Park, T. Mandai, K. Ueno, K. Dokko, M. Watanabe, J. Phys. Chem. C 118 (2014) 17362–17373.
[152] Z. Zhang, P. Zhang, Z. Liu, B. Du, Z. Peng, ACS Appl Mater. Interfaces 12 (2020) 11635–11642.
[153] L. Suo, Y.-S. Hu, H. Li, M. Armand, L. Chen, Nat. Commun. 4 (2013) 1481.
[154] S. Dörfler, H. Althues, P. Härtel, T. Abendroth, B. Schumm, S. Kaskel, Joule 4 (2020) 539–554.
[155] C. Yang, P. Li, J. Yu, L.-D. Zhao, L. Kong, Energy 201 (2020) 117718.
[156] M. Zhao, B.-Q. Li, X.-Q. Zhang, J.-Q. Huang, Q. Zhang, ACS Cent Sci. 6 (2020) 1095–1104.
[157] Z. Wen, Y. Hu, X. Wu, J. Han, Z. Gu, Adv. Funct. Mater. 23 (2013) 1005–1018.
[158] X. Yu, A. Manthiram, ChemElectroChem 1 (2014) 1275–1280.
[159] X. Yu, A. Manthiram, J. Phys. Chem. C 118 (2014) 22952–22959.
[160] X. Yu, A. Manthiram, J. Phys. Chem. Lett. 5 (2014) 1943–1947.
[161] S. Xin, Y.-X. Yin, Y.-G. Guo, L.-J. Wan, Adv. Mater. 26 (2014) 1261–1265.
[162] R. Carter, L. Oakes, A. Douglas, N. Muralidharan, A.P. Cohn, C.L. Pint, Nano Lett. 17 (2017) 1863–1869.
[163] Y.-X. Wang, J. Yang, W. Lai, S.-L. Chou, Q.-F. Gu, H.K. Liu, D. Zhao, S.X. Dou, J. Am. Chem. Soc. 138 (2016) 16576–16579.
[164] Z. Qiang, Y.-M. Chen, Y. Xia, W. Liang, Y. Zhu, B.D. Vogt, Nano Energy 32 (2017) 59–66.
[165] Y.-M. Chen, W. Liang, S. Li, F. Zou, S.M. Bhaway, Z. Qiang, M. Gao, B.D. Vogt, Y. Zhu, J. Mater. Chem. A 4 (2016) 12471–12478.
[166] D. Ma, Y. Li, J. Yang, H. Mi, S. Luo, L. Deng, C. Yan, M. Rauf, P. Zhang, X. Sun, Adv. Funct. Mater. 28 (2018) 1705537.
[167] B.-W. Zhang, T. Sheng, Y.-D. Liu, Y.-X. Wang, L. Zhang, W.-H. Lai, L. Wang, J. Yang, Q.-F. Gu, S.-L. Chou, Nat. Commun. 9 (2018) 4082.
[168] B.-W. Zhang, T. Sheng, Y.-X. Wang, S. Chou, K. Davey, S.-X. Dou, S.-Z. Qiao, Angew. Chem. Int. Ed. 131 (2019) 1498–1502.
[169] S. Wei, S. Xu, A. Agrawral, S. Choudhury, Y. Lu, Z. Tu, L. Ma, L.A. Archer, Nat. Commun. 7 (2016) 11722.
[170] X. Xu, D. Zhou, X. Qin, K. Lin, F. Kang, B. Li, D. Shanmukaraj, T. Rojo, M. Armand, G. Wang, Nat. Commun. 9 (2018) 3870.
[171] Z.W. Seh, J. Sun, Y. Sun, Y. Cui, ACS Central Sci. 1 (2015) 449–455.
[172] W. Luo, C.-F. Lin, O. Zhao, M. Noked, Y. Zhang, G.W. Rubloff, L. Hu, Adv. Energy Mater. 7 (2017) 1601526.
[173] Y. Zhao, L.V. Goncharova, A. Lushington, Q. Sun, H. Yadegari, B. Wang, W. Xiao, R. Li, X. Sun, Adv. Mater. 29 (2017) 1606663.
[174] H. Wan, W. Weng, F. Han, L. Cai, C. Wang, X. Yao, Nano Today 33 (2020) 100860.
[175] J. Yue, F. Han, X. Fan, X. Zhu, Z. Ma, J. Yang, C. Wang, ACS Nano 11 (2017) 4885–4891.
[176] X. Yu, A. Manthiram, Small Methods 1 (2017) 1700271.
[177] Y. Xu, G. Zhou, S. Zhao, W. Li, F. Shi, J. Li, J. Feng, Y. Zhao, Y. Wu, J. Guo, Adv. Sci. 6 (2019) 1800981.
[178] W. Chu, X. Zhang, J. Wang, S. Zhao, S. Liu, H. Yu, Energy Storage Mater. 22 (2019) 418–423.
[179] L. Kong, C. Yan, J.-Q. Huang, M.-Q. Zhao, M.-M. Titirici, R. Xiang, Q. Zhang, Energy Environ. Mater. 1 (2018) 100–112.
[180] Z. Zhao-Karger, M. Fichtner, MRS Commun. 7 (2017) 770–784.
[181] S.-H. Chung, A. Manthiram, Adv. Mater. 31 (2019) 1901125.
[182] W. Li, S. Cheng, J. Wang, Y. Qiu, Z. Zheng, H. Lin, S. Nanda, Q. Ma, Y. Xu, F. Ye, Angew. Chem. Int. Ed. 55 (2016) 6406–6410.
[183] H.D. Yoo, I. Shterenberg, Y. Gofer, G. Gershinsky, N. Pour, D. Aurbach, Energy Environ. Sci. 6 (2013) 2265–2279.
[184] P. Saha, M.K. Datta, O.I. Velikokhatnyi, A. Manivannan, D. Alman, P.N. Kumta, Prog. Mater. Sci. 66 (2014) 1–86.
[185] O. Tutusaus, R. Mohtadi, ChemElectroChem 2 (2015) 51–57.
[186] I. Shterenberg, M. Salama, Y. Gofer, E. Levi, D. Aurbach, MRS Bull. 39 (2014) 453–460.
[187] H.S. Kim, T.S. Arthur, G.D. Allred, J. Zajicek, J.G. Newman, A.E. Rodnyansky, A. G. Oliver, W.C. Boggess, J. Muldoon, Nat. Commun. 2 (2011) 427.
[188] Z. Zhao-Karger, X. Zhao, D. Wang, T. Diemant, R.J. Behm, M. Fichtner, Adv. Energy Mater. 5 (2015) 1401155.
[189] T. Gao, M. Noked, A.J. Pearse, E. Gillette, X. Fan, Y. Zhu, C. Luo, L. Suo, M.A. Schroeder, K. Xu, J. Am. Chem. Soc. 137 (2015) 12388–12393.
[190] Z. Zhang, Z. Cui, L. Qiao, J. Guan, H. Xu, X. Wang, P. Hu, H. Du, S. Li, X. Zhou, Adv. Energy Mater. 7 (2017) 1602055.
[191] A. Du, Z. Zhang, H. Qu, Z. Cui, L. Qiao, L. Wang, J. Chai, T. Lu, S. Dong, T. Dong, Energy Environ. Sci. 10 (2017) 2616–2625.
[192] T. Gao, S. Hou, F. Wang, Z. Ma, X. Li, K. Xu, C. Wang, Angew. Chem. Int. Ed. 56 (2017) 13526–13530.
[193] T. Gao, S. Hou, F. Wang, Z. Ma, X. Li, K. Xu, C. Wang, Angew. Chem. Int. Ed. 129 (2017) 13711–13715.
[194] X. Zhou, J. Tian, J. Hu, C. Li, Adv. Mater. 30 (2018) 1704166.
[195] X. Yu, A. Manthiram, ACS Energy Lett. 1 (2016) 431–437.
[196] H. Du, Z. Zhang, J. He, Z. Cui, J. Chai, J. Ma, Z. Yang, C. Huang, G. Cui, Small 13 (2017) 1702277.
[197] X. Li, T. Gao, F. Han, Z. Ma, X. Fan, S. Hou, N. Eidson, W. Li, C. Wang, Adv. Energy Mater. 8 (2018) 1701728.
[198] L.-P. Wang, Z. Zhao-Karger, F. Klein, J. Chable, T. Braun, A.R. Schür, C.-R. Wang, Y.-G. Guo, M. Fichtner, ChemSusChem 12 (2019) 2286–2293.
[199] T. Gao, X. Li, X. Wang, J. Hu, F. Han, X. Fan, L. Suo, A.J. Pearse, S.B. Lee, G.W. Rubloff, Angew. Chem. Int. Ed. 128 (2016) 10052–10055.
[200] H. Yang, L. Yin, J. Liang, Z. Sun, Y. Wang, H. Li, K. He, L. Ma, Z. Peng, S. Qiu, Angew. Chem. Int. Ed. 130 (2018) 1916–1920.
[201] X. Yu, M.J. Boyer, G.S. Hwang, A. Manthiram, Chem 4 (2018) 586–598.
[202] Y. Guo, H. Jin, Z. Qi, Z. Hu, H. Ji, L.-J. Wan, Adv. Funct. Mater. 29 (2019) 1807676.
[203] J.-Q. Huang, Q. Zhang, H.-J. Peng, X.-Y. Liu, W.-Z. Qian, F. Wei, Energy Environ. Sci. 7 (2014) 347–353.
[204] X. Yu, A. Manthiram, Adv. Energy Mater. 5 (2015) 1500350.
[205] S.-H. Chung, A. Manthiram, J. Phys. Chem. Lett. 5 (2014) 1978–1983.
[206] J.-Q. Huang, T.-Z. Zhuang, Q. Zhang, H.-J. Peng, C.-M. Chen, F. Wei, ACS Nano 9 (2015) 3002–3011.
[207] S.-H. Chung, P. Han, R. Singhal, V. Kalra, A. Manthiram, Adv. Energy Mater. 5 (2015) 1500738.
[208] Z. Li, C. Zhou, J. Hua, X. Hong, C. Sun, H.-W. Li, X. Xu, L. Mai, Adv. Mater. 32 (2020) 1907444.
[209] T. Yim, S.H. Han, N.H. Park, M.-S. Park, J.H. Lee, J. Shin, J.W. Choi, Y. Jung, Y.N. Jo, J.-S. Yu, Adv. Funct. Mater. 26 (2016) 7817–7823.
[210] Z.A. Ghazi, X. He, A.M. Khattak, N.A. Khan, B. Liang, A. Iqbal, J. Wang, H. Sin, L. Li, Z. Tang, Adv. Mater. 29 (2017) 1606817.
[211] Y. Tian, G. Li, Y. Zhang, D. Luo, X. Wang, Y. Zhao, H. Liu, P. Ji, X. Du, J. Li, Adv. Mater. 32 (2020) 1904876.
[212] N. Wang, B. Chen, K. Qin, E. Liu, C. Shi, C. He, N. Zhao, Nano Energy 60 (2019) 332–339.
[213] T. Zhou, W. Lv, J. Li, G. Zhou, Y. Zhao, S. Fan, B. Liu, B. Li, F. Kang, Q.-H. Yang, Energy Environ. Sci. 10 (2017) 1694–1703.
[214] L. Li, L. Chen, S. Mukherjee, J. Gao, H. Sun, Z. Liu, X. Ma, T. Gupta, C.V. Singh, W. Ren, Adv. Mater. 29 (2017) 1602734.
[215] J. Sun, G. Zheng, H.-W. Lee, N. Liu, H. Wang, H. Yao, W. Yang, Y. Cui, Nano Lett. 14 (2014) 4573–4580.
[216] S. Bai, X. Liu, K. Zhu, S. Wu, H. Zhou, Nat. Energy 1 (2016) 1–6.
[217] L. Jiao, C. Zhang, C. Geng, S. Wu, H. Li, W. Lv, Y. Tao, Z. Chen, G. Zhou, J. Li, Adv. Energy Mater. 9 (2019) 1900219.
[218] Z. Zhou, B. Chen, T. Fang, Y. Li, Z. Zhou, Q. Wang, J. Zhang, Y. Zhao, Adv. Energy Mater. 10 (2020) 1902023.
[219] H.O. Ford, L.C. Merrill, P. He, S.P. Upadhyay, J.L. Schaefer, Macromolecules 51 (2018) 8629–8636.
[220] X. Yu, A. Manthiram, Adv. Energy Mater. 7 (2017) 1700561.
[221] J. Tan, D. Liu, X. Xu, L. Mai, Nanoscale 9 (2017) 19001–19016.
[222] X. Ma, W. Luo, M. Yan, L. He, L. Mai, Nano Energy 24 (2016) 165–188.
[223] Y. Yang, X. Liu, Z. Dai, F. Yuan, Y. Bando, D. Golberg, X. Wang, Adv. Mater. 29 (2017) 1606922.
[224] Y. Wu, N. Liu, Chem 4 (2018) 438–465.
[225] P. Harks, F.M. Mulder, P.H.L. Notten, J. Power Sources 288 (2015) 92–105.
[226] J. Wan, W. Bao, Y. Liu, J. Dai, F. Shen, L. Zhou, X. Cai, D. Urban, Y. Li, K. Jungjohann, Adv. Energy Mater. 5 (2015) 1401742.
[227] A.M. Tripathi, W.-N. Su, B.J. Hwang, Chem. Soc. Rev. (2018) 736–851.
[228] M. Yan, P. He, Y. Chen, S. Wang, Q. Wei, K. Zhao, X. Xu, Q. An, Y. Shuang, Y. Shao, Adv. Mater. 30 (2018) 1703725.
[229] P. He, G. Zhang, X. Liao, M. Yan, X. Xu, Q. An, J. Liu, L. Mai, Adv. Energy Mater. (2018) 1702463.
[230] J. Nelson, S. Misra, Y. Yang, A. Jackson, Y. Liu, H. Wang, H. Dai, J.C. Andrews, Y. Cui, M.F. Toney, J. Am. Chem. Soc. 134 (2012) 6337–6343.
[231] J. Conder, R. Bouchet, S. Trabesinger, C. Marino, L. Gubler, C. Villevieille, Nat. Energy 2 (2017) 17069.
[232] X. Xu, C. Niu, M. Duan, X. Wang, L. Huang, J. Wang, L. Pu, W. Ren, C. Shi, J. Meng, Nat. Commun. 8 (2017) 460.
[233] Y. Yuan, K. Amine, J. Lu, R. Shahbazian-Yassar, Nat. Commun. 8 (2017) 15806.
[234] J.Y. Huang, L. Zhong, C.M. Wang, J.P. Sullivan, W. Xu, L.Q. Zhang, S.X. Mao, N.S. Hudak, X.H. Liu, A. Subramanian, Science 330 (2010) 1515–1520.
[235] J.W. Wang, X.H. Liu, S.X. Mao, J.Y. Huang, Nano Lett. 12 (2012) 5897–5902.
[236] N. Liu, Z. Lu, J. Zhao, M.T. McDowell, H.-W. Lee, W. Zhao, Y. Cui, Nat. Nanotechnol. 9 (2014) 187.
[237] J. Sun, H.-W. Lee, M. Pasta, H. Yuan, G. Zheng, Y. Sun, Y. Li, Y. Cui, Nat. Nanotechnol. 10 (2015) 980.
[238] Z.-H. Xie, Z. Jiang, X. Zhang, J. Electrochem. Soc. 164 (2017) A2110–A2123.
[239] S.D. Lacey, J. Wan, A. von W. Cresce, S.M. Russell, J. Dai, W. Bao, K. Xu, L. Hu, Nano Lett. 15 (2015) 1018–1024.
[240] L. Lin, K. Yang, R. Tan, M. Li, S. Fu, T. Liu, H. Chen, F. Pan, J. Mater. Chem. A 5 (2017) 19364–19370.
[241] S.-Y. Lang, Y. Shi, Y.-G. Guo, R. Wen, L.-J. Wan, Angew. Chem. Int. Ed. 56 (2017) 14433–14437.

[242] S.-Y. Lang, Y. Shi, Y.-G. Guo, D. Wang, R. Wen, L.-J. Wan, Angew. Chem. Int. Ed. 55 (2016) 15835–15839.
[243] D.B. Williams, C.B. Carter, The Transmission Electron Microscope, Springer, 1996.
[244] M. Cuisinier, P.-E. Cabelguen, S. Evers, G. He, M. Kolbeck, A. Garsuch, T. Bolin, M. Balasubramanian, L.F. Nazar, J. Phys. Chem. Lett. 4 (2013) 3227–3232.
[245] J. Gao, M.A. Lowe, Y. Kiya, H.D. Abruña, J. Phys. Chem. C 115 (2011) 25132–25137.
[246] M.A. Lowe, J. Gao, H.D. Abruña, RSC Adv. 4 (2014) 18347–18353.
[247] A. Robba, A. Vizintin, J. Bitenc, G. Mali, I. Arčon, M. Kavcic, M. Žitnik, K. Bucar, G. Aquilanti, C. Martineau-Corcos, Chem. Mat. 29 (2017) 9555–9564.
[248] H. Kim, J.T. Lee, A. Magasinski, K. Zhao, Y. Liu, G. Yushin, Adv. Energy Mater. 5 (2015) 1501306.
[249] O. Pecher, J. Carretero-González, K.J. Griffith, C.P. Grey, Chem. Mat. 29 (2016) 213–242.
[250] J. Xiao, J.Z. Hu, H. Chen, M. Vijayakumar, J. Zheng, H. Pan, E.D. Walter, M. Hu, X. Deng, J. Feng, Nano Lett. 15 (2015) 3309–3316.
[251] H. Wang, N. Sa, M. He, X. Liang, L.F. Nazar, M. Balasubramanian, K.G. Gallagher, B. Key, J. Phys. Chem. C 121 (2017) 6011–6017.
[252] K.A. See, M. Leskes, J.M. Griffin, S. Britto, P.D. Matthews, A. Emly, A. Van der Ven, D.S. Wright, A.J. Morris, C.P. Grey, J. Am. Chem. Soc. 136 (2014) 16368–16377.
[253] F. Wang, Z. Zuo, L. Li, F. He, Y. Li, Nano Energy 68 (2020) 104307.
[254] W. Chen, T. Lei, T. Qian, W. Lv, W. He, C. Wu, X. Liu, J. Liu, B. Chen, C. Yan, Adv. Energy Mater. 8 (2018) 1702889.
[255] Y. He, Y. Qiao, Z. Chang, X. Cao, M. Jia, P. He, H. Zhou, Angew. Chem. Int. Ed. 131 (2019) (1904) 11900–11904.
[256] W. Zhu, A. Paolella, C.-S. Kim, D. Liu, Z. Feng, C. Gagnon, J. Trottier, A. Vijh, A. Guerfi, A. Mauger, Sustainable Energy Fuels 1 (2017) 737–747.
[257] C.-N. Lin, W.-C. Chen, Y.-F. Song, C.-C. Wang, L.-D. Tsai, N.-L. Wu, J. Power Sources 263 (2014) 98–103.
[258] X. Yu, H. Pan, Y. Zhou, P. Northrup, J. Xiao, S. Bak, M. Liu, K.-W. Nam, D. Qu, J. Liu, Adv. Energy Mater. 5 (2015) 1500072.
[259] M.U. Patel, R. Demir-Cakan, M. Morcrette, J.-M. Tarascon, M. Gaberscek, R. Dominko, ChemSusChem 6 (2013) 1177–1181.
[260] M.U. Patel, R. Dominko, ChemSusChem 7 (2014) 2167–2175.
[261] H. Marceau, C.-S. Kim, A. Paolella, S. Ladouceur, M. Lagacé, M. Chaker, A. Vijh, A. Guerfi, C.M. Julien, A. Mauger, J. Power Sources 319 (2016) 247–254.
[262] J. Fang, W. Shen, S.H.S. Cheng, S. Ghashghaie, H.K. Shahzad, C.Y. Chung, J. Power Sources 441 (2019) 227202.
[263] G. Cohn, L. Ma, L.A. Archer, J. Power Sources 283 (2015) 416–422.
[264] G. Tan, R. Xu, Z. Xing, Y. Yuan, J. Lu, J. Wen, C. Liu, L. Ma, C. Zhan, Q. Liu, Nat. Energy 2 (2017) 17090.
[265] C. Yang, S. Xin, L. Mai, Y. You, Adv. Energy Mater. (2020) 2000974.
[266] K. Fu, Y. Yao, J. Dai, L. Hu, Adv. Mater. 29 (2017) 1603486.
[267] R.S. Carmichael, Physical Properties of Rocks and Minerals, CRC Press Boca Raton, 1989.